THE UNIVERSITY OF OKLAHOMA

GRADUATE COLLEGE

PETROGRAPHY, MINERALOGY, AND GEOCHEMISTRY OF THE CHAMOSITIC IRON ORES OF NORTH-CENTRAL LOUISIANA

A DISSERTATION

SUBMITTED TO THE GRADUATE FACULTY

in partial fulfillment of the requirements for the

degree of

DOCTOR OF PHILOSOPHY

by

HERSHEL LEONARD JONES

Norman, Oklahoma

1969

PETROGRAPHY, MINERALOGY, AND GEOCHEMISTRY OF THE

CHAMOSITIC IRON ORES OF NORTH-CENTRAL LOUISIANA

APPROVED BY

Charles J. Mankin

Arnulf P. Hagen

David B. Vitts

Harvey Scott

Arthur J. Myers

DISSERTATION COMMITTEE

ACKNOWLEDGMENTS

The writer is grateful to Dr. Charles J. Mankin for directing this research and for making available the equipment and financial support of the University of Oklahoma School of Geology and Geophysics and the Oklahoma Geological Survey. Thanks are also due to Drs. Harvey Blatt, Arnulf P. Hagen, David B. Kitts, and Arthur J. Myers for reading the manuscript.

Initially, this investigation was subsidized by the Louisiana Geological Survey, and special thanks are due to Mr. Leo W. Hough, Louisiana State Geologist, for making available the facilities and financial support of the Survey. Special credit is also due to Harry Rowland and James Welch, geologists of the Louisiana Survey, for their invaluable assistance in obtaining and processing the cores necessary for this study. Dr. James M. Coleman, Louisiana Coastal Studies Institute, assisted in radiography studies. The Louisiana Highway Department graciously loaned the drilling equipment and crew necessary for obtaining the cores. Dr. James P. Morgan, then director of the Louisiana Coastal Studies Institute, kindly made available the Institute's specialized core barrel, essential for coring operations peculiar to this study. Dr. C. O. Durham,

Jr., Chairman, Department of Geology, Louisiana State University, initially endorsed this project for a dissertation and lent his support in the early stages of the investigation.

When the writer transferred to the University of Oklahoma in 1965, Mr. Leo Hough approved funds to help with the expense of transporting the cores, and later in 1967, he was instrumental in helping to obtain financial support, essential for completion of this project, from the United States Bureau of Mines. The financial assistance so generously supplied by the Bureau of Mines during the period from October, 1966 to August, 1969 is most sincerely appreciated. Mr. Kenneth J. Hughes, Director, Bartlesville Petroleum Research Center, U.S. Bureau of Mines, was the writer's Bureau of Mines supervisor during this study. He is to be highly commended for a fine job of coordinating the project through the University of Oklahoma advisor, Dr. Charles J. Mankin.

Credit is due various members of the University of Oklahoma Chemistry Department and Department of Botany and Microbiology for making available equipment necessary for this study, especially Drs. Glenn Dryhurst, Assistant Professor of Chemistry, and Elroy L. Rice, Professor of Botany. Dr. Sherril D. Christian, Professor of Chemistry, offered many helpful suggestions regarding gas chromatography analysis. Mr. Richard Pogue, Chemistry graduate student, willingly gave technical advice on analysis by atomic absorption spectrophotometry.

Many thanks are due to Dr. Jon N. Weber of Penn State University for his helpful advise on paleosalinity studies, to Dr. F. C. Loughnan, then Visiting Professor, School of Geology and Geophysics, University of Oklahoma, for technical assistance and helpful advice, to Dr. Konrad B. Krauskopf, Stanford University, for helpful comments during his recent visit to the University of Oklahoma.

Mr. Kenneth A. Sargent kindly assisted in the spectrochemical analysis. Gratitude is also expressed to Mr. W. H. Bellis and Mr. Clayton R. Nichols for their technical assistance, and to Mr. Clayton Nichols, Mr. David Bucke, Mr. Edward Gafford, and other fellow graduate students for helpful discussions of the study. A special vote of thanks is extended to Mr. Garrett L. Morrison, the writer's office mate, for his technical advice and many helpful suggestions throughout this endeavor.

Special thanks are due to two old Army buddies, Fred Janezic, M.S., Kansas State University, and Roy Parrott, B.S., Michigan State University, for helping in the preparation and loading of the cores for transport to Oklahoma during a very trying period in the writer's life.

Finally, the writer is indebted to his wife, Genevieve E. Jones, for editing and typing the manuscript, and for other invaluable assistance throughout this endeavor.

CONTENTS

TABLES

ILLUSTRATIONS

Figure Page

Plate Page

PETROGRAPHY, MINERALOGY, AND GEOCHEMISTRY OF THE CHAMOSITIC IRON ORES OF NORTH-CENTRAL LOUISIANA

INTRODUCTION

Purpose of Investigation

In North-central Louisiana sideritic chamosite lentils within the Upper Cook Mountain-Lower Cockfield (Upper Claiborne) sequence, Middle Eocene, alter during weathering to brown ore consisting of goethite veins and ledges distributed in the altered parent lentils. An investigation of the areal extent, volume, and potential economic quality of these Middle Eocene sedimentary iron ores was conducted by the Louisiana Geological Survey in cooperation with the Louisiana State University School of Geology during the period from 1959 to 1962.

Because the initial investigation was primarily an economic survey of the secondary brown iron ores, only a knowledge of the bulk chemistry of these deposits was essential; therefore, the lack of detailed studies of the petrography, mineralogy, and geochemistry of the unweathered parent chamosite beds during the initial investigation prevented paragenesis and petrofabric interpretations as well as detailed mineralogical identification. As a result, the location of

the iron in relationship to the minerals of the assemblage constituting the parent bed was also incompletely known. That portion of the iron not structurally coordinated in siderite or iron-bearing clay minerals could be present in interlayer or other ion exchange positions and/or as free amorphous iron oxide. This lack of information prevented a clear understanding of the mechanism of transformation of the iron-bearing minerals of the unaltered parent bed to the brown ore of the weathered beds.

An understanding of the relationships of all the minerals in these deposits is important, but the relationship of the siderite to the minerals in the unaltered parent bed and to the brown ore in the altered bed poses one of the most significant problems as far as possible future industrial development is concerned. Prior to deep drilling accompanying this study, siderite had been observed in surface or near surface exposures and in shallow drill holes. However, little was known about the mineralogy of the unaltered parent material below the present zone of oxidation. From such limited observations siderite could either be an intermediate phase in the transition from green to brown ore, contemporaneous with the enclosing glauconite, or formed during diagenesis. If the first hypothesis is correct, siderite should be formed only in the transition zone between the green and brown ore bodies; but if the mode of origin fits either of the latter cases, then siderite could feasibly occur throughout the entire bed

with no relationship to the topographic position of the bed. "Eckles (1938, p. 41, 46, 47) considered the siderite associated with the East Texas glauconite to be a secondary alteration and replacement of the glauconite occurring near and beneath the water table at the base of the brown ore," (in Durham, 1964, p. 28).

If siderite should persist throughout the parent bed in concentrations as great as those present in green ore samples from surface or near-surface exposures, it would add significantly to the economic potential of these deposits. Analyses of such material as reported by Durham (1964, p. 58) indicate that nearly half of the iron content in these green ores, averaging 34.84 percent, may be present as siderite. Removal of the carbon dioxide and water of hydration, averaging approximately 15 and 5 percent respectively, of these samples by roasting increased the iron content to approximately 45 percent by reducing the weight of the total sample. The presence of such a high available iron content in the enormous green ore reserves available (over 121 million long tons mapped) could add significantly to the economic potential of these iron ore deposits. Durham (1964) recognized this and recommended that studies of the unaltered parent bed be made to resolve the question.

Therefore, the primary purpose of this investigation was to conduct a detailed study of the mineralogy, petrography and geochemistry of the green ore and to supplement similar studies of the brown

ores where necessary and to utilize these data to explain the petrogenesis. This information would shed much light on the environment of deposition of these deposits and allow speculation on the location, lithology, and climate of the source area for the iron and its mode of transportation and concentration.

Previous Investigations

The Louisiana Geological Survey in cooperation with the Louisiana State University School of Geology conducted an investigation of the areal extent, volume, and quality of these sedimentary ores of north-central Louisiana from 1959 to 1962. The writer was a member of the investigating team and a detailed study of three of the major districts was prepared by him as a separate report (Jones, 1962). Subsequently, the collective results of work by the writer and various individuals working on this project was compiled, supplemented, and published as Geological Bulletin No. 41 entitled "Iron Ore of Central North Louisiana," by Clarence O. Durham, then Director of Research, Louisiana Geological Survey, and Professor of Geology, Louisiana State University (Durham, 1964).

Several cursory surveys of strictly an economic and stratigraphic nature were conducted prior to the Louisiana Survey's more detailed work, and these investigations are referenced in detail in both of the above-mentioned reports.

Location

The major iron ore deposits of north-central Louisiana are in an area approximately forty miles in length and twenty miles in width which trends northwest-southeast between the northeast portion of Webster Parish and the south-central part of Lincoln Parish. This includes most of central and southern Claiborne Parish, western and southern Lincoln Parish, and the northernmost part of Bienville Parish (Figure 1). The development of present topography and/or facies changes within the parent ore bed result in isolated ore districts within this overall region, but these are normally quite extensive (Figure 2).

Ore deposits in areas other than those outlined above are known, but these were not studied in detail either because of their marginal quality or because of their remoteness from the major deposits. For example, deposits are known in northeastern Webster Parish, most of Claiborne and Lincoln Parishes, portions of Jackson and Union Parishes, and northern Bienville Parish.

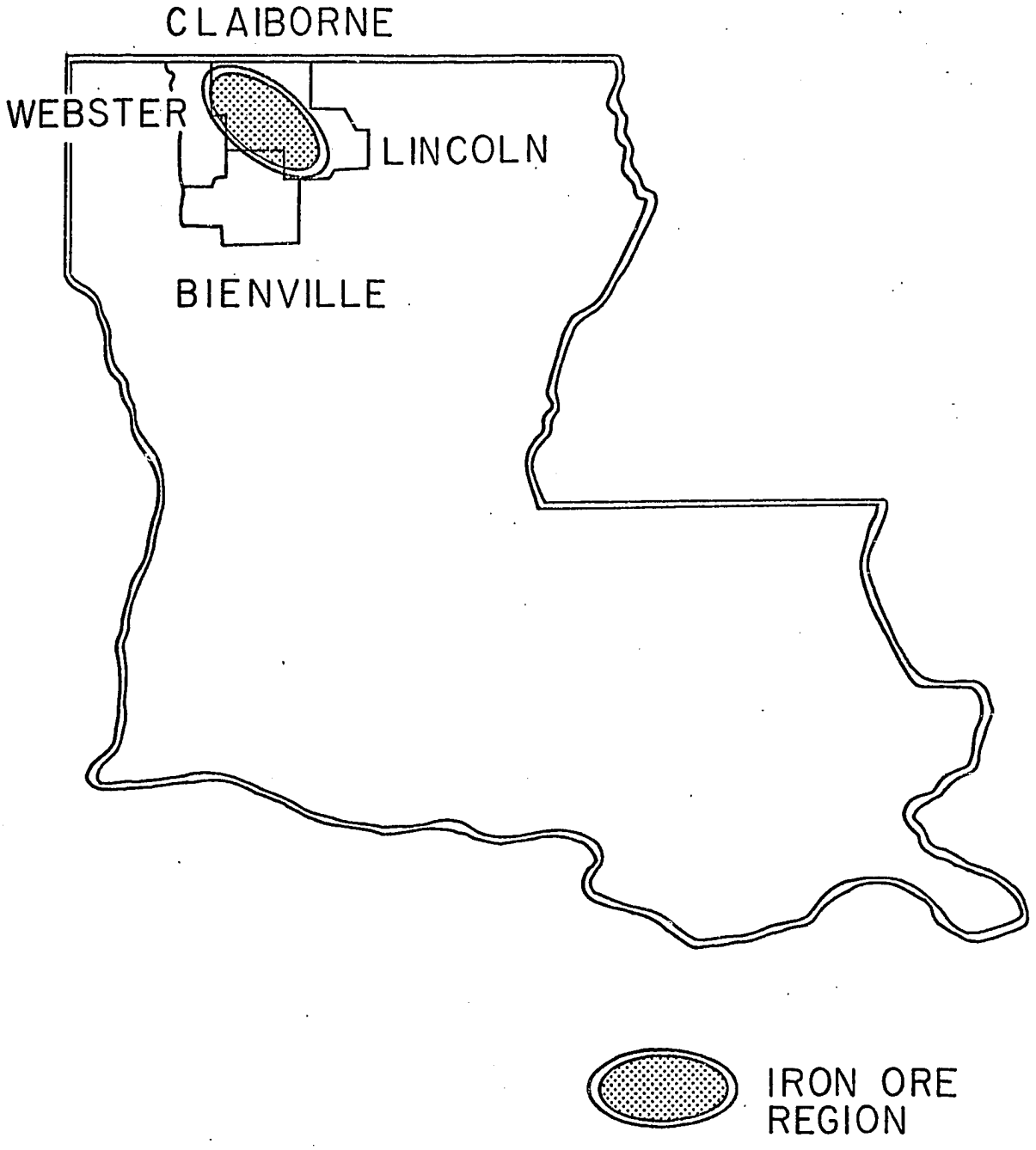

Figure 1. Map of Louisiana showing general location of the iron region.

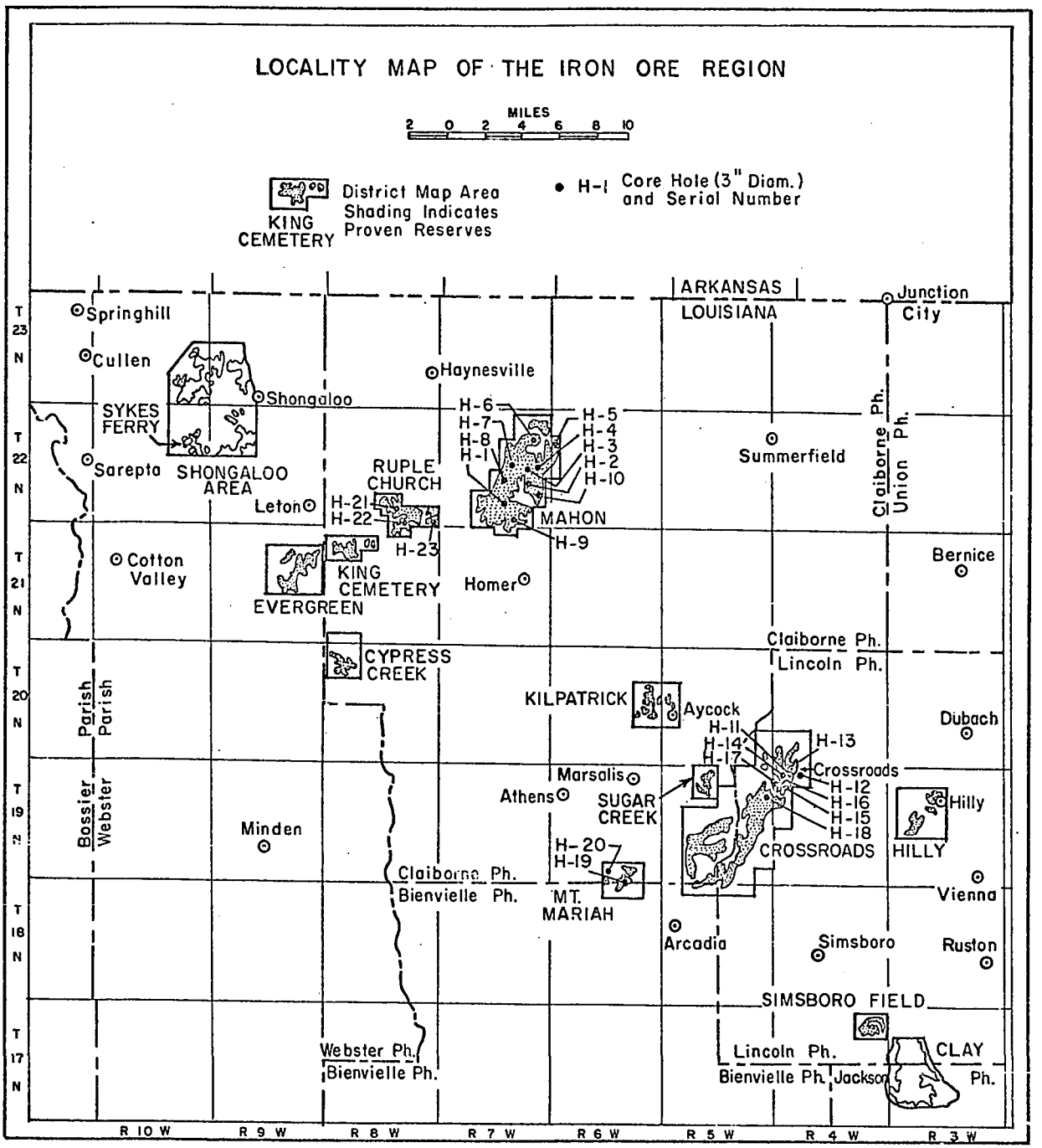

Figure 2. Locality map of the iron ore region showing position of proven reserves and location of coring sites. Modified after Durham, (1964, Plate 2).

GEOLOGIC SETTING

The following resume of the geologic setting of the area of investigation is a modified version of that contained in the writer's master's thesis (Jones, 1962).

In the area of investigation, the nearly flat-lying surface beds of the Claiborne group (Middle Eocene) constitute a part of the extensive D'Arbonne structural platform* of only slight regional dip (Figure 3). This platform is separated from the structurally higher Sabine platform to the southwest by a monocline of gentle northeasterly dip. The Sabine platform is a prominent surface feature of northwestern Louisiana and adjacent parts of Texas. It is underlain by older sediments of the Wilcox group (Paleocene-Eocene). "The Sabine and D'Arbonne platforms are bounded on the south by the Angelina-Caldwell flexure, which extends southwest-northeast through central Louisiana, and is the northern edge of southerly Gulfward-dipping beds" (Durham, 1964,

---

*This area was originally called the Claiborne platform by Durham and White (1960) but was subsequently redesignated the D'Arbonne platform for the largest watershed in its confines by Durham (1964). "This substitution is done in order to avoid confusion of the term 'Claiborne' with the Claiborne sequence which actually forms the platform's terrain but is named from Claiborne Bluff in Alabama" (Durham, 1964, p. 11).

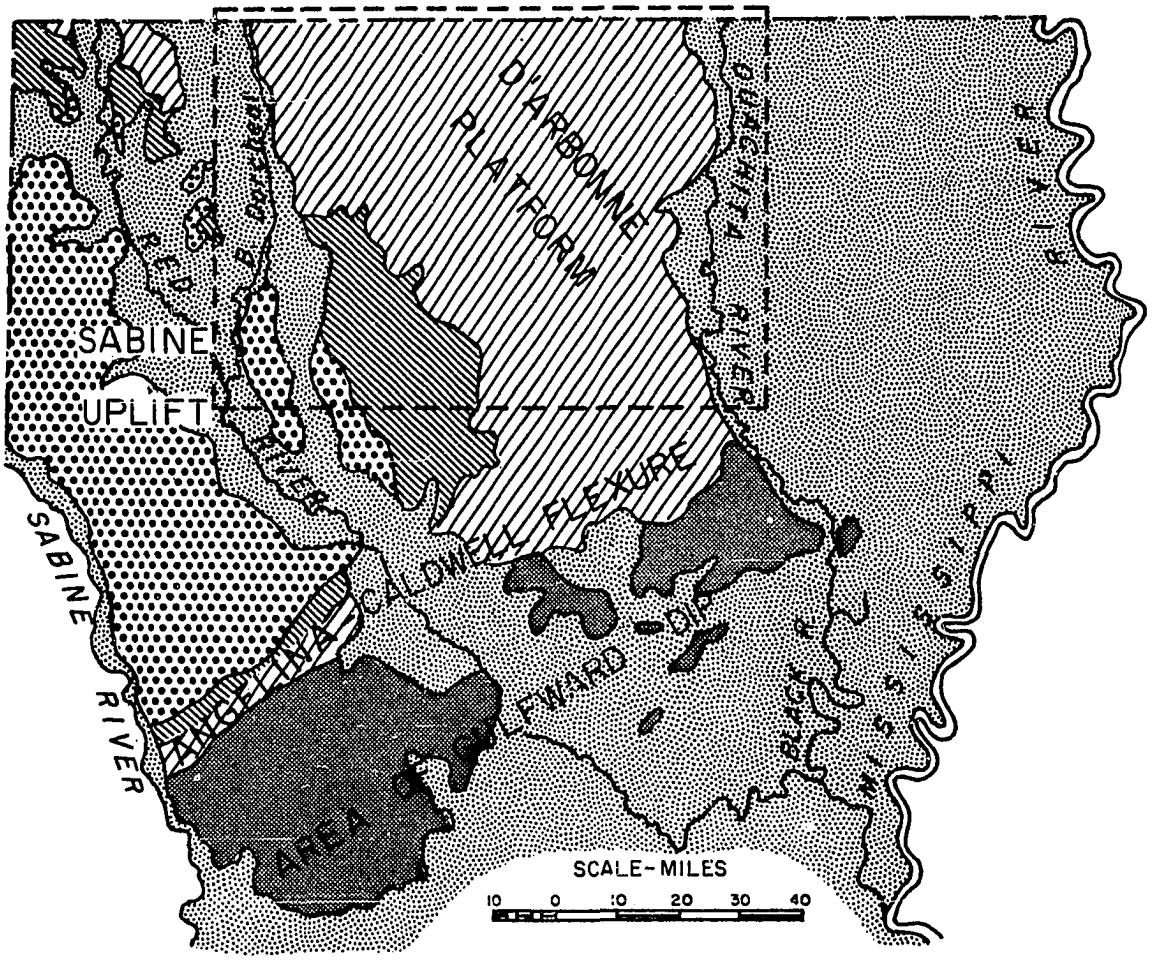

GEOLOGIC MAP
OF
NORTH AND CENTRAL LOUISIANA

- Recent Alluvium and Pleistocene Terraces
- Jackson and younger Tertiary beds
- Upper Claiborne (Cook Mt. and Cockfield)
- Lower Claiborne (Sparta and older beds)
- Wilcox and older beds

Figure 3. General geologic map of north and central Louisiana showing major structural features and occurrences of Tertiary sediments. Modified after Durham (1964, Plate 1).

p. 11) (Figure 3).

The structural configuration changes with depth, and the southwestern edge of the D'Arbonne platform is underlain by the North Louisiana Syncline whereas the Monroe uplift underlies it to the east. The Monroe uplift does not exhibit a surface expression on the D'Arbonne platform even though it is a prominent North Louisiana subsurface structural feature. The surface position of the northeasterly dipping monocline separating the Sabine and D'Arbonne platforms overlies the axis of the subsurface North Louisiana syncline.

According to Durham (1964, p. 11-12):

> The northwestward projection of the North Louisiana syncline axis into the area north of the Sabine platform is marked by a saddle, with surface expression, between the structurally lower D'Arbonne platform to the east and the northeastward extension of the East Texas embayment to the west in Texas (the Pittsburg syncline of Murray, 1961), and between the structurally higher Sabine platform to the south and the southward dipping inner margin of the Gulf Coastal Province in Arkansas to the North.

The distribution of salt dome structures, most of which have surface expression, is controlled by the subsurface portion of the North Louisiana syncline. For example in the southern portion of the area of study a large rim syncline peripheral to the Minden salt dome reflects the subsurface Minden basin, which is the most pronounced negative feature along the axis of the North Louisiana syncline.

Although local subsidiary structures, e.g., Homer, Haynesville, Athens, Sugar Creek, Hico-Knowles, Simsboro, and Ruston, exhibit surface

expressions on the D'Arbonne platform, the general absence of dip over the area results in exposures being limited to only a small portion of the Eocene sequence. As a result of the alternating marine and non-marine cyclic pattern characteristic of North Louisiana Tertiary deposits, the middle Eocene Claiborne Group overlying the Wilcox deltaic complex (Paleocene-Lower Eocene) is subdivided into alternating marine and non-marine formations from the oldest, Carrizo (non-marine), through Cane River (marine), Sparta (non-marine), Cook Mountain (marine) to the youngest, Cockfield (non-marine). In the general study area only the upper Sparta, Cook Mountain, and lower Cockfield are exposed. Sparta is only exposed on local structural highs and formations younger than lower Cockfield do not exist in the area because it is structurally too high.

The lithology of the marine beds normally consists of glauconitic,* fossiliferous clay or marl, whereas the non-marine units are characterized by sands, silts, and clays which may be carbonaceous or interbedded with lignite, and are commonly crossbedded. A further characteristic of the lithology of the area is the transitional and intertonguing nature of the contacts between the marine and non-marine units in contrast with the sharper boundaries exhibited farther

---

*Glauconite as used in this report is strictly a field term applied to small greenish pellets of iron-rich clay and is not to be misconstrued to represent the mineral glauconite. The actual clay mineral was found to be chamosite in samples tested.

gulfward. Due to the area's inland position, contacts must be arbitrarily selected at key mapping horizons which may be present within the transitional sequence. In the study area this is especially true of the Cook Mountain-Cockfield contact. As a result, non-marine channel sands are placed within the Middle and Upper Cook Mountain, and glauconitic marginal marine beds are placed within the Lower Cockfield.

STRATIGRAPHY

General

Normally only beds of the Cook Mountain and lower Cockfield Formations of the Claiborne Group (Middle Eocene) are exposed in the area of consideration. "However, lower Cook Mountain beds, as well as the underlying upper Sparta beds, are well exposed in the southwestern portion of the iron ore region where higher structural elevations occur along the foot of the northeastward dipping monocline which separates the Sabine from the D'Arbonne platform" (Durham, 1964, p. 17). Beds of the Sparta Formation are also exposed on some of the local subsidiary structures on the platform (Jones, 1962). For example, beds of the upper Sparta are exposed on the Sugar Creek structure (Jones, 1962). The Sparta and Cane River Formations come to the surface on the Arcadia piercement salt structure (Worley, 1962), and practically the total thickness of the Sparta is exposed on the Homer dome (Durham, 1964). Very slight northeasterly regional dip of the Tertiary beds constituting the D'Arbonne platform results in progressively younger sediments northeastward; consequently, in the northeastern part of the area only Cockfield and upper Cook Mountain beds

are exposed. Due to the structural attitude of this platform, the upper Cook Mountain and lower Cockfield Formations are the most extensively exposed stratigraphic units within the area of study.

In this study detailed stratigraphic descriptions are restricted to the siderite - chamosite facies within the upper Cook Mountain and lower Cockfield Formations because a detailed study of these facies is the prime interest of this report. The stratigraphy of the brown ore, formed by weathering of these facies, is discussed in two earlier reports on the north-central Louisiana iron ores (Jones, 1962; Durham, 1964). The general stratigraphy and stratigraphic relationships of the area are comprehensively covered in two Louisiana State University theses. A thesis by the writer (Jones, 1962), produced as part of the Louisiana Survey's iron ore project, treats the Sugar Creek area in southeastern Claiborne, northern Bienville, and western Lincoln Parishes. A thesis by Worley (1962), produced in connection with this same project, covers the Arcadia dome area in northeastern Bienville, southeastern Claiborne and southwestern Lincoln Parishes. These reports are in the Louisiana State University Library and on open file in the Louisiana Geological Survey office.

Stratigraphic Subdivisions

The leaf-bearing, lignitic, non-marine Sparta silts and clays are overlain directly by the fossiliferous, glauconitic, arenaceous

Dodson member of the Cook Mountain transgressive marine phase. These strata are in turn overlain by the extremely fossiliferous calcareous clay beds of the Milams member of the inundative Cook Mountain marine phase. The transgressive and inundative units of the Cook Mountain marine phase are overlain consecutively by four, unnamed, locally mappable, transitional marine units: a lower silt and clay member, a middle sand member, an upper clay and silt member, and an uppermost sand member* (Figure 4). Collectively the beds above the non-marine Sparta represent the entire Cook Mountain marine phase and the early phase of the subsequent Cockfield regression (Durham, 1964). Subsequent to deposition of the marine Milams member, a gradual but fluctuating retreat of the sea is interpreted from the transitional and intertonguing nature of the deposits of the upper Cook Mountain and lower Cockfield Formations. The regression is reflected in the increasing coarseness of the detrital material, and the fluctuating character of this regression is further attested to by the intermittent occurrence of several chamosite lentils within these marginal marine facies. Martin (1943, 1954) postulated that these deposits formed along a fluctuating deltaic shoreline, and Durham (1964) agreed after pointing out the variability of the stratigraphy of these members.

---

*Utilization of the term "uppermost sand" means only that this sand is the youngest formation occurring in the area and should not be misinterpreted as representing its position as a member within any scheme of stratigraphic nomenclature (Durham, 1964).

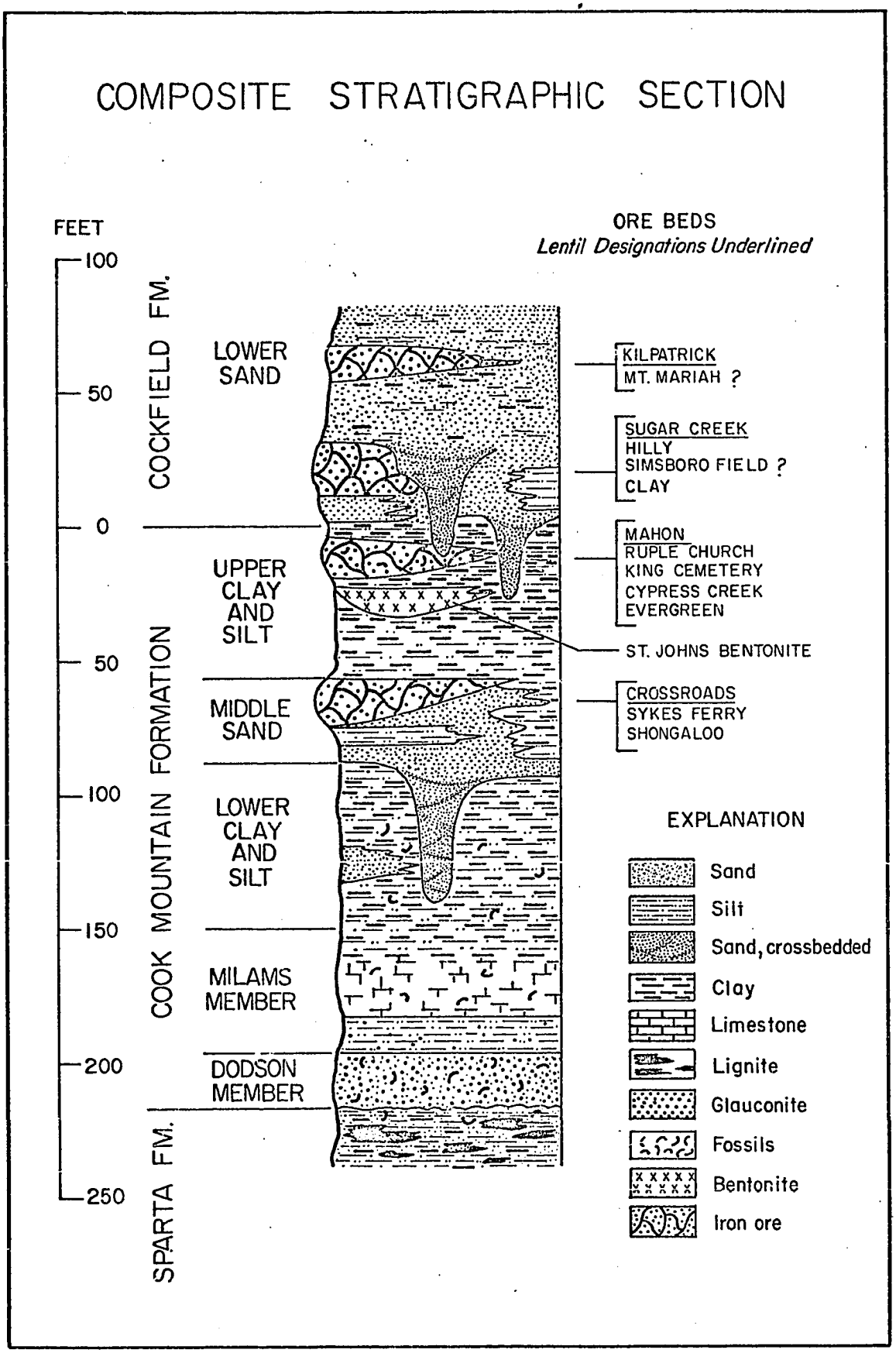

Figure 4. Composite stratigraphic section showing position of chamosite lentils. From Durham (1964, Figure 3) as modified after Jones (1962, Plate III).

That gradual regression began after deposition of the Milams member is interpreted from the absence of abundant marine fossils and the presence of a few glauconitic beds in the overlying silt and clay member. The nature of these deposits implies a shallow, nearshore transitional environment of deposition, such as Durham's (1964) shallow, nearshore prodeltaic environment. The increased coarseness of the clastic sands of the overlying middle sand member reflects a further regression of the then existing environment of deposition. The fact that these crossbedded sands partially replace the underlying clay and silt member and locally fill channels extending deeply into it help to substantiate this observation. The sand filling these channels is channel-bedded and commonly contains "clay balls" and other reworked material from the underlying clay and silt member. These phenomena point to a stream origin for the channel and its deposits. The presence of abundant glauconite in the upper sands of the middle sand member is suggestive of nearshore and shoreline deposits (Durham, 1964). Return of conditions similar to those existing during deposition of the lower clay and silt member occurred during the deposition of the overlying upper clay and silt member, as suggested by sparingly fossiliferous clays and silts containing interbedded glauconite beds. In this member the St. John's bentonite bed occurs discontinuously yet is widespread enough so that its upper surface forms a good mapping horizon.

The lithology of the overlying sand member, and youngest Tertiary unit present in the area, suggests a return to environmental conditions similar to those existing during deposition of the middle sand member. This sand member is composed of two facies. In the northern part of the area the sand facies is non-chamositic and locally channel-bedded. These channel-bedded sands are similar to those of the middle sand member and are also thought to be stream laid. Environmental conditions change southward and in the Gulfward southern part of the area this facies in part overlies and in part intertongues with a nearshore transitional marine sand facies characterized by interbedded chamosite and infrequent fossils. "These two facies of upper most sand are so transitional and intimately interbedded in many places that it is impossible to map them separately, although locally, as where the non-marine facies occur in channels within the glauconitic deposits of the shoreline facies, they are readily distinguishable" (Durham, 1964, p. 20). Durham (1964) included both facies in the uppermost sand member which he assigned to the lower Cockfield and designated the lower sand member.

The intertonguing and transitional nature of the upper Cook Mountain and lower Cockfield Formations greatly complicates selection of a formational boundary between the marine Cook Mountain and the overlying, supposedly non-marine Cockfield. In order to include all marine beds in the area in the Cook Mountain Formation, the boundary

would have to be placed above the uppermost chamosite lentil in the uppermost sand member. This would mean placing the boundary above the Kilpatrick lentil which is more than 50 feet above the base of the uppermost sand. This is not a satisfactory boundary, however, because the chamosite lentils pinch out northward, and there the contact is conveniently drawn at the base of the uppermost sand member just above the bentonite (Durham and White, 1960). "Since separation of the glauconitic and non-glauconitic facies of the uppermost sand is impractical on a regional basis, assignment of the entire uppermost sand to the Cockfield appears to be a logical solution even though nearshore glauconite facies are thus grouped with the Cockfield" (Durham, 1964, p. 21). The arbitrary placement of the boundary just above the bentonite bed is convenient because this datum is easily recognized and is widely distributed over the area.

Within the upper three members, four chamosite lentils are the primary ore-formers in the area: the "crossroads" lentil at the top of the middle sand member, the "Mahon" lentil in the upper part of the upper clay and silt member, the "Sugar Creek" lentil near the base of the lower Cockfield sand member, and the "Kilpatrick" lentil near the top of the lower Cockfield sand member. A combination of slight northeasterly regional tilt of the D'Arbonne platform combined with the fluctuating character of these lentils result in the restriction of outcrop areas of certain of these lentils to specific geographic

locations, from whence came the name of the lentils; however, outcrops of one or the other of these lentils occur extensively over the approximately 1000 square mile area considered.

Regional Correlations

Although exact regional correlation of the north-central Louisiana iron ore deposits, on a lentil by lentil basis, with those of the East Texas iron ores is not possible, recent evidence based on regional correlation studies and ore similarities indicate that the Louisiana ores are equivalent in age to those of the East Texas North Basin. On the basis of a regional correlation study around the flanks of the Sabine platform, Smith (1957) concluded that the East Texas North Basin iron ores also belong to the Cook Mountain rather than to the Weches (Cane River) marine facies of the preceding cycle to which the East Texas South Basin ores belong (Durham, 1964). This contradicts Eckles' (1938) interpretation of an equivalent Weches age for the East Texas North Basin and South Basin ores. The dissimilarity of characteristics of South and North Basin ores emphasized in the geological report on the East Texas ores also makes age equivalency of these iron ore bodies questionable. Eckles recognized 17 differences which are tabulated in that publication (Eckles, 1938). According to Durham (1964, p. 25), "Characteristics of the ore of central North Louisiana match 15 of 17 characteristics of the East Texas North Basin type.

This is an added indication that the North Basin ores are Cook Mountain as are those in Louisiana rather than Weches, as are those of the East Texas South Basin."

In the geological report on the Central North Louisiana ores, Durham regionally correlates on a member basis the Cook Mountain-lower Cockfield stratigraphic pattern of Central North Louisiana to the Central Texas subdivisions described by Stenzel in 1939 (Durham, 1964, p. 22). Regional correlation of the Central North Louisiana Cook Mountain-lower Cockfield subdivisions on a member by member basis with those of the type section of Huner (1939) to the south in Winn Parish is also attempted in that report (Durham, 1964, p. 22).

METHODS OF INVESTIGATION

The geology of the brown ore deposits is determinable from surface or near surface exposures because once exposed to oxidizing and leaching conditions above the present ground water table the parent bed is converted to brown ore. In order to acquire unoxidized parent material, however, it was necessary to select drilling locations where the parent bed could be encountered deep below the present zone of oxidation. This was accomplished by interpretation of the position of the bed in relationship to topography from structural, isopachous, and topographic maps. Due to the size of the area of study, approximately 1000 square miles, it was necessary to choose strategically located drilling sites that offered samples representative of the average lithology and thickness of the parent bed and to encounter the bed topographically as low as possible.

Deep-seated cores essential for this study were eventually obtained in the late Spring and Summer of 1965 only after several abortive coring attempts during the early Spring of 1965. The difficulty in coring these deposits results from the inconsistencies in physical properties of the constituents of the parent bed in cross

section. Sections of tightly cemented, indurated ore alternate with less tightly cemented, friable sand-size ore which is subject to loss by dispersion during coring operations involving drilling fluids. Drive-type coring was highly unsuccessful because of the extreme hardness of the indurated portions of the bed. It was only after a specialized rotary coring device, a ten-foot Dampco core barrel with a modified core catcher, was obtained and a knowledge of specific drilling mud concentrations and drilling pressures were acquired that good recovery operations were achieved. When these problems had finally been mastered, an average of greater than 85 percent recovery was achieved. A total of twenty-two three-inch diameter cores of the complete parent bed were taken from predetermined sites within the area. These cores are designated by the prefix "H", and the numbers run chronologically throughout the entire region (Figure 3).

Once obtained, these cores were prepared for transport back to the lab by cutting them into five-foot sections which were placed in halves of plastic tubing, wrapped with aluminum foil, and sealed with wax. On arrival at the lab the cores were prepared for analytical work. First they were split in half longitudinally and a 3/8 inch section was taken from the center for X-radiography studies. The remainder of the core was then examined under high magnification and 40 representative samples were selected to be thin sectioned. Subsequently, the excess material from these 40 samples was utilized in

qualitative and quantitative analysis by X-ray diffraction and fluorescence, emission spectroscopy, and differential thermal analysis.

Initially, a study of the optical properties of the constituent minerals in thin section was conducted by means of a petrographic microscope to facilitate identification, mineralogical associations, and description. This technique proved to be the most effective method of determining changes in the original mineralogy and structure resulting from diagenesis. Identification of clay minerals, particularly those showing poor crystallinity, is not always infallible in thin section; therefore, X-ray diffractograms and information from differential thermal analysis were utilized to compliment mineral identification.

The presence of amorphous iron oxide in untreated samples created extreme difficulty in obtaining diffractograms of either the random powder slides or preferentially-oriented slides of clay fractions. This undesired iron was removed utilizing the dithionite-citrate technique proposed by O. P. Mehra and M. L. Jackson (1960). The theory and analytical procedures for this process are included in the clay mineralogy section and Appendix A. The total free iron oxide extracted from these samples by this technique was determined by atomic absorption spectrophotometry.

Further dispersion of the dithionite-citrate treated clays by boiling in a 2 percent Na_2CO_3 solution for 5 minutes was attempted on

one of the samples. The diffraction pattern of sedimented slides of this material showed some improvement in the intensity and definition of the clay peaks, but the results obtained from samples treated by the dithionite-citrate technique were in general so good that it was unnecessary to continue this procedure.

Large samples of the bulk material were crushed to pass through a 120 mesh screen. Amorphous iron coatings were then removed from these samples by means of the dithionite-citrate technique. The treated samples were dispersed in distilled water and further disaggregated and dispersed by means of the ultrasonic transducer. Size fractionation of selected treated samples was performed by a combination of decantation and high speed centrifugation methods in hopes of obtaining more nearly monomineralic samples of clay-sized particles. The less-than-one micron equivalent spherical diameter particles were segregated from the suspended sample by fluid withdrawal according to Stokes' Law settling graphs. The fraction less-than-one micron was further subdivided into 1-1/2, 1/2-1/4, 1/4-1/8, and 1/8-1/16 micron fractions by continuous flow centrifugation. The identity and nature of the size-fractioned clays was determined by X-ray diffraction and thermal stability and phase transformation studies. A high temperature oven was utilized to conduct high-temperature structural stability studies, and differential thermal analysis, effluent gas analysis and gas chromatography analysis were utilized in determining the nature of

the reactions detected. Differential thermal analyses were conducted using a Robert L. Stone model DTA-13 M furnace and recording assembly. Gas liberated by the samples during the reactions produced by the heating furnace was detected by EGA. It was then collected and analyzed by means of gas chromatography.

Magnetically susceptable siderite was selectively removed from the bulk sample by using the Frantz Magnetic separator and random powder diffraction patterns were obtained of this material.

Bruce Williams Laboratories in Joplin, Missouri performed quantitative wet chemical analyses on 33 samples randomly selected from cores of the parent chamosite bed. Subsequently, a complete silicate analysis of 17 samples, aliquots of core samples utilized in other tests, was achieved by quantitative X-ray fluorescence analysis utilizing the Siemens vacuum X-ray spectrometer. Seven of the samples analyzed by Bruce Williams were utilized as standards in fluorescence analysis. The H_2O+, H_2O-, and CO_2 content of these samples was determined by Mr. John Schleicher, with the Illinois Geological Survey.

The Jarrel-Ash 1.5 meter Wadsworth Mount Grating Spectrometer housed in the Oklahoma Geological Survey was utilized for quantitative trace element analysis. X-radiograms of 3/8 inch sections of selected core material were obtained by placing 12 inch lengths of core material between a source of X-radiation and a twelve-inch section of emulsion film. The X-radiography unit in the Nuclear Science Building on the

Louisiana State University Campus was utilized for this purpose.

The techniques and procedures employed in this study are discussed in detail in Appendix A.

PETROGRAPHY

Unaltered Chamosite Facies

Even though these deposits are of different ages and occur at different stratigraphic levels, they represent almost identical environments of deposition as suggested by the nature of the deposits in the lentils. The lithology and structure of these facies are identical in every respect, and even the character of the sediments immediately above and below these lentils are typically similar. This is not too unusual, however, because these deposits represent the alternating transgressive and regressive sequences of the same major regressive phase.

The thickness of the chamosite lentils exceeds 15 feet in the gulfward southern portion of some of these lentils but their thicknesses gradually decrease toward the landward flanks until they finally disappear through facies changes. These facies consist predominantly of light to dark green sand-sized chamosite grains with varying amounts of detrital quartz grains and other detrital minerals (e.g., muscovite, feldspar, etc.). Normally these grains are tightly cemented by a microcrystalline siderite cement which ranges in color from clear to reddish brown

to dark brown depending on the degree of oxidation of the siderite. The tightly cemented sections are resistant to mechanical disaggregation as evidenced by the extreme difficulty in drilling these sections. Some sections within the facies are less strongly cemented and are consequently more susceptible to disaggregation because they are more friable. The more tightly cemented grains are also normally less affected by chemical alteration. These deposits have been extensively bored and burrowed by worms and other small benthonic organisms. These bore and burrow holes have been filled by lighter-colored siderite or sideritic muds and this contrast in color commonly gives the deposits a mottled appearance (Plate I). The concentration of these secondary structures ranges from extensive to sporadic, but they are invariably present. These features are commonly more indurated than the enclosing material and weathering or mechanical disaggregation of the exposed surface of these deposits commonly results in the protrusion of these structures as small tubules or nodular objects.

Locally within the chamosite bed the siderite content increases sufficiently to form beds from approximately two inches up to nearly six inches in thickness. These beds are rarely pure siderite and normally contain some chamosite and/or associated detrital mineral grains (e.g., quartz). Normally these siderite beds are composed of the same basic constituents as the bed above and below but with a much higher percentage of siderite cement. In places, however, the beds may

Plate I

SELECTED X-RADIOGRAPHS

A. X-radiograph of a three-inch interval (37.00-37.25 feet) of core H-1 showing extensive worm borings (light areas) in general discordant to sedimentary bedding in clayey material from the upper transition zone to the overlying bed. Borings are filled with less compact silty material.

B. X-radiograph of a three-inch interval (37.75-38.00 feet) of core H-1 showing borings filled with secondary, compact siderite (dark lineations) in sideritic chamosite clay from the upper part of the main bed. Dark, elongated chamosite oolites are seen in the center of the radiograph whereas a rounded oolite (dark) is present near the right edge of the picture three-fourths of the distance from the bottom. Small, concentric oolite located left of center, in lighter area, near top of radiograph, exhibits alternating light and dark shells indicating areas of iron-richer and iron-poorer minerals or alternating zones of oxidized and non-oxidized chamosite.

C. X-radiograph of a seven-inch interval (50.00-50.60 feet) of core H-1 showing transition from extensively bored (light areas) chamositic clays of the lower part of the main bed to more compact clays of the underlying bed with less borings.

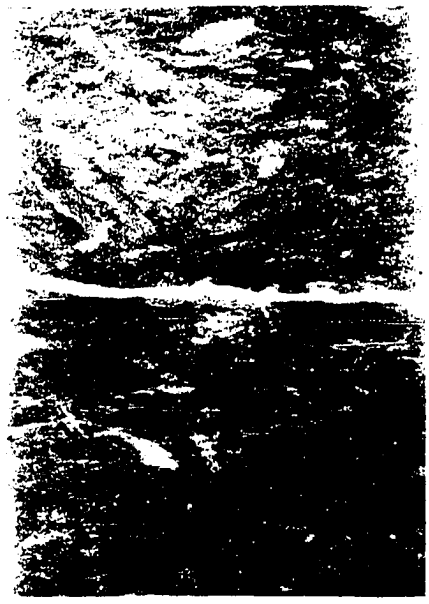

A

B

C

Plate I

be composed almost entirely of microgranular siderite. Siderite beds may occur at any stratigraphic position within the parent facies, but they characteristically occur near the top and bottom of the unit.

The chamosite grains constituting the bulk of these glauconite lentils are all sand-sized but have a variety of shapes. The smaller grains tend to be round whereas the larger grains are commonly elongated. There may be no direct correlation between grain size and vertical position within the bed, but larger grains commonly occur near the top and bottom of the bed whereas smaller grains are normally found near the central portion of the bed. The surfaces of unweathered chamosite grains are normally smooth and shiny in appearance, but the surfaces of weathered grains are chemically etched and pitted, and normally contain a coating of secondary alteration product, a light gray clayey material.

The siderite cement enclosing the constituent grains ranges in form from microgranular, microcrystalline to cryptocrystalline. The grains are normally clear, ranging in color from a slight reddish brown tinge to darker shades of red, depending on the degree of oxidation. In places, the cementing material is white microgranular calcite cement indicating local changes to environmental conditions favorable to the precipitation of calcite.

In many places there are thin intervals of less tightly cemented chamosite which are friable and crumble readily. The

constituents of such intervals are characteristically more altered than those of the tightly cemented material. Any siderite cement present is highly oxidized, and the constituent chamosite grains are highly altered, exhibiting dull gray clayey coatings and pitted surfaces. The presence of a variable, dark gray clayey matrix in portions of these intervals gives them a dull appearance. There seems to be a direct correlation between decreasing siderite cement and increasing clayey matrix material, suggesting that all of the clay is not an in situ alteration product. A white or yellowish, microgranular, clayey material is in places randomly distributed through these intervals giving them a speckled or "salt-and-pepper" appearance. A similar material in the Northampton Iron Ore deposits was identified by Bannister (in Taylor, 1949, p. 36) as consisting of allophane and halloysite together with hydrated aluminum sulphates.

Locally, the occurrence of high concentrations of light green chamositic mud matrix causes a marked change in the appearance of the parent bed. These intervals are characteristically extensively bored and burrowed and commonly contain random light gray sideritic clay stringers. The bore holes and burrows have subsequently been filled with light to dark gray siderite and this contrast in colors gives this interval a mottled appearance. The high siderite cement content normally present in tightly cemented zones decreases in these sections with a resulting increase in chamositic and sideritic muds and detrital

quartz sand grains. These changes indicate a shallowing of the depositional environment. In these less tightly cemented zones, the siderite cement and chamosite grains are more oxidized and chemically altered, respectively, than similar constituents in more tightly cemented intervals indicating that this change in environmental conditions included an increase in oxidation potential and chemical reactivity. These intervals may occur anywhere in the bed, but they characteristically occur near the top and bottom when present.

The main body of the chamositic bed characteristically grades vertically in both directions through a thin interval of highly oxidized chamositic siderite into a fine-grained quartz sandstone with a high content of carbonaceous matter. Typically the sandstone is composed predominantly of clear, angular to sub-rounded detrital quartz grains containing variable quantities of muscovite mica, carbonaceous matter, chamosite grains, and light gray sideritic mud. Small- to medium-sized chert pebbles are randomly distributed throughout this clayey sandstone sequence directly overlying the chamosite bed in a core (H-6) from the northern part of the area. The carbonaceous matter is present as fine- to large-sized fibrous particles resembling charcoal and in places as long rod-like bodies resembling carbonized plant twigs. The light gray sideritic mud occurs as randomly dispersed, indurated clay stringers and as a matrix or cementing material for the quartz sand. The lower portion of these

zones, particularly where the chamosite and sideritic mud content is fairly high, is commonly extensively bored and burrowed. However, the chamosite and sideritic clay decrease in a direction away from the chamosite bed, resulting in less clayey, more friable sandstone which does not exhibit the borings and burrows. The presence of fine-grained, angular to sub-rounded quartz sand; fine, clayey mud matrix; and persistent, fragile carbonaceous matter in these sands point to a low energy reducing environment.

The gradation of siderite-chamosite deposits into similar clayey sandstone units above and below the main bed probably represents a gradual fluctuation in environmental conditions from a quiet, back-swamp or lagoonal environment to a near-shore, shallow marine environment followed by a return to conditions similar to those prior to the deposition of the chamosite.

Altered Chamosite Facies

Once exposed to surface or near-surface conditions, chemically reactive waters attack the chamosite and siderite, oxidizing and leaching their iron content, and concentrating the iron as geothite in veins or ledges within an associated clayey matrix produced by decomposition and leaching of the iron-bearing silicate minerals. The nature of the weathered parent material is dependent upon the extent of leaching of the iron-bearing minerals and the nature and percentage

of other minerals originally present. In the case of incomplete leaching, the residue consists of limonite-stained silt or clay sized matrix material containing partially leached chamosite grains and detrital quartz grains. The leached chamosite grains commonly exhibit an outer thin rim of dark brown goethite, but the interior of these grains consists of a yellow, homogeneous, silt-sized material with a clayey consistency. Some of the detrital grains contain a thin coating of clear, glassy-looking silica, diagenetically produced by concentration of the silica released upon decomposition of the iron-bearing silicate minerals. Where leaching and segregation of the iron content have gone to completion, the end product is a light tan to gray clay or silt with some ghosts of relict chamosite grains and a variable content of detrital quartz grains. In places, oxidation proceeded without subsequent migration of the iron into veins or ledges. In such situations the end product is a dull brown, massive, homogeneous ironstone with only incipient vein development, if present at all.

Goethite veins and ledges assume horizontal, concentric or boxwork patterns, or a combination of these, depending on the control exerted on mineralizing surface waters by the permeability of the parent bed during weathering (Plates II and III). In most instances the concentration of goethite as horizontal ledges seems to be the result of higher permeability along bedding planes within the parent bed or along its upper or lower contacts (Plate IIA) allowing the

Plate II

SELECTED PHOTOGRAPHS

A. Road metal quarry near center sec. 9, T19N, R6W, 2 miles east of Athens showing a thick, continuous, horizontal limonite ledge near the top of the brown ore bed (Figure 14, Durham, 1964). Artificial terraces controlling field erosion by forming breaks in slope similar to that formed by the limonite ledge can be seen on hillside behind quarry.

B. Remnant of once continuous brown ore bed in quarry in north part of area A, Kilpatrick district showing thin, horizontal veins and ledges in thick massive parent bed (Figure 9, Durham, 1964).

A

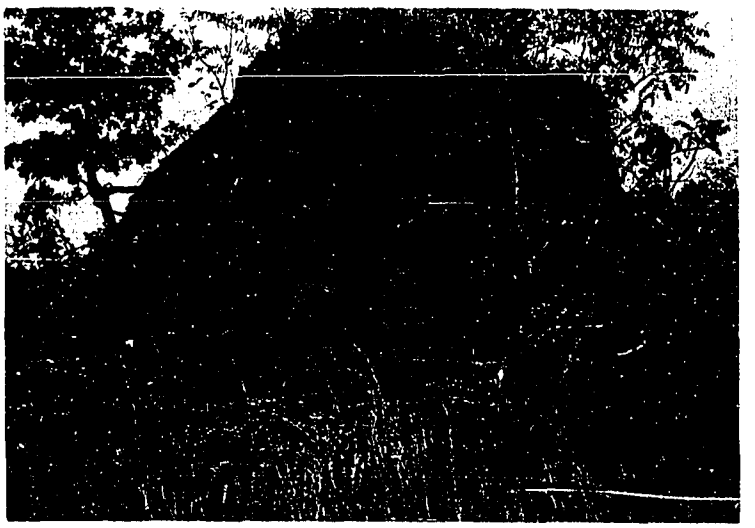

B

Plate II

Plate III

SELECTED PHOTOGRAPHS

A. "Residual boulder of green ore, in area D, Kilpatrick district, showing gradational development of exfoliation 'shells' during process of alteration to brown ore. Only the non-layered core is still green," (Figure 7, Durham, 1964, p. 34).

B. North quarry face in area D, Kilpatrick district showing boxwork and concentric patterns of iron ore development resulting from completion of the exfoliation process (Figure 8, Durham, 1964). Altered residual boulder is seen at upper right.

A

B

Plate III

passage of mineralizing waters, but thin horizontal ledges have also been observed in thick homogeneous parent material (Plate IIB). However, ledges occurring at the top or bottom of parent beds are normally thicker and more persistent than horizontal beds within the parent bed itself. The structural form of such thick ledges is quite different from that of thinner ledges. They are normally continuous bodies with horizontal laminations or irregular bodies with crumbly interiors. Boxworks and concentric patterns occur in thick homogeneous parent beds. Concentration of goethite by downward percolating surface waters along fracture or joint patterns or other surface water circulation routes within the parent bed accounts for the boxwork patterns. Concentric or spheroidal patterns (Plate IIIA) are the result of exfoliation weathering of residual blocks of green chamosite ore as discussed by Durham (1964, p. 31-32):

> The veins and ledges frequently have a concentric or shell-like orientation although a smaller boxwork pattern may interupt or complement it. This is due to exfoliation weathering on the surface of residual blocks of green ore (figs. 5-8). Original dimensions of the individual blocks are apparently determined by vertical and horizontal joint systems and range from less than one foot to ten feet (fig. 11). Progressive development of the oxidation shells at the expense of the unaltered blocks produces the spheroidal weathering effect, so that the remaining unaltered green ore may occur in rounded 'boulders' in some cases four or five feet in diameter. Several road metal pits in the region have exposed such boulders. They are particularly well developed within the northernmost quarry in the Kilpatrick district (area D, pl. 9) where quarrying operations have left several of them discarded on the floor of the pit or else still in place in the walls of the pit (figs. 6, 7, 10).

> In other areas, the bed is completely oxidized but the concentric arrangement of the iron ore veins indicates that the oxidation process passed through a similar stage during development of the brown ore (fig. 5).

The veins and ledges constituting the boxworks (Plate IIIB) and concentric patterns and some horizontal ledges are typically thin (1/10 inch to $1\frac{1}{4}$ inches in thickness) bodies which characteristically exhibit a smooth metallic surface. Close observation of these surfaces in many cases reveals the presence of tightly cemented detrital quartz grains and faint outlines of relict chamosite pellets replaced by goethite. Ledges may reach thicknesses in excess of one foot, and the surface form and texture are considerably different from that of the thinner veins and ledges. These ledges may exist as thin, platy subhorizontal layers or they may be more massive with mammillary and botryoidal shapes. "Infrequently, rounded concretions of ore with a cockscomb surface due to an internal radial pattern occur among the thicker ledges" (Durham, 1964, p. 31).

All stages of weathering and segregation, from fresh unaltered green chamosite through oxidized brown glauconite in which only incipient veining is apparent to complete development of goethite veins in a clay matrix, may be observed in present outcrops. Only in the latter instance, however, is high grade ore produced. The extent of oxidation of the parent bed depends on its position in relation to the permanent water table and the amount and type of overburden. Descending,

oxidizing surface water must have free access to the parent bed in order to free the iron, allowing concentration in veins elsewhere. Overlying, permeable beds, like sand, allow free movement of oxidizing water whereas clay retards the movement of water due to its impermeable nature. The present water table normally marks the downward limit of weathering, because free oxygen available for oxidation normally does not extend below the water table. Thus, the weathering zone does not extend deeper than 15 or 20 feet, and closely conforms to the present topography which suggests that alteration occurred during or after establishment of the present topography.

MINERALOGY

General

Unweathered Parent Bed

The fresh parent ore bed consists essentially of green or gray-green chamosite oolites and pellets in a matrix of clear or pale yellow microcrystalline siderite or less commonly in a matrix of green chamositic mud. In places oolites predominate and are separated only by thin siderite or chamosite cement and in other instances less abundant oolites are scattered through a matrix of siderite or of chamositic mud. Averaged point counts of the constituent minerals in selected size fractions yield 53 percent siderite, 42 percent chamosite, with the remaining 5 percent composed of detrital quartz, feldspar, mica, and other minor accessory minerals. Typical chamosite oolites with the pronounced concentric or onion-ring structure are present in these deposits, but they are normally associated with pellet-like grains and rounded clay-like bodies which may or may not have been oolites prior to diagenesis. In general, variation in the nature of the oolites is irregular and sporadic, typically resulting in mixed assemblages of oolites. Kaolinite is widespread and occurs both as randomly distributed

fine grains and as fine mosaic-like masses of crystals in chamositic oolites and mud matrix. Illite is rarely present in the main bed but it commonly occurs in the transition zones. Minor quantities of a 14 Å clay mineral with an expandable structure occurs in some places in the main bed and more commonly in the transition zones.

Fine-grained clear or cloudy siderite with subordinate calcite forms the dominant matrix material for these rocks. Locally, chamositic mud or calcite is the dominant matrix material. Siderite is also present as granular masses and secondary spherulites in chamositic muds. It is also an active replacement mineral and commonly replaces chamosite, detrital quartz, and organic matter.

Limonite and/or goethite is a common constituent of these ores, occurring as rinds around oolites, as amorphous stains or coatings, or as finely divided crystals.

Detrital quartz is a prominent constituent of these deposits, but it normally constitutes less than 5 percent by weight of the total rock sample.

Microcline, orthoclase, and plagioclase (?) feldspar grains are characteristically present in subordinate quantities. Detrital muscovite mica is widespread in these rocks, but it is never abundantly present except in the transition zones. Minor accessory minerals in these deposits include detrital grains of rutile, zircon, tourmaline and garnet. The organic remains of plant material are present in

places, but for the most part they have been subsequently replaced by siderite which in turn has commonly been oxidized to a high birefringent reddish brown material.

Pyrite is widely distributed, but it is normally not abundant. Mainly it occurs in granular aggregates widely distributed in the groundmass, but locally it partially or even completely replaces chamosite oolites, matrix, and organic material. Magnetite is rarely present in these rocks and when present it exists as small, randomly distributed granules in matrix.

Collophanite is present in limited quantities in these deposits and local increases in its abundance are normally associated with an increase in calcite. Some of the phosphorous occurring in these deposits may be present in allophane (?) which is widely distributed.

The Weathered Rocks

Weathering processes associated with the present land surface have resulted in definite changes in the mineralogy of the original parent bed. Although weathering for the most part is related to present topography, evidence from deep-seated cores indicates that at least part of the weathering predates that associated with the present topography.

The mineral changes are similar to those described by Taylor

(1949) from the Northampton Sand Ironstone Formation of England. In some instances alteration of the original iron-bearing minerals takes place without subsequent redistribution of secondary iron but in others the iron has been leached from the parent minerals and redistributed within the altered parent bed.

Mineralogy of the Unweathered Parent Bed

Minerals of the Oolites

The oolites occur in a variety of sizes and shapes. In size they range from 0.2 mm up to 0.5 mm, averaging 0.3 mm, and in shape they range from spheroidal, ellipsoidal, elongated to vermicular. A mixture of these morphological types is typical of these deposits (Plate IVA). In general, the different morphological types appear to reflect different modes of origin rather than subsequent changes in shape after genesis.

Spheroidal and ellipsoidal oolites normally have a pronounced concentric, or onion-ring structure resulting from the growth of fine-grained chamosite or clay flakes around a detrital nucleus (e.g., quartz, feldspar, limonite) (Plate IVB). This arrangement of finely crystalline material tangentially to a succession of spheroidal or ellipsoidal growth surfaces results in the direction of the slow ray being tangent to the oolite. Many such oolites exhibit a well-marked extinction cross under crossed nichols (Plate IVC). The aggregate birefringence

Plate IV

SELECTED PHOTOMICROGRAPHS

A. Various forms of chamosite grains in fine-grained siderite cement. Shapes range from spheroidal, ellipsoidal, elongated, to vermicular. Thin section H-19-32. Plain light (X12½).

B. Chamosite oolite in center of picture showing concentric structure resulting from growth of fine-grained chamosite around a detrital quartz nucleus. Thin section H-21-37. Plain light (X50).

C. Chamosite oolite in center of picture exhibiting a well-marked extinction cross under crossed nichols. Thin section H-21-36. Crossed nichols (X12½).

D. Chamosite oolite just above center with concentric structure exhibiting alternating shells of lighter and darker chamosite, reflecting changes in physico-chemical conditions during growth. Concentric chamosite oolite to right of center has round limonite core. Thin section H-1-9. Plain light (X50).

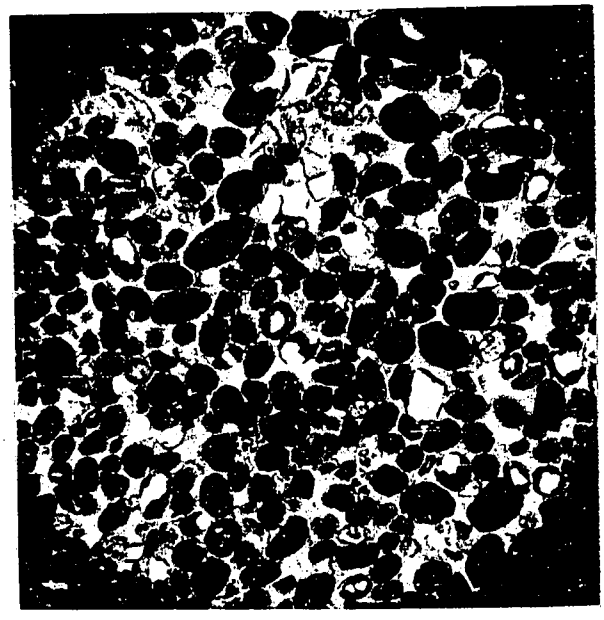

A

B

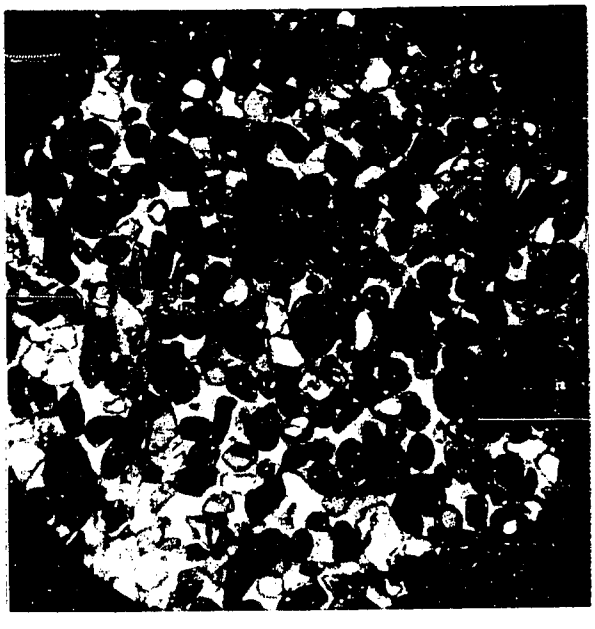

C

D

Plate IV

Plate V

SELECTED PHOTOMICROGRAPHS

A. Concentric chamosite oolite in center of picture with an oxidized, rounded portion of an older chamosite crystal. Siderite is replacing quartz grains randomly scattered in field of view. Chamosite replacing quartz grain to upper left of center. Thin section H-21-36. Plain light (X50).

B. Ellipsoidal pellet-like grains having no concentric structure. Grains consist of chamosite (green), intimately mixed quartz (larger light-colored grains), kaolinite flakes (small light-colored flakes), and other mineral inclusions. In center of picture quartz grain is partially replaced by siderite releasing silica which migrated outward and recrystallized to form an outer rim of chalcedony. Thin section H-21-37. Crossed nichols (X50).

C. Rounded bodies of yellowish green chamositic mud similar in size and form to true oolites but are thought to be rolled fragments of chamositic mud ("False oolites"). Grain in extreme right of center merges imperceptibly into mud matrix. Several "oolites" are replaced by siderite. Thin section H-1-6. Crossed nichols (X50).

D. Large vermicular chamosite grain in center of picture exhibiting alternating light and dark green stringers of chamosite. Bent tabular crystal immediately below left boundary of vermicular grains consists of colorless kaolinite plates alternating with thin, yellowish green chamositic mud. Oxidized siderite spherulites are randomly dispersed in chamositic mud matrix. Thin section H-1-1. Crossed nichols (X50).

A

B

C

D

Plate V

Plate VI

SELECTED PHOTOMICROGRAPHS

A. Slightly rounded microcline grain in center of photomicrograph is replaced along twinning and cleavage planes by chamosite. Thin section H-1-5. Crossed nichols (X50).

B. Quartz grain to right of center is replaced around the outer extremities and along fracture planes by chamosite. Ellipsoidal pellet-like chamosite oolite to extreme left of center containing quartz grains and kaolinite flakes. Thin section H-1-15. Plain light (X50).

C. Siderite spherulites in chamositic muds, in places coalescing, produced by recrystallization of siderite originally disseminated through the chamosite muds. Many spherulites have silt particles which were apparently in their path as they grew. Thin section H-1-2. Plain light (X50).

D. Slightly oxidized and in places replaced chamosite oolites in matrix of light yellow calcite. Secondary calcite growth perpendicular to the exterior surfaces of the enclosed grains gives the groundmass a radial appearance. Many of the quartz grains were partially replaced by siderite before deposition of the calcite. Thin section H-11-30. Crossed nichols (X12$\frac{1}{2}$).

A

B

C

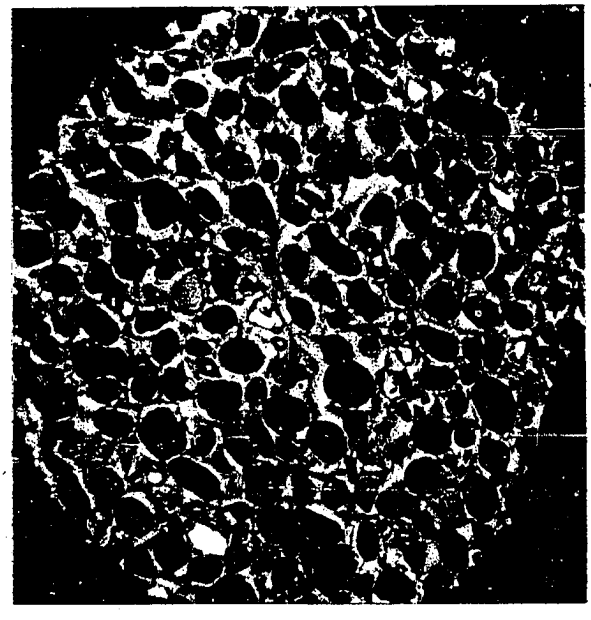

D

Plate VI

Plate VII

SELECTED PHOTOMICROGRAPHS

A. Quartz grain, partially enclosed by chamosite, to upper right of center contains barely visible, long tourmaline or rutile needles. Other quartz grains (light colored grains) contain small, rounded inclusions exhibiting third- or fourth-order green and red interference colors. Thin section H-1-15. Crossed nichols (X50).

B. Quartz grain in near center of photomicrograph is replaced by coarsely crystalline siderite. Isolated remnants of the original intact quartz grain (white color) are surrounded by light yellow siderite. Thin section H-21-37. Crossed nichols (X50).

C. Detrital chalcedony grain in center of field of view showing distinct radial aggregate structure between crossed nichols. Thin section H-21-38. Crossed nichols (X50).

D. Fibrous organic matter replaced in part by pyrite (black) and siderite (dark brown). The siderite has been subsequently oxidized. Thin section H-11-27. Plain light (X12$\frac{1}{2}$).

A

B

C

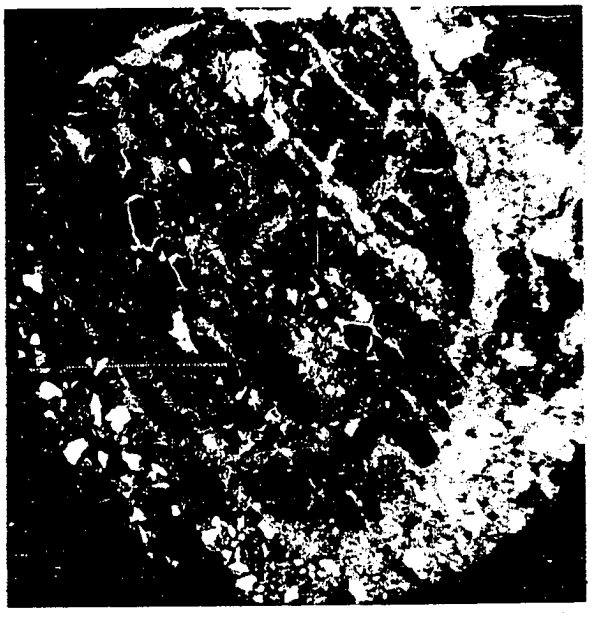

D

Plate VII

of most such oolites is normally low.

Oolites with concentric structure commonly exhibit alternating shells of green and brown material, reflecting changes in physico-chemical conditions during growth (Plate IVD). Sporadic increases in the oxidation potential of the depositional environment result in oxidation of the outer extremities of the growing chamosite grain. Subsequent return to reducing conditions proceed with growth of another green shell of chamosite. Some oolites show up to three or four stages of chamositization.

Oolites commonly have a central core of material showing no concentric structure. This core may be a portion of a chamosite crystal or structureless green chamositic mud (Plate VA). Taylor (1949) reported similar oolites from the Northampton Sand Ironstone Formation of Britain. The coarser crystalline material of the core is normally oxidized to a brownish or yellowish color, reflecting two contrasting environments of formation. This core is surrounded by concentric growth rings of green chamosite indicating that the fragment suffered partial oxidation prior to its incorporation in the oolites. Some oolites contain either an angular or rounded core of limonite (Plate IVD). Other oolites contain oxidized cores of structureless chamositic mud. These cores may be rounded but some are also angular. Some detrital grains have only a thin outer rind of light green chamosite or chamositic mud. Other types of foreign bodies may also serve as nuclei

for some oolites (e.g., coarsely crystalline siderite, zircon crystals, feldspar crystals, apatite crystals, or a portion of an earlier oolite).

Ellipsoidal pellet-like grains are commonly intimately mixed with the true oolites or may locally be the predominant oolite present (Plate VB). These are similar to mineralized faecal pellets described by Porrenga (1965) which are now being formed in recent sediments of the Niger and Orinoco deltas. These pellets do not have a concentric structure, and characteristically they consist of chamosite intimately mixed with quartz, kaolinite, and other mineral inclusions. According to Porrenga, animals feeding on bottom sediments consume detrital mineral fragments and produce faecal pellets composed of an intimate mixture of organic and inorganic material. He advocates that synsedimentary or early diagenetic mineralization of these faecal pellets produces poorly ordered authigenic chamosite. The iron content would increase during diagenesis. Kaolinite may be quite abundant in some of these pellets. Kaolinite may exist as small colorless flakes or as mosaic-like masses of grains forming good rouleaux (Plate VB).

Rounded bodies of yellowish green chamositic mud or light green cryptocrystalline clay similar in size and form to true oolites locally form the dominant oolite type or are intimately mixed with oolites and pellets (Plate VC). These are the "false oolites" of Cayeux (1922) referred to by Taylor (1949) in his discussion of the Northampton Sand Ironstone Formation. This type is closely associated

with a chamositic mud matrix, and the "oolites" commonly merge imperceptibly into the matrix (Plate VC). Many such occurrences appear to be associated with local reworked zones in which the oolites are preferentially oriented along the sides of many burrows. Extensive replacement of such "oolites" by siderite is commonly observed (Plate VC). Most of the "false oolites" are thought to be rolled fragments of chamositic mud, but those composed of light green cryptocrystalline clay commonly show a radial growth structure. A thin outer shell of light green mud may form around some grains of yellowish green chamosite. Some of the "rolled oolites" exhibit a flattened, distorted form.

Vermicular chamosite grains are in places associated with the other types (Plate VD). Alternating light and dark stringers of chamosite or chamositic mud, commonly crisscrossing, constitute these tabular grains. Many of these grains have discontinuous inclusions of colorless chamosite (?) alternating with light green cryptocrystalline chamosite. This effect gives the vermicular crystals a kind of "hourglass" structure. This particular type resembles in appearance vermicular chlorotoid grains, but the optical properties are more similar to those of chamosite, and X-ray diffractograms of these samples do not reveal the presence of chlorotoid. Other grains exhibiting a vermicular form consist of bent, colorless kaolinite plates alternating with thin, yellowish green, chamositic mud (Plate VD).

Chamosite occurs in colors from dark green, light green, yellowish green to reddish brown, depending upon the degree of oxidation. Many oolites exhibit yellow, yellow brown, or even reddish brown tints, apparently due to partial oxidation of the chamosite. The optical properties are variable for the different types discussed but optical properties also commonly vary within any one type. Some exhibit weak birefringence whereas others are almost isotropic. Pleochroism in some of the oolites is similar to that described by Taylor (1949) for oolites in the Northampton ores (i.e., green or yellow green for rays vibrating at right angles to the cleavage, deep olive green for rays vibrating parallel to it). The refractive index appears to increase with increase in depth of color as suggested by Taylor but normally ranges between 1.61 and 1.65. As with Taylor's Northampton ores (1949, p. 18), "It appears possible that the depth of colour and variation in optical properties of the material composing the ooliths are in part determined by the percentage of clay associated with the chamosite."

Chamosite is normally without doubt the dominant mineral present in "oolites", no matter what type, but, as pointed out before, kaolinite occurs both as fine grains and as mosaic-like masses of crystals in the pellets and "false oolites." Kaolinite is normally not readily discernible under a microscope in oolites with a marked concentric structure, but X-ray diffractograms of the clay residue

left after removal of the chamosite with warm 10 percent HCl invariably reveal the presence of kaolinite. Chemical analysis of the clay-sized fraction separated from these samples yield compositions which are not typical for chamosite but suggest a mixture of chamosite and kaolinite. The relative proportion of kaolinite in the oolites is variable, but in general it increases in oolites near the lower and upper transition zones. In the transition zones the oolites and matrix may be predominantly kaolinite.

Chamosite is an active replacement mineral and some of the chamosite grains are secondary. Orthoclase, microcline and perthite are readily etched and replaced by chamosite (Plate VIA). Replacement normally starts around the outer extremity of the grain but proceeds more rapidly along twinning and cleavage planes which form zones of weakness within the feldspar structure. All stages of alteration were observed. In some instances, only the outer surfaces had been altered, in others only along selected cleavage or twinning planes, and in others only isolated remnants suggest the original identity of the grain. When completely replaced by chamosite, the relict structure of the original feldspar crystal is commonly indicated by the retention of the wavey extinction characteristic of the original twinning. The feldspar crystals commonly have undergone some rounding prior to diagenetic alteration. The replacement of detrital quartz by chamosite is much more difficult to explain in terms of structural change, yet

this phenomenon occurs extensively in these deposits (Plate VIB). Replacement occurs at abraded edges and proceeds readily along fracture zones and other planes of weakness (e.g., along planes of inclusions). Partially replaced grains commonly exhibit crisscrossing stringers of chamosite which isolate patches of quartz. All stages of replacement, from partial to nearly complete, have been observed.

In some oolites, the central detrital nucleus has been partially replaced by siderite prior to incorporation of the grain in the oolite. Others may include one or more concentric zones of siderite, either as a replacement phenomenon or as direct crystallization about the then existing surface. In either case, the presence of siderite marks a temporary change in physico-chemical conditions favorable to precipitation of siderite rather than chamosite. As suggested by Taylor (1949), this might be due to an increased supply of carbon dioxide which would either result in carbonation of the outer skin of the oolite or in direct precipitation of siderite in place of chamosite. Some oolites have a thin outer shell of siderite which commonly has been oxidized to form a reddish brown outer rim. Some oolites have been extensively or even completely replaced by siderite (Plate VC). Other oolites have irregular cores of coarsely granular siderite which is probably related to an earlier replacement phenomenon. It is difficult to determine how many oolites have been completely replaced by siderite because once replaced all trace of the concentric structure is lost. The siderite

associated with the oolites is always more coarsely crystalline than that of the groundmass, and it is normally yellow whereas that of the groundmass is normally colorless or light gray.

Some oolites contain limonite cores and some oolites are partially oxidized, but no oolites consisting wholly of limonite like those described by Taylor for the Northampton ores were observed in these deposits. Some oolites have one or more concentric zones of limonite alternating with green chamosite.

Taylor (1949) reported fine granules of magnetite in some chamosite oolites of the Northampton Sand Ironstone, but similar occurrences of magnetite were not observed in these ores. Fine granules of magnetite are, however, found in the groundmass in some places.

Minerals of the Groundmass

Siderite occurs extensively throughout these deposits and is the predominant mineral constituting the groundmass. It is also present as granular aggregates and spherulites in chamositic muds.

In general, the siderite of the groundmass is extremely fine-grained and is either colorless or pale yellow in color. The textural relationships of the matrix to the constituent chamosite grains indicate that it is syndepositional. Primary siderite commonly displays prominent rhombohedral cleavage planes.

Secondary replacement siderite locally forms all or a major

portion of the groundmass. It is more coarsely crystalline than primary siderite and it is normally pale yellow rather than colorless. Paritally replaced grains or relict outlines of completely replaced grains are distinguishable in much of the coarsely crystalline matrix. The secondary replacement siderite is commonly optically continuous with the colorless primary siderite in the groundmass and the secondary siderite of the partially replaced grains. This probably means that the replacement siderite postdates the deposition of the groundmass because the secondary siderite would tend to crystallize in continuity with the primary siderite.

Where siderite occurs in the form of spherulites in chamositic muds, they are normally small but they coalesce in places to form local siderite sheets (Plate VIC). The spherulites appear to be secondary minerals produced by recrystallization of siderite originally disseminated through the chamosite muds. Siderite in the spherulites is present either as finely fibrous crystals or sector-like crystals radially arranged. The siderite is commonly colorless or light yellow, but roughly concentric zones within the spherulites are commonly defined by being colored in various shades of brown. Other spherulites have been strongly oxidized and are now dark brown (Plate VD). As pointed out by Williams, Turner and Gilbert (1954), some have nuclei of silt particles which were apparently in their path as they grew, and the fine clay particles in the matrix appear to have been pushed aside

and crudely oriented by growth of many of the spherulites.

X-ray diffractograms of siderite magnetically separated from the deposits yield peaks characteristic of typical siderite (Figure 5). Differential thermal analysis curves of this material are also typical of siderite (Figure 5). They show a strong endothermic peak at approximately 525°C followed by a strong exothermic peak around 550°C, and a minor exothermic peak at approximately 810°C. Although the endothermic peak and the first exothermic peak are due to the decomposition of the mineral and oxidation of the FeO produced, respectively, the minor exothermic reaction is most probably due to a change in iron types. Effluent gas analysis curves show a strong peak around 525°C corresponding to the release of CO_2 during decomposition of the mineral (Figure 5). Analysis of the gas liberated at this temperature by gas chromatography yielded CO_2.

Chamosite mud is a common constituent of the groundmass, even though it is subordinate to siderite and its occurrence seems to be rather restricted in extent. In some instances, the mud matrix predominates with only scant ooliths and minor quantities of siderite randomly dispersed throughout. In many places, however, these muds contain considerable quantities of recrystallized siderite in the form of spherulites. In some places, numerous light green, rounded clay oolites are set in a subordinate matrix of light green chamositic mud. These oolites appear flattened and commonly merge imperceptibly into the mud

H-1-7 Magnetically Separated Siderite

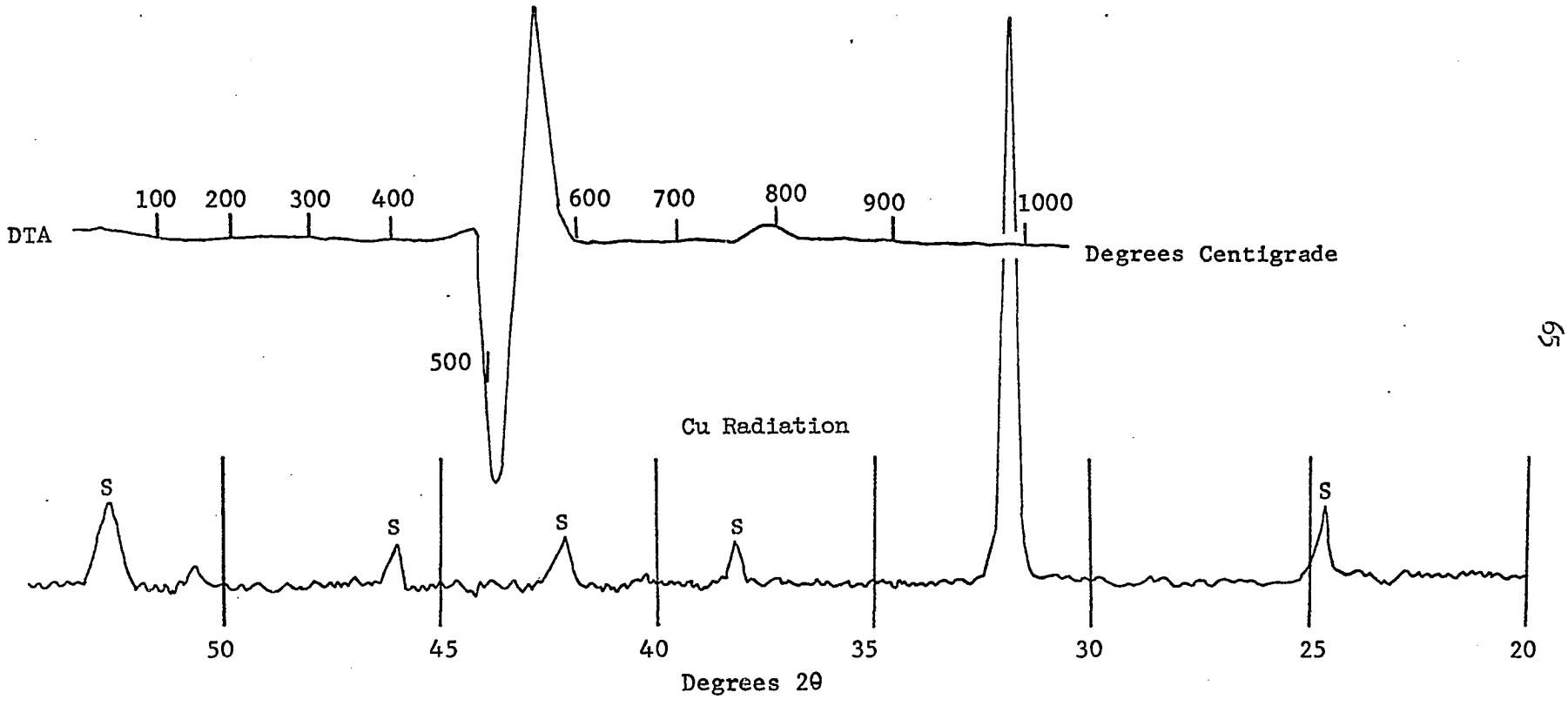

Figure 5. DTA diagram and randomly oriented X-ray diffractogram of siderite.

matrix. The mud and its constituents commonly have been extensively reworked and replaced by siderite. Siderite stringers transverse many of these zones and replace everything in their path.

Kaolinite is invariably present in these muds. It may be present as mosaic-like masses of kaolinite crystals or as bent kaolinite flakes interlayered with chamosite. In some places it is too finely divided to be distinguished under a microscope, but analyses by X-ray diffraction reveal the presence of at least some kaolinite. The chamositic mud content increases considerably toward the transition zones, and the relative proportion of kaolinite in these muds increases.

A minor quantity of calcite is closely associated with the granular siderite in the groundmass of these deposits. It is normally finely granular like the siderite matrix; consequently, it is only distinguishable from the siderite in X-ray diffractograms and DTA patterns. Calcite of organic origin was not detected in these rocks. Locally and rarely, calcite enrichment results in calcite becoming the dominant matrix material (Plate VID). In such occurrences, oolites and partially replaced detrital quartz are set in a matrix of recrystallized calcite. Calcite crystal growth proceeds perpendicular to the exterior surfaces of enclosed constituent minerals giving the groundmass a radial appearance. Many of the quartz grains seem to have been partially replaced by siderite prior to deposition of the calcite, and many of the oolites appear to be more oxidized than usual. This type of

occurrence is rare and then it is restricted to thin layers or to small rounded or nodular bodies.

X-ray diffractograms of samples containing such high quantities of calcite yield peaks typical of calcite (Figure 6). Differential thermal analysis curves are also typical for calcite. They show a strong endothermic peak at approximately 800°C which corresponds to decomposition of the mineral. Effluent gas analysis curves show a strong peak at approximately 800°C corresponding to release of CO_2 during breakup of the calcite structure (Figure 6). Analysis of the gas liberated at this temperature yielded CO_2.

Other Constituents

Of the remaining constituents, quartz is the most abundant. The relative quantity of quartz grains varies in most of the thin sections examined, but it is invariably present, either as separate grains and/or as nuclei of chamosite grains, and constitutes an average of 5 percent of the total mineralogical assemblage. Quartz is commonly present in quantities less than one percent but may constitute as much as 25 percent of the total sample. The relative quartz content characteristically increases toward the transition zones and the landward flanks of the lentils, but it may also increase locally. When present in abnormally high quantities, it drastically reduces the iron content by reducing the proportions of siderite and chamosite present.

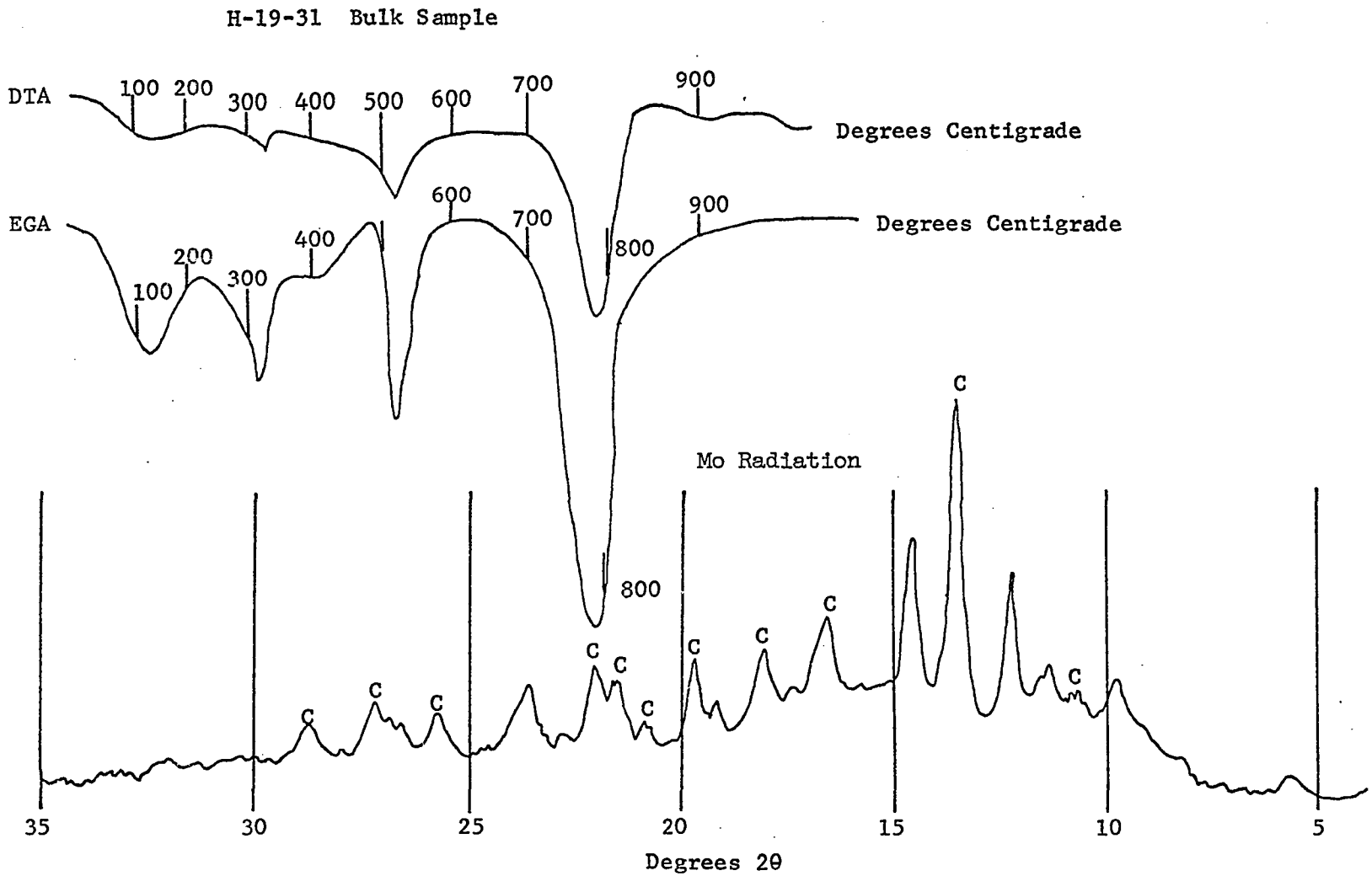

Figure 6. DTA and EGA diagrams and randomly oriented X-ray diffractogram depicting the presence of calcite.

Characteristically, the quartz grains are subangular to subrounded particles ranging in size from very fine to medium sand. Practically all of the quartz grains contain idiomorphic crystalline inclusions in varying amounts. Rutile and tourmaline needles are rarely present (Plate VIIA), but the majority of the microlites are small, rounded inclusions exhibiting third- or fourth-order green and red interference colors, characteristic of carbonates. The latter inclusions may be randomly distributed, but they also form intersecting chains or planes of inclusions.

In these slides extinction types range from straight to "slightly undulose" to "strongly undulose", according to Folk's classification of reworked sedimentary quartz (1959). Some grains exhibit semi-composite extinction, but this is rare. Quartz grains with straight to slightly undulose extinction represent the majority of grains present.

Quartz overgrowths were not observed in these slides, but this does not preclude the possibility that they were at one time present because the outer rims of most grains have been severely etched and replaced by either siderite or chamosite.

The outer rims of most quartz grains have been etched and replaced by siderite and all or a major portion of many grains have been replaced by this mineral. This process of replacement starts along the outer extremities of the grain and then proceeds along fracture

planes or other zones of weakness in the mineral structure (Plate VIIB). The relict outline of many of the original grains is all that remains to suggest its former identity. Some silica released during replacement of quartz by siderite migrates outward and precipitates to form an outer rim of chalcedony (Plate VIIB). Other quartz grains have larger outer rims of chalcedony with little or no associated replacement siderite.

A few detrital chalcedony grains were observed in these thin sections (Plate VIIC), but most of the chalcedony is present either as an authigenic and/or secondary diagenetic mineral. Between crossed nichols these detrital grains show a distinctive radial aggregate structure. In these radial groups the small crystals converge toward the center of the individual particle, and this radial uniformity of orientation produces, with crossed nichols, a dark cross parallel to the positions of extinction. The outer margins of such grains are normally embayed by chamosite or they may be etched and replaced by siderite.

Feldspar grains constitute less than one percent of the total mineralogical assemblage, but they are present in varying amounts in almost every thin section studied. Microcline and orthoclase are the most prominent feldspars present, but perthite is also present. Unweathered microcline has the so-called "gridiron" or "quadrille" structure, with two sets of lamellae at right angles. The twin

lamellae are normally spindle shaped and the extinction wavy. It is extremely difficult to distinguish most orthoclase grains from quartz because the orthoclase grains are untwinned. Tabular feldspar grains exhibiting good cleavage are readily identifiable but identification of less distinctive grains must be made by comparison of the refractive indices, that for orthoclase being less than that of Canada balsam and quartz. Many of the orthoclase grains appear cloudy due to incipient alteration in contrast with quartz which is normally clear. Plagioclase is rare or absent in these thin sections.

No well-rounded feldspar grains were observed; most are subangular to subrounded. Some grains in a few samples are even subangular to angular. It is frequently difficult to determine the original shape and surface texture of the feldspar grains because the exteriors of most grains have been severely etched and frequently replaced by chamosite or siderite. Orthoclase forms the nucleus for some chamosite grains.

Muscovite was the only detrital mica observed in these deposits. It is widespread, but it is never abundantly present, except in the transition zones. There it may form a major part of the mineral assemblage. Normally it occurs in long, thin, tabular crystals, and it is colorless to pale green in thin section. It is readily recognizable due to its strong birefringence; it normally exhibits interference colors of the upper second order.

Collophanite is present in limited quantities in these deposits. A marked increase of phosphorous in samples containing an abnormally high calcite content is explained by an increase in collophanite in the form of rounded grains. These grains are commonly colorless but may be snow white. They are normally isotropic and exhibit moderate relief, refractive index greater than balsam. Preliminary petrographic examination and chemical analysis of samples of surface or near-surface green ore by the U.S. Bureau of Mines also indicated that collophanite was the principal phosphorous-bearing mineral in the green ore (Durham, 1964, p. 52).

Quantitatively the percentage of phosphate-bearing minerals in these rocks is relatively insignificant compared to the other constituents, but the relative percentage of phosphorous in these deposits would be significant in terms of potential economic value. "The phosphorous content, and its possible use as a byproduct, is a factor in the selection of a processing technique designed for this ore," (Durham, 1964, p. 51).

Pyrite is widely distributed, but it is normally not abundant. Mainly it occurs in granular aggregates widely distributed in the groundmass, but locally it partially or completely replaces chamosite oolites, matrix material, and organic matter (Plate VIID). All X-ray analyses of samples containing an unusually high sulfur content show pyrite to be present. Differential thermal analysis curves show a

strong endothermic peak around 470°C which corresponds to decomposition of the pyrite crystal structure. Effluent gas analysis patterns also show a strong peak at this temperature, corresponding to the release of sulfur dioxide during collapse of the pyrite structure (Figure 7). Analysis of the gas released at this temperature confirmed that it was SO_2.

Mineralogy of the Weathered Rocks

Minerals of the Altered Oolites and Groundmass

The resulting change in the mineralogy of both the oolites and the groundmass depends on whether the alteration of the iron-bearing minerals was accompanied by subsequent migration of the iron to other areas, and it also depends on the extent of leaching of the original minerals. Infrequently, alteration of the iron-bearing minerals takes place without subsequent redistribution of the iron, but normally the iron has been leached from these minerals and redistributed within the altered parent bed.

In the first case, the chamosite oolites have been altered to or replaced by high birefringent limonite. The presence of high birefringent limonite stain on the constituents of the groundmass makes it extremely difficult to distinguish individual minerals of the groundmass, but it appears that the original siderite cement has been altered directly to limonite retaining the original mineral form. The

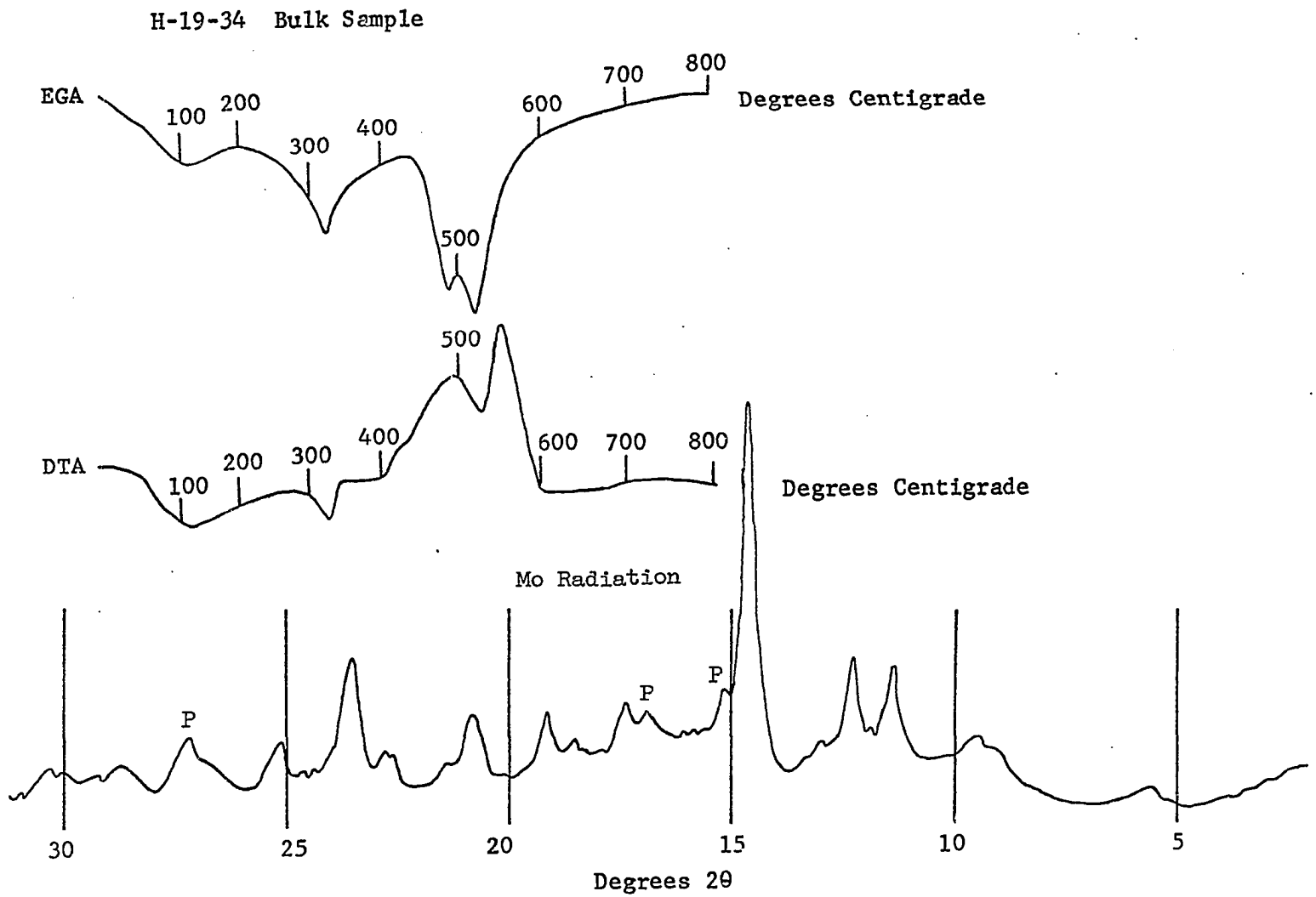

Figure 7. EGA and DTA diagrams and randomly oriented X-ray diffractogram depicting the presence of Pyrite.

spatial relationships of the other constituent minerals to the altered iron minerals also remain essentially the same as those in the original rock, and the non-iron bearing minerals appear to be essentially unaltered.

In the second case, the iron has been either partially or completely leached from all iron-bearing minerals and concentrated along selected planes in the weathered parent bed in the form of veins, box-works, or ledges. Where extensive leaching has occurred, only faint outlines of the original chamosite oolites remain. The residual material of the original oolite is a light tan to gray clayey material, appearing to consist predominantly of fine-grained kaolinite flakes. Less extensively altered oolites retain the original structure. The partially altered oolite may consist of an exterior shell of pale yellow to brown scaly material surrounding an aggregate of unoriented fibers or granules. Others consist of outer rims of light-colored earthy material with a core of cryptocrystalline aggregates. Still others exhibit an outer, thin rim of dark brown limonite or goethite with an interior consisting of yellow, homogeneous, silt or clay-sized material with a clayey consistency.

Where leaching and segregation of the leached iron have gone to completion, attempts to distinguish between matrix and oolites are no longer feasible. The residual material now consists of light tan to gray clay, or less commonly of yellow or yellow brown birefringent

clayey material, containing relict outlines of chamosite grains and stable residual grains (e.g., quartz, feldspar, muscovite). Some of the detrital grains contain a thin coat of clear, glassy-looking silica resulting from concentration of silica released during decomposition of iron-bearing silicate minerals. Identification of kaolinite and illite in the clayey matrix is not always possible under magnification, but X-ray diffractograms of this material always reveal its presence.

Pyrite originally present in the groundmass is absent. It is readily oxidized and the sulfur released is thought to be redistributed elsewhere, possibly as gypsum because it is found in some parts of the transition zones between the altered and unaltered portion of the parent bed. The calcite normally present as matrix material was also not observed in altered sequences. It possibly went into solution and was redeposited in the transition zones because small stringers and concretions of calcite are commonly found there. Thin ledges of siderite are also found in many parts of the transition zone. This probably represents secondary deposition of iron as siderite in the presence of organic matter because distinct, solid ledges of siderite are not normally found in the unaltered parent bed.

A white, powdery material is commonly observed in the altered clayey matrix material. A similar material was observed by Taylor in the Northampton Sand Ironstone Formation. According to Taylor (1949,

p. 36), "X-ray examination of this by Dr. F. A. Bannister has shown that it is in part amorphous, in part finely crystalline and apparently consists of allophane and halloysite together with hydrated aluminum sulphates to which the names basaluminite and hydrobasaluminite have been given (Bannister and Hollingsworth, 1948)." So far, the writer has not isolated enough of this material to analyze by X-ray diffraction.

Minerals of the Secondary Iron Bodies

These features normally consist of high birefringent limonite or goethite with varying amounts of incorporated chamosite grains and detrital quartz and feldspar. Some of the chamosite oolites have been severely leached of their iron content and others have been altered to or replaced by limonite. Some incorporated chamosite oolites have undergone little alteration.

X-ray analysis of the iron veins give diffractograms characteristic of goethite (Figure 8). Differential thermal analysis of this material shows one strong endothermic peak at approximately 325°C which corresponds to dehydration of the ferrous oxide (Figure 8).

F-50 Selected Goethite Vein

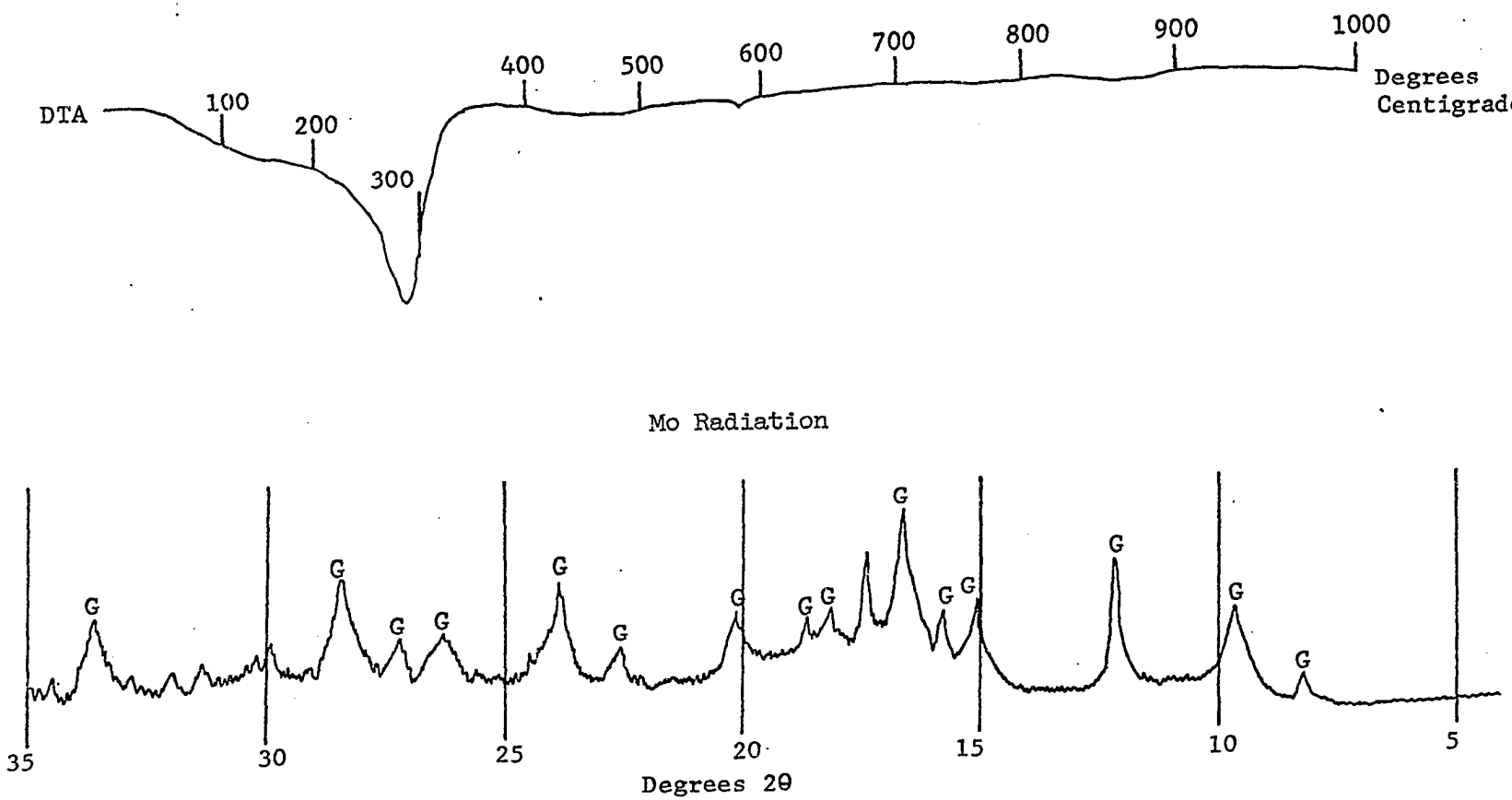

Figure 8. DTA diagram and randomly oriented X-ray diffractogram depicting the presence of goethite.

CLAY MINERALOGY

General

During this investigation studies of 48 samples were conducted by X-ray diffraction methods. Diffractograms were obtained of both the bulk samples and of the clay-sized fractions of size-fractioned samples. Identification of the clay minerals in these samples was based upon X-ray diffraction characteristics of oriented clay aggregates and their response to heat treatment, acid treatment, and solvation with ethylene glycol. Differential thermal analyses, effluent gas analyses, and gas chromatography analyses were also utilized as identification aids.

Three clay minerals, poorly-ordered chamosite, b-axis disordered kaolinite, and dioctahedral illite, were definitely identified in these deposits. Minor quantities of a 14 Å clay mineral with an expandable lattice, possibly nontronite, was also detected. Chamosite and kaolinite are normally the only two clay minerals found in the main body of the bed whereas illite and nontronite (?) are mostly restricted to the transition zones. Chamosite is by far the predominant clay mineral in the main portion of the bed, so much so that sedimented

slides of the clay minerals reveal only the presence of chamosite. Even though the presence of kaolinite is not revealed in such slides, X-ray analysis of the residue of the acid-treated samples nearly always reveals its presence. Powder patterns of samples not treated with acid also commonly show the presence of kaolinite.

Analytical Techniques

Diffractograms of randomly-oriented powder slides and preferentially-oriented slides of clay fractions were obtained by using the Siemens X-ray diffractometer and automatic recorder. Nickel-filtered Cu (K-alpha) and zirconium-filtered Mo (K-alpha) radiation generated at 35 KV and 18 ma was employed. The presence of amorphous iron oxide in untreated samples created extreme difficulty in obtaining diffractograms of either the random powder slides or preferentially oriented slides of clay fractions. For example, when the untreated powder slides were bombarded with characteristic copper radiation, iron fluorescence masked the diffraction peaks of the weaker clay reflections.

Cu K alpha radiation cannot be used with ferrous materials because it will cause fluorescent radiation from the iron in the specimen (Cullity, 1959, p. 166). The characteristic wavelength of Cu K alpha (1.542 Å) is shorter than the K absorption edge of iron (1.743 Å), thus exciting iron fluorescent radiation. In order to prevent this situation the characteristic wavelength used should be

longer than the K absorption edge of the specimen. Characteristic radiations of Co K alpha (1.790 Å), Fe K alpha (1.937 Å), and Cr K alpha (2.291 Å) are all sufficient for analysis of samples similar to these, but the unit available was not equipped with either of these tubes. This problem was somewhat overcome, however, by utilizing Mo K alpha (0.711 Å) radiation. This characteristic wavelength is considerably shorter than the K absorption edge of iron and naturally excites iron fluorescent radiation, but the intensity of the hard, diffracted molybdenum radiation is sufficiently greater than the iron fluorescent radiation, after filtration, to give fairly well-defined diffraction peaks. A zirconium filter (K edge = 0.689 Å) was utilized because it has a greater absorption for the fluorescent Fe K alpha (1.937 Å) radiation contributing to the background than for the Mo K alpha (0.711 Å) radiation forming the diffraction lines. This line of reasoning is in accordance with the general rule which states, "....if it is impossible to use a wavelength longer than the K absorption edge of the specimen, choose one which is considerably shorter and use a proper filter" (Cullity, 1959, p. 167).

Preparation of oriented slides of the clay fractions for X-ray diffraction studies proved to be the most difficult and frustrating part of this study. Initially, the normal procedure of preparing sedimented slides was followed. Bulk samples ground to less than 250 mesh were dispersed in distilled water and further disaggregated and

dispersed by means of an ultrasonic transducer (Powerton Autosonic, Model PA-3001). The less-than-four micron equivalent spherical diameter particles were acquired from the suspension by utilizing the differential settling velocities according to Stokes' law. This suspended material was sedimented on glass slides and then dried in an oven at approximately 55°C. Normally this procedure preferentially aligns the clay fraction and enhances the basal diffraction maxima by orienting the c-crystallographic axis of the clay minerals normal to the slide. However, the presence of amorphous iron oxide coatings in these samples prevented complete dispersion of the layer silicate clays which prevented subsequent parallel orientation and sufficient concentration of these clays for strong diffraction peaks. One broad amorphous-like diffraction peak, covering the entire 2θ span normally occupied by several clay peaks, was obtained from the first sedimented slides X-rayed. Information from these diffractograms made it evident that these clay minerals were either extremely poorly crystalline or that the presence of amorphous iron oxide was causing this anomaly. One of the samples was size-fractioned into 1-1/2, 1/2-1/4, 1/4-1/8, and 1/8-1/16 micron fractions by continuous flow centrifugation using a Lourdes (Model LCA-1) super-centrifuge, and each of these size fractions was X-rayed to see if this phenomenon was characteristic of all clay-size fractions. The same unsatisfactory results were obtained from sedimented slides of each of these size fractions.

At this time it became necessary to determine if iron oxide coatings were responsible for this phenomenon. In the search for a satisfactory method of removing iron oxide coatings and crystals of iron oxides, the writer conducted numerous time-concentration experiments with different weak acids (e.g., acidic, formic). Slight improvement in the random powder patterns was achieved using 10 percent HAc over different time ranges, but totally unsuccessful results were obtained in every case with the sedimented slides of samples so treated.

Subsequently, a search of the literature revealed that numerous techniques have been utilized in the past for removal of amorphous iron oxides with varying degrees of success and failure. In choosing a technique several factors had to be considered. The process should selectively remove oxide coatings without attacking the iron structurally coordinated in the iron-bearing clay minerals present. Further, it should not attack the layer silicate minerals with resulting increase or decrease in cation exchange capacity, and ideally the technique should be fast and free from analytical difficulties. Such a technique was proposed by O. P. Mehra and M. L. Jackson (1960). Their dithionite-citrate-bicarbonate method employs sodium dithionite ($Na_2S_2O_4$) as a reducing agent, sodium bicarbonate as a buffer, and sodium citrate as a chelating or complexing agent for iron. Operation at a neutral pH makes it possible to achieve the prerequisites mentioned above. Sedimented samples treated by this technique gave well-defined diffraction

patterns facilitating identification of the clay minerals. Marked improvement in random powder patterns and DTA curves was also achieved. X-ray diffraction patterns of samples of both the treated and untreated material were obtained for comparison purposes. The analytical procedures for this process are included in Appendix A.

Clay Minerals of the Unaltered Parent Bed

Chamosite

The term chamosite derives its origin from "chamoson," the type locality of the original clay mineral. The clay mineral to which the name chamosite was first given has the 14 Å chlorite structure (Orcel et al, 1949), but other minerals which have subsequently been described as chamosite have the 7 Å kaolin-type structure. Orcel, Henin, and Caillere (1949) introduced the name "berthierine" for the kaolin- or serpentine-type minerals to avoid using one name for two distinct minerals. Nelson and Roy (1958) proposed the name "septachlorite" for the four minerals amesite, chamosite, greenalite, and cronstedtite because they are structurally characterized by serpentine-like layers with $d_{001} \simeq 7$ Å. The usage of the term chamosite for both forms will probably persist, however, because chamosites which occur in extensively widespread sedimentary ironstone deposits are of the 7 Å type and the common usage of the term "chamosite-siderite mudstones" is deeply ingrained.

X-ray diffractograms of oriented clay aggregates invariably yield only two distinguishable peaks, 7.12 Å and 3.56 Å (Figure 9). These are characteristic of the first and second orders of ferrous chamosite. Poorly-ordered chamosites commonly exhibit only the first- and second-order diffraction peaks, and this phenomenon is characteristic of all the chamosites in these deposits. Porrenga (1965) suggests that there is a direct correlation between depth of burial and the degree of ordering in chamosites. He contends that all chamosites of Miocene and younger age are poorly ordered and that chamosites of Mesozoic age and older are more ordered.

Diffraction peaks representing the first and second orders of ferrous chamosite are sharp and well defined for some samples while for others, the peaks are broader and less well defined. The degree of definition and sharpness is probably a function of the stacking arrangements of the layers making up the chamosite unit cell. Brindley (1951) showed that variation of powder diagrams of 7 Å chamosites could be explained by the presence of both orthogonal (with no a-axis layer displacements) and monoclinic (with regular a/3 shifts between all layers) stacking of layers. According to Brown (1961, p. 105), "The number, positions and intensities of the reflections depend on the proportions of the monoclinic and orthogonal forms, on the composition of the mineral, and on the state of oxidation." He suggests that the better ordered chamosites are rich in iron and the less well-ordered

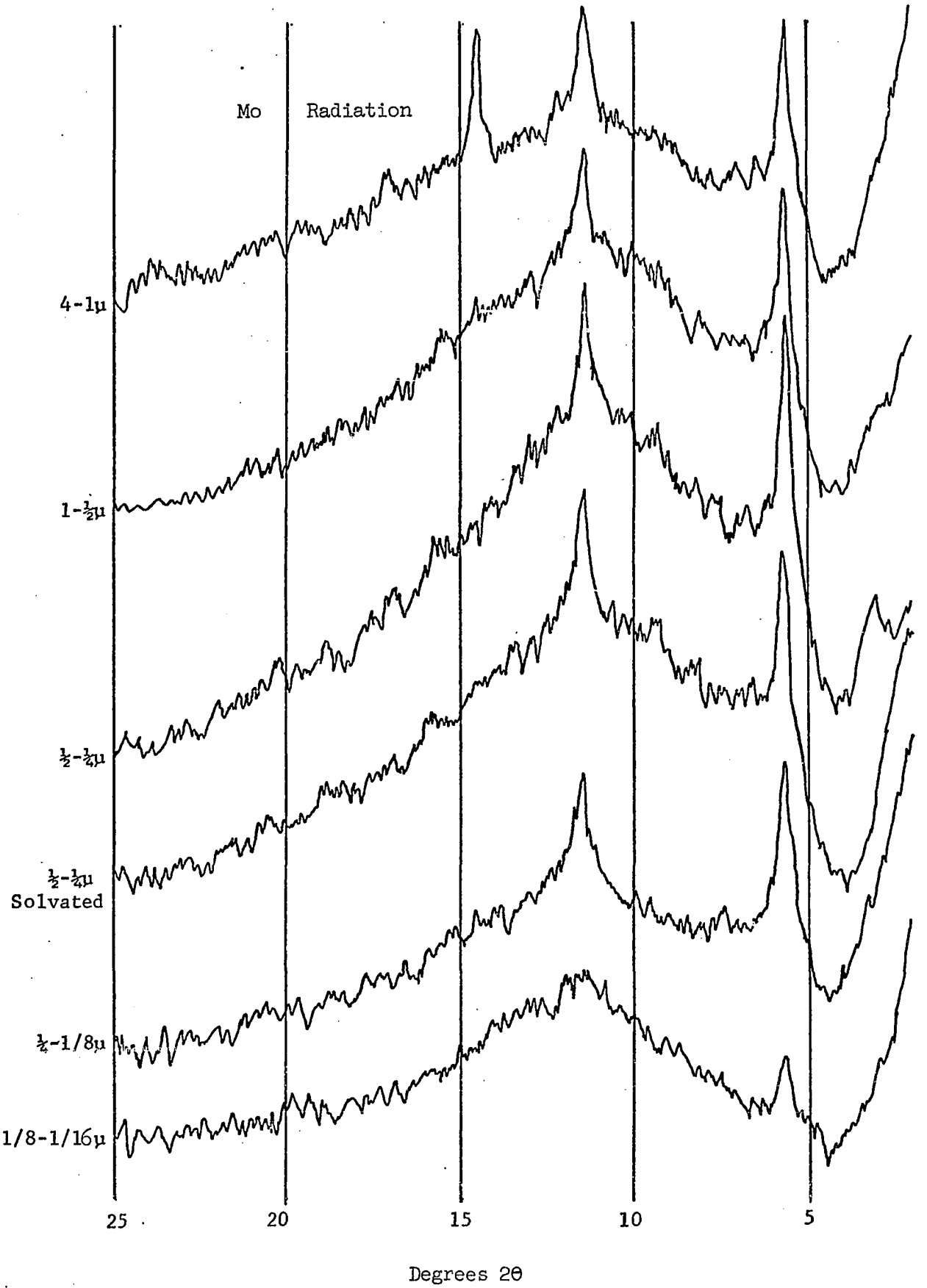

Figure 9. X-ray diffractograms of oriented selected size fractions of Sample H-1-2 showing variation in mineralogy with particle size and effects of glycolation on the $\frac{1}{2}$-$\frac{1}{4}$ micron size fraction

ones contain less iron and more aluminum and that the oxidation increases the disorder.

Two representative samples, one from the main body of the bed (H-1-2) and the other from the transition zone (H-1-1) were size-fractioned into 4-1, 1-1/2, 1/2-1/4, 1/4-1/8, and 1/8-1/16 micron size fractions to see if there was any variation in mineralogy with particle size. Oriented X-ray diffractograms of selected size fractions of sample H-1-2 are shown in Figure 9. The two peaks characteristic of ferrous chamosite are present in each size fraction. In addition, there is a peak at 2.79 Å in the 4-1 micron fraction. This peak is the most intense peak of siderite and shows that fine-grained siderite remains with the less-than-four micron fraction during size fractionation. The chemical determination of an abnormally high CO_2 content in this size fraction confirms this conclusion.

In the 1/2-1/4 micron size fraction, a small peak at 14.3 Å is most probably attributable to the presence of a small quantity of montmorillonite. Upon solvation of this size fraction with ethylene glycol, the peak disappeared. The expansion of montmorillonite upon solvation would ideally result in a peak around 2° 2θ, but its absence there is not too surprising because this is the low-angle, high-scattering region of molybdenum radiation where resolution is extremely low to non-existant. A similar 14 Å clay mineral was also observed from samples of the transition zone, as evidenced in sample H-1-1

(Figure 13). This mineral occurs in every size fraction of sample H-1-1 and upon solvation the peak disappeared as in sample H-1-2.

At first, this 14 Å peak was thought to be a super order representing mixed layering of kaolinite and chamosite. If this had been the case, however, the peak should have remained unchanged in its original position because the lattice of neither of these minerals is expandable.

The chamosite peaks representing the 1/8-1/16 micron size fraction are less well defined and less sharp than those of the larger size fractions. This can be attributed either to the effect of a decrease in crystallinity with extremely small particle size or to the effect of line broadening due to fine particle size (Cullity, 1959, p. 97).

According to Brown (1961, p. 106):

> Brindley and Youell (1953) showed that by heating a natural and essentially ferrous chamosite in air at 300-400°C, the colour changed from green, through yellow, to brown as the ferrous ions became oxidized to ferric, and at the same time the unit-cell parameters contract (see Table II.8). The results can be understood in relation to the positions occupied by the iron atoms in the octahedrally coordinated layer. Since this layer is only a small fraction, about 1/3, of the entire layer thickness, c contracts less than a and b. The contraction is the result of changing Fe^{2+} ions, of radius 0.83 Å, to Fe^{3+} ions of radius 0.67 Å.

The d_{001} decreases from 7.11 Å to 7.06 Å (Table 1).

Figure 10 shows the results of heat treatment on the same selected size fractions of sample H-1-2. The small percent contraction

TABLE 1

CHANGES IN THE STRUCTURE OF CHAMOSITE WHEN HEATED TO APPROXIMATELY 400°C IN THE PRESENCE OF OXYGEN (CORRESPONDING TO THE CONVERSION OF FERROUS TO FERRIC CHAMOSITE) FROM BROWN (1961, P. 106)

	Ferrous Form	Ferric Form	Percent Contraction on Oxidation
a	5.41A°	5.25A°	3.0
b	9.38	9.10	3.0
d(001)	7.11_5	7.06	0.8

In addition to structural changes, chemical analysis and X-ray pattern intensities show that some outer $(OH)^-$ ions of the octahedral layer are converted to $(O)^{-2}$ and some are driven off completely. Oxidation and dehydration reactions corresponding to conversion of ferrous to ferric chamosite are represented (Brindley and Youell, 1953) as follows:

$$Fe^{+2} + (OH)^- \rightleftharpoons (Fe)^{+3} + (O)^{-2} + H^+$$

$$(OH)^- \rightleftharpoons \tfrac{1}{2}H_2O + \tfrac{1}{2}(O)^{-2}$$

THEORETICAL FORMULA OF 7A-CHAMOSITE

$$(Al, Fe^{+3}, Fe^{+2}, Mg)_6 (Si_3Al) O_{10} (OH)_8$$

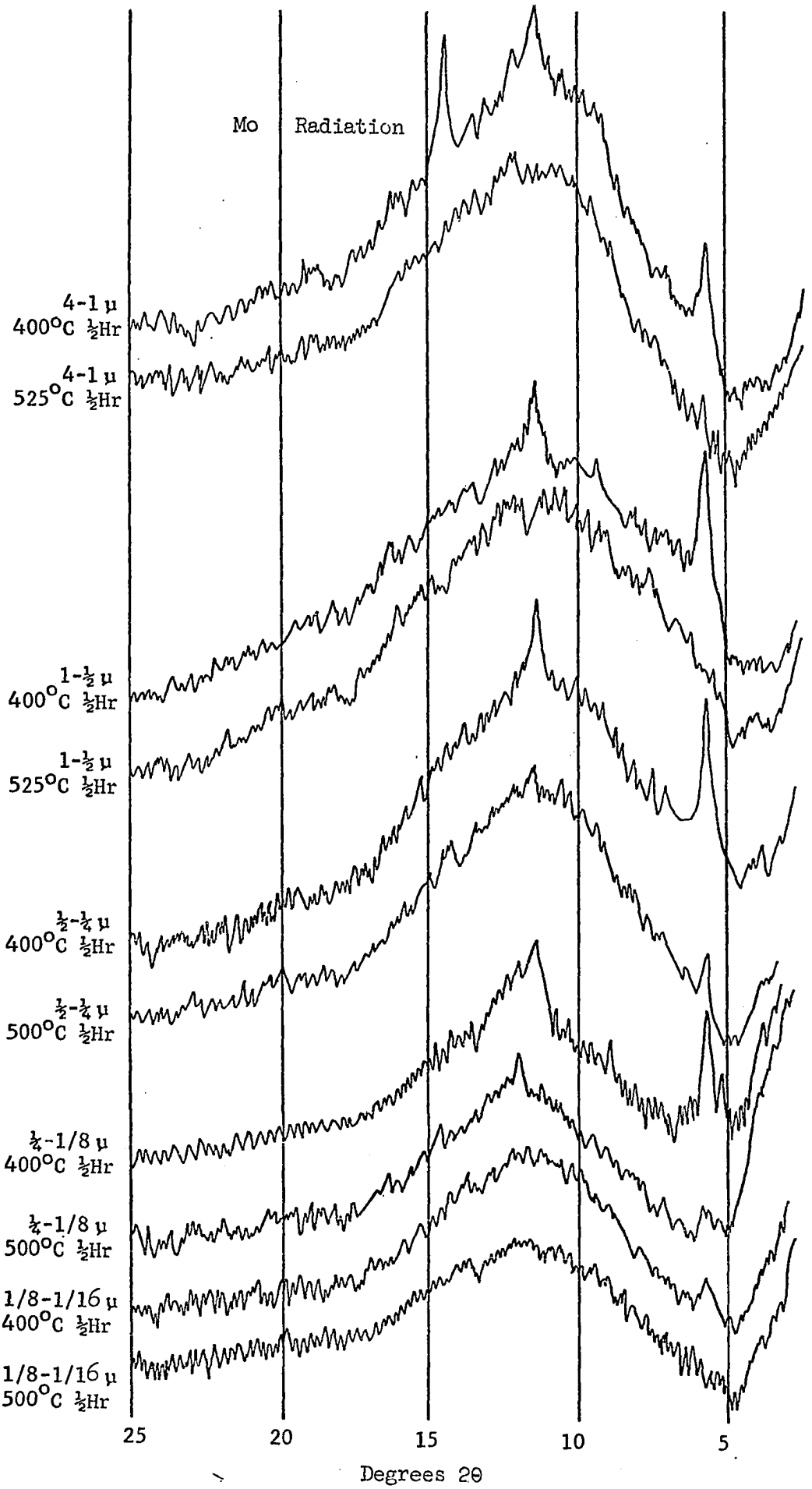

Figure 10. Effects of heat treatment on oriented X-ray diffractograms of selected size fractions of sample H-1-2.

in the c-crystallographic direction makes it difficult to distinguish between actual change due to oxidation and change due to experimental error, but in general there was a shift of the d_{001} peaks toward higher 2θ values, corresponding to a decrease in the unit cell parameter in the c direction. This helps confirm that this clay mineral is indeed ferrous chamosite. The absence or reduction of the chamosite peaks by 525°C shows that the mineral structure has been completely or partially destroyed by the time this temperature is reached.

Figure 11 exhibits DTA and EGA curves of selected size fractions of sample H-1-2. In general, DTA curves show a strong endothermic peak at approximately 100°C, corresponding to loss of interlayer and adsorbed water. EGA curves show a peak in approximately the same area confirming the release of water vapor during low temperature dehydration. DTA curves exhibit a broad, strong exothermic peak between approximately 250° and 400°C, normally peaking around 300°C. This peak corresponds to oxidation of ferrous to ferric chamosite on heating in the presence of oxygen. EGA curves show a broad peak over this same region, corresponding to liberation of water during the oxidation process. Oxidation and dehydration reactions corresponding to conversion of ferrous to ferric chamosite are represented (Brindley and Youell, 1953) in Table I. According to Brown (1961, p. 106):

> The mechanism of the oxidation process can be described as follows: each Fe^{2+} ion on 'oxidation' becomes an Fe^{3+} ion and liberates an electron, which in turn reacts with an

Figure 11. Differential thermal analysis and effluent gas analysis of selected size fractions of sample H-1-2.

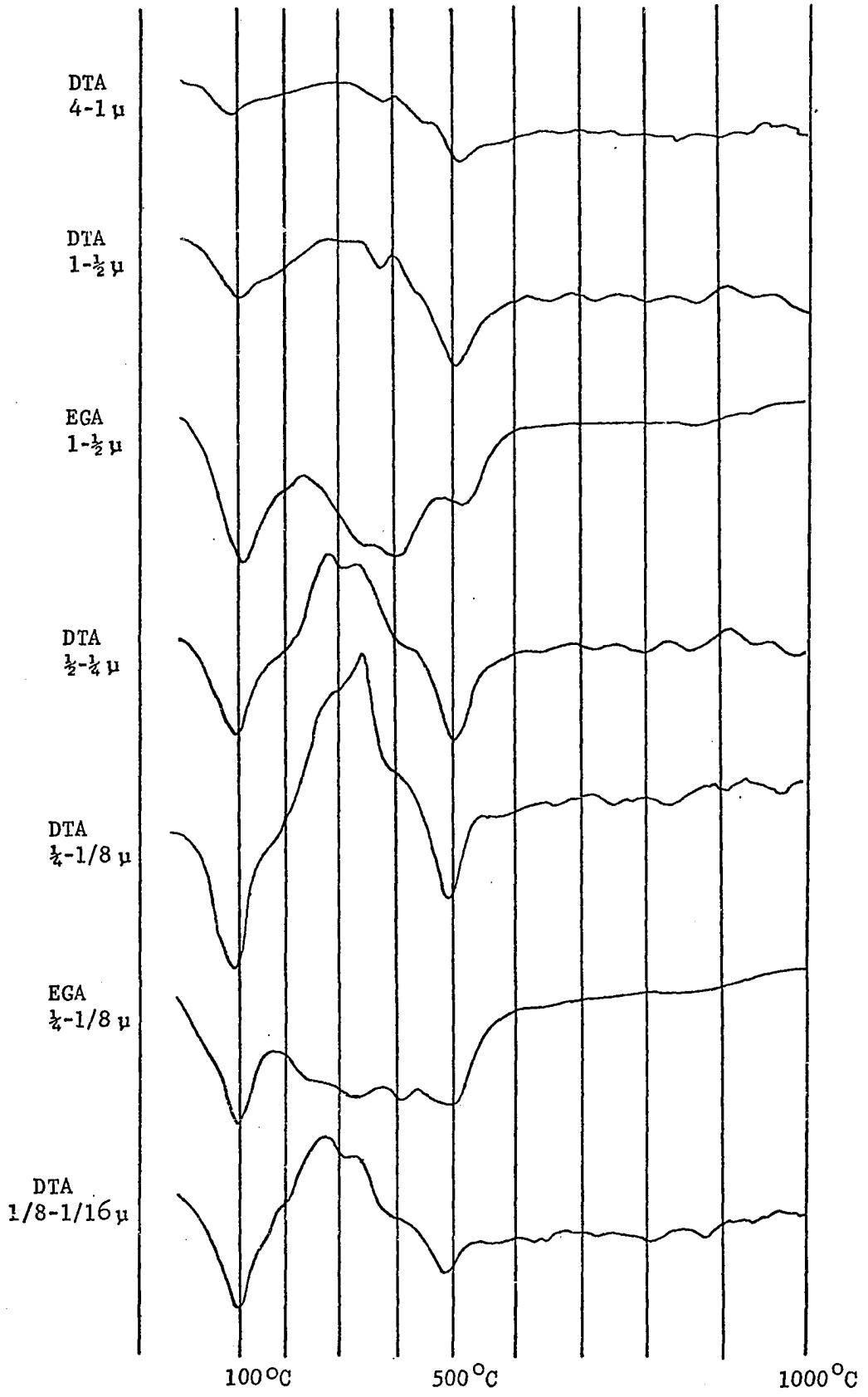

> $(OH)^-$ ion which becomes O^{2-}. The liberated proton, H^+, is removed as water by aerial oxidation. The process does not take place in the absence of atmospheric oxygen. At the same time, a partial dehydration occurs which appears to be confined to the external sheet of hydroxyl ions in the layer structure.

DTA curves show a strong endothermic peak around 500°C which corresponds to the collapse of the chamosite structure. A corresponding EGA peak in the same general area, corresponds to the release of water vapor during collapse of the structure.

Figure 12 displays X-ray diffractograms of the randomly oriented 1-1/2 micron size fraction of sample H-1-2 showing the effects of utilizing differently prepared samples and the effects of acid treatment. As demonstrated earlier, diffractograms of sedimented slides only yield peaks characteristic of the first and second orders of ferrous chamosite, but diffractograms of powder patterns of the same sample yield additional peaks characteristic of b-axis disordered kaolinite. This is thought to result from preferential alignment of minor quantities of kaolinite flakes due to slight compaction of loosely consolidated sample during loading of the sample holder. An oriented layer will give enhanced basal reflections permitting rather small percentages of kaolinite to be recognized. The acid treated sample with the chamosite removed exhibits peaks characteristic of b-axis disordered kaolinite. Also noted is a shift of the 001 peak (7.12 Å) toward lower 2θ values (7.18 Å), corresponding to an increase

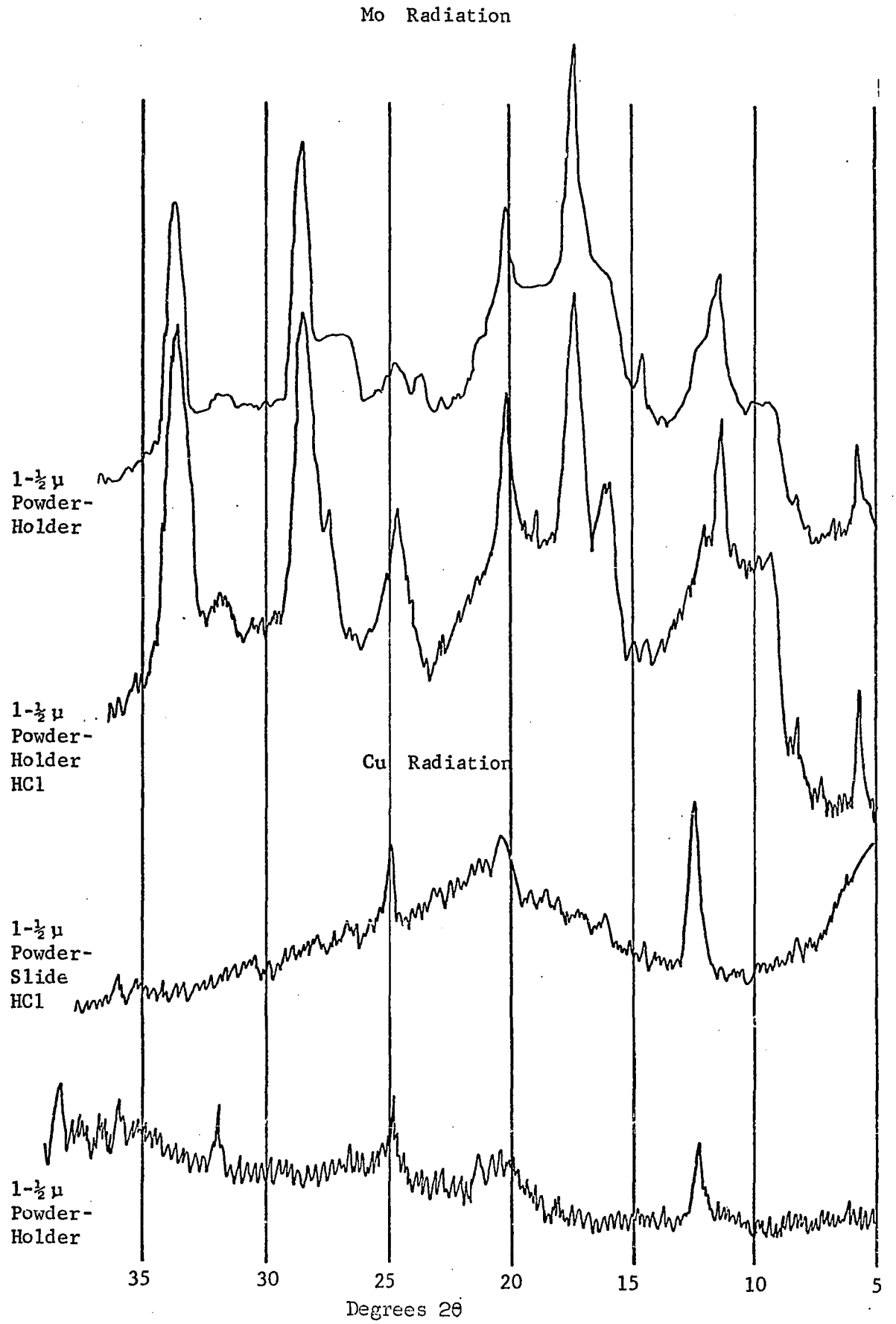

Figure 12. X-ray diffractograms of the randomly oriented 1-$\frac{1}{2}$ micron size fraction of sample H-1-2 showing the effects of acid treatment and the effects of utilizing differently prepared samples and different radiation types.

in the d-spacing of the (001) peak. The d-spacing of ferrous chamosite is approximately 7.11 Å and that for b-axis disordered kaolinite corresponds to approximately 7.18 Å.

Kaolinite

As pointed out earlier, kaolinite is invariably present in samples from these deposits, even though its presence may not be detectable under magnification. The relative proportion of kaolinite varies within the main part of the bed, but it invariably increases in abundance toward the transition zone.

Sample H-1-1 from the transition zone was chosen as a typical sample to illustrate the effects of an increase in kaolinite content in the clay-sized fraction of the transition zone. Figure 13 displays oriented X-ray diffractograms of selected size fractions of this sample, showing variation in mineralogy with particle size and effects of glycolation of the 1/8-1/16 micron size fraction. The difficulty of identifying kaolinite in the presence of chamosite, which gives reflections near to those of kaolinite, is once again clearly demonstrated in this sample. Peaks representing the basal reflection of kaolinite would normally lie on the high spacing, low 2θ, side of the d_{001} of chamosite, but the separation is insufficient for the reflections to be seen. For mixtures of the minerals, the 2θ values of the resulting peaks are intermediate between those normally found

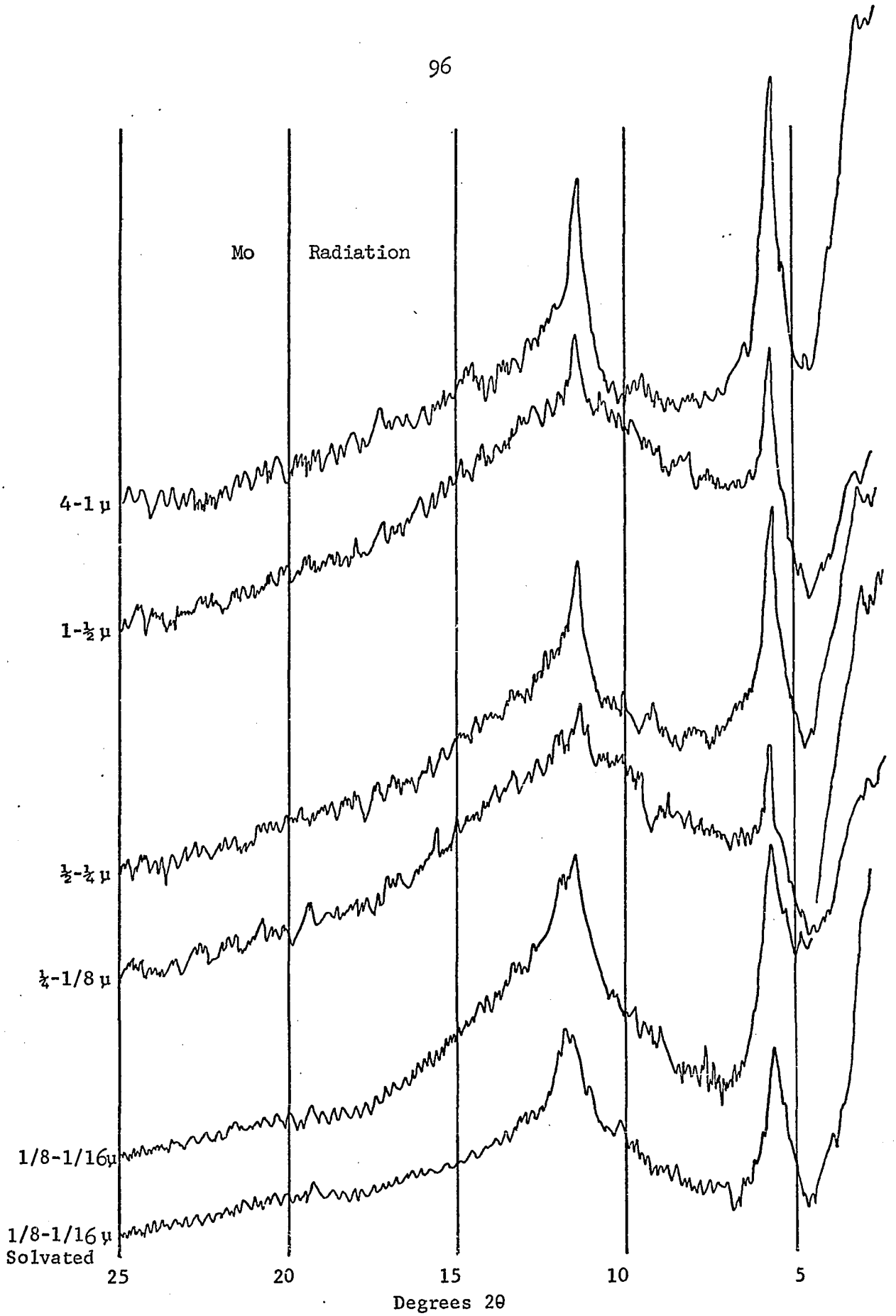

Figure 13. X-ray diffractograms of oriented selected size fractions of sample H-1-1 showing variation in mineralogy with particle size and effects of glycolation of the 1/8-1/16 micron size fraction.

for each separate mineral, and the exact 2θ value possibly depends on the relative proportions of the two minerals present. For example, in this sample the composite basal reflection averages approximately 7.15 Å which is not characteristic of that of either chamosite (7.11 Å) or of b-axis disordered kaolinite (7.18 Å).

Identification of the particular kaolinite variety from diffractograms of oriented slides of mixtures of kaolinite and chamosite, is not possible, as evidenced from diffractograms of sample H-1-1. A slight shift of the basal reflections to a lower d-spacing (averaging 7.15 Å) was detected when heating the selected size fractions of sample H-1-1 to 400°C. However, this shift was not as pronounced as that for sample H-1-2, where the proportion of chamosite was much greater (Figure 14). The composite peaks representing the first and second orders of mixed chamosite and kaolinite are greatly reduced or destroyed by heating to 500-525°C. If the lattice structure of kaolinite had persisted to a higher heating temperature than that of chamosite, then identification of the particular kaolinite variety would have been possible from the remaining peaks. But this was not the case because both structures were destroyed at about the same temperature.

In general DTA and EGA curves of selected size fractions of sample H-1-1 yielded peaks similar to those discussed for sample H-1-2, but curves for the 1-1/2 micron size fraction treated with warm 10

Figure 14. Effects of heat treatment on X-ray diffractograms of oriented selected size fractions of sample H-1-1.

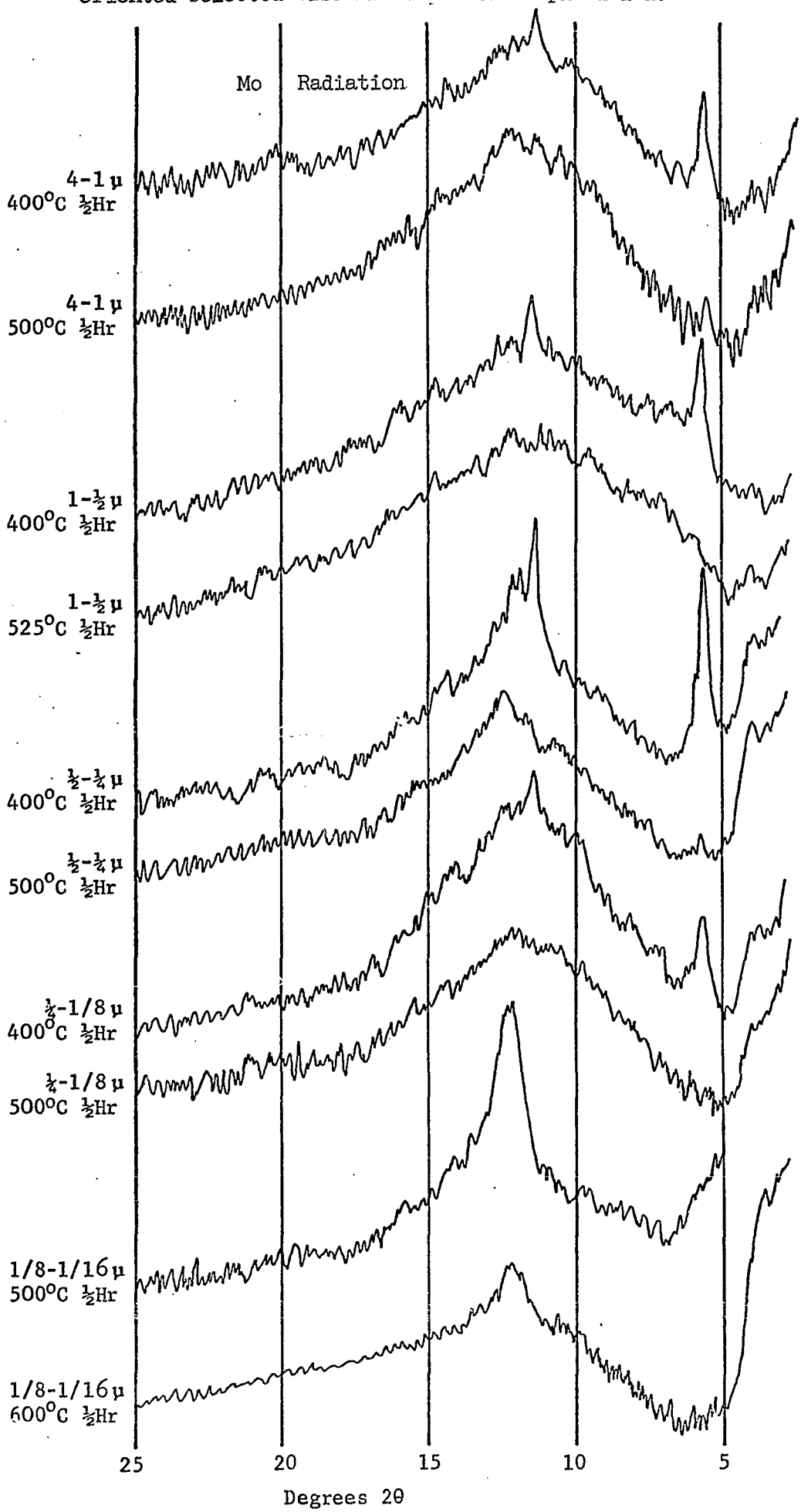

percent HCl gave quite a different pattern (Figure 15). The DTA curve shows a strong endothermic peak around 100°C, corresponding to loss of H_2O- and a strong endothermic peak at approximately 550°C, corresponding to dehydroxylization of kaolinite. The EGA curve for this size fraction shows two peaks at approximately the same temperatures as those of the DTA peaks. This confirms loss of water vapor during the dehydration and dehydroxylization of kaolinite, as suggested by the two DTA endothermic peaks. Conspicuously absent in the DTA and EGA curves of this acid-treated sample is the strong exothermic peak normally occurring around 300°C, corresponding to oxidation of ferrous to ferric chamosite. Acid treatment has removed the chamosite but kaolinite remains to yield DTA and EGA curves typical of kaolinite.

True identification of the kaolinite variety present in this sample is possible only from diffractograms of powder samples (Figure 16). In addition to the composite peaks representing the first and second orders of mixed chamosite and kaolinite, the diffractogram of the untreated specimen shows additional peaks characteristic of b-axis disordered kaolinite. As discussed previously, preferential alignment of kaolinite flakes during loading of the holder probably accounts for these additional peaks. The diffractogram of the acid-treated sample exhibits a succession of peaks characteristic of b-axis disordered kaolinite. The peak positions are located at the correct 2θ values for this variety of kaolinite, but the relative intensities of the peaks

Figure 15. Differential thermal analysis and effluent gas analysis of selected size fractions of sample H-1-1.

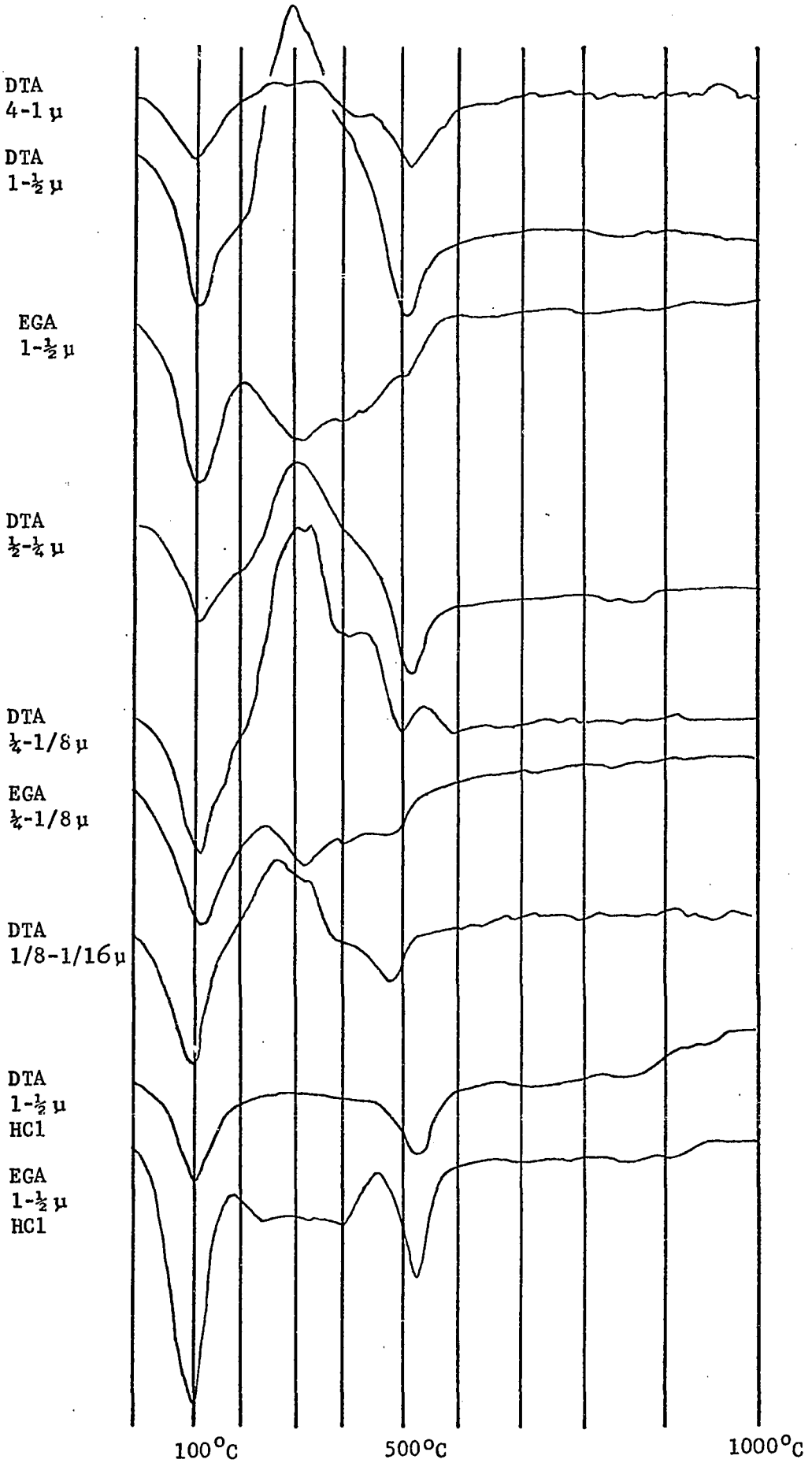

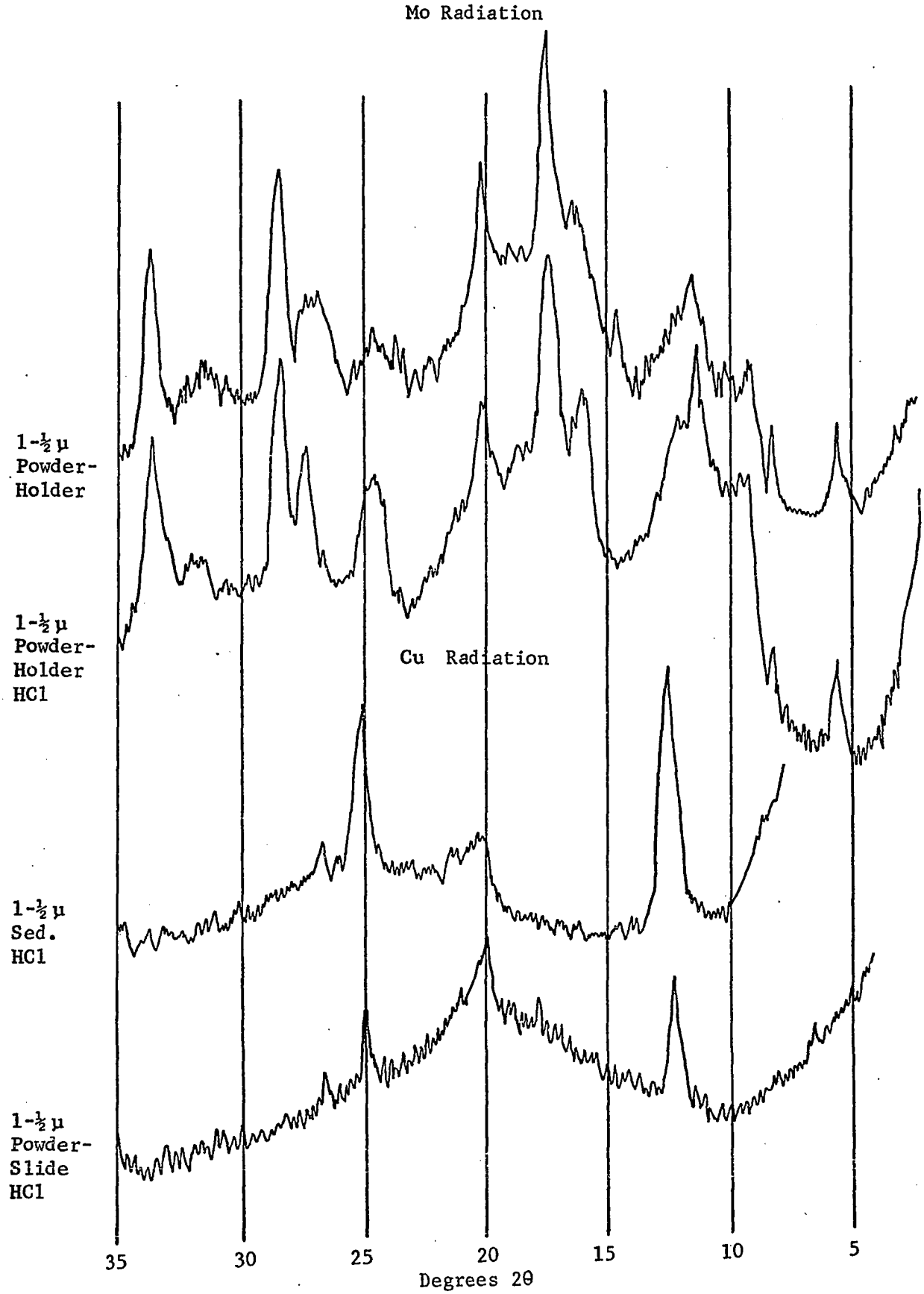

Figure 16. X-ray diffractograms of the randomly oriented 1-½ micron size fraction of sample H-1-1 showing the effects of acid treatment and the effects of utilizing differently prepared samples and different radiation types.

vary from those listed for typical b-axis disordered kaolinite. This phenomenon is thought to result from abnormally enhanced reflections due to preferential alignment of kaolinite flakes during loading of the sample holder.

Some of the reflections in this diffractogram exhibit a broadened or blurred appearance. As suggested by Brown (1961, p. 64-65):

> When kaolin clays from different sources are examined by X-ray diffraction, considerable variations are found in the degree of structural regularity. Disorder in the lattice produces blurring and weakening of reflections, and usually of particular groups of reflections, depending on the disordering process.
>
> The feature most commonly observed is that reflections with k index not a multiple of 3 (this can be abbreviated to the statement $k \neq 3n$) tend to be weak or missing, while reflections with $k = 3n$ tend to be largely unaffected.
>
> The results are readily interpreted in terms of random layer displacements parallel to the b axis of $nb/3$. In the idealized layer structure, the OH ions in the wholly hydroxyl layer lie in lines parallel to the b axis and at intervals of $b/3$. Therefore the structural layers can be displaced parallel to b by $nb/3$, without altering the OH-O bonds between the adjacent layers. Such displacements can be expected to occur rather easily because no marked energy changes are involved. The net result of these displacements is that the Al and Si atoms occupy a number of positions statistically in the average unit cell.

Illite

Minor illite is characteristically found in the transition zones and its abundance increases progressively toward the overlying and underlying beds where it becomes a prominent constituent of these beds. Illite is a mica type clay mineral with a 10 Å c-axis spacing.

The structure of illite is much the same as that of muscovite, but illite contains less potassium and more water than muscovite. According to Brown and Norish (1952) this may be explained by the partial substitution of the hydronium ion (H_3O^+) for the K^+ ion. The (060) reflection of the illite in these deposits averages approximately 1.50 Å which is characteristic of the dioctahedral type.

Selected size fractions of sample H-1-1 reveal the presence of illite, and this sample is typical of the occurrence of illite in the transition zones (Figure 13). The presence of illite is not readily evident in the coarser size fractions of Figure 11, but the relative increase of illite with respect to chamosite in the finer size fractions results in more pronounced peaks representing the first, second, and third orders of illite, 4.06° 2θ (10.04 Å), 8.12° 2θ (5.02 Å), and 12.25° 2θ (3.33 Å) respectively. Peaks representing the first and second orders are small and poorly defined but the peak representing the third order is very intense and better defined.

In the coarser micron fractions, down to 1/2-1/4 micron size, the presence of the most intense third order is indicated only by a slight hump on the high 2θ side of the more intense second-order chamosite peak, which occurs at 11.45° 2θ (3.56 Å). The one large peak occurring in this region actually consists of two peaks, but the illite peak is represented only as a hump on the larger peak because the more intense chamosite peak overlaps on the less intense

illite peak. Starting with the 1/4-1/8 micron fraction, the relative proportion of illite increases rapidly and the relative intensities of the chamosite and illite peaks essentially reverse so that in the 1/8-1/16 micron fraction the third-order illite peak becomes the main peak with the second order of chamosite represented as a hump on the low 2θ side of the illite peak.

In this sample the presence of illite becomes more apparent as the sample is heated to temperatures sufficient to partially or completely destroy chamosite (Figure 14). Structurally, illite is stable at much higher temperatures than either chamosite or kaolinite; therefore, illite remains after destruction of both these minerals, as seen in Figure 14. The 1/2-1/4 micron fraction exhibits this phenomenon very well. A double peak, consisting of the second and third orders of chamosite and illite respectively, persists up to 400°C, but by 500°C the chamosite structure has been essentially destroyed and the illite peak becomes the prominent peak. The 1/8-1/16 micron fraction also shows this phenomenon well. By the time the sample is heated to 500°C illite is the prominent peak, and it is still distinctly present at 600°C.

The effect that varying amounts of illite in this sample has on the DTA and EGA curves is not readily evident in Figure 15, but the 1/4-1/8 micron fraction has a slight endothermic peak at approximately 600°C. This peak probably represents dehydroxylization of illite

because both chamosite and kaolinite lose their structurally coordinated water at a much lower temperature. Curves for the other size fractions do not exhibit distinct peaks characteristic of reactions involving only illite, but many of the patterns show double peaks in the areas of the exothermic peak and second endothermic peak. Perhaps these double peaks indicate dehydroxylization at different temperatures of mixtures of chamosite, kaolinite, and illite because the structurally coordinated water would be held more tightly for illite than for the other two. Another clay mineral with an expandable 14 Å lattice structure is also present in this sample. Perhaps this mineral is nontronite and the shoulders on some of the exothermic peaks at approximately 400°C can be attributed to exothermic reactions by nontronite. Nontronites commonly exhibit midrange endotherms from 300-500°C.

A greater number of illite peaks, which in general are better defined, appear in diffractograms of powdered samples held in aluminum holders. Determination of the illite type on the basis of the 2θ value of the (060) reflection is possible from such diffractograms (Figure 16). The illite peak at 7° 2θ, corresponding to the third order, is sharper and better defined in powder patterns than in sedimented patterns.

Clay Minerals of the Weathered Bed

Weathering associated with the present topography leached the iron from the chamosite structure resulting in disruption of the

crystal structure. X-ray diffractograms of samples from the altered parent bed invariably reveal the presence of kaolinite and illite, but chamosite is absent from extensively leached samples (Figure 17). Removal of chamosite increases the relative percentages of kaolinite and illite and this increase is seen in diffractograms by an increase in reflection intensities for these two minerals. Kaolinite is definitely present in larger quantities than is illite but the relative proportion of each mineral is not of great significance to this study.

In less extensively leached rocks, it is possible that some chamosite remains, but as pointed out earlier, it is extremely difficult to distinguish from kaolinite, especially when the kaolinite content is higher than chamosite.

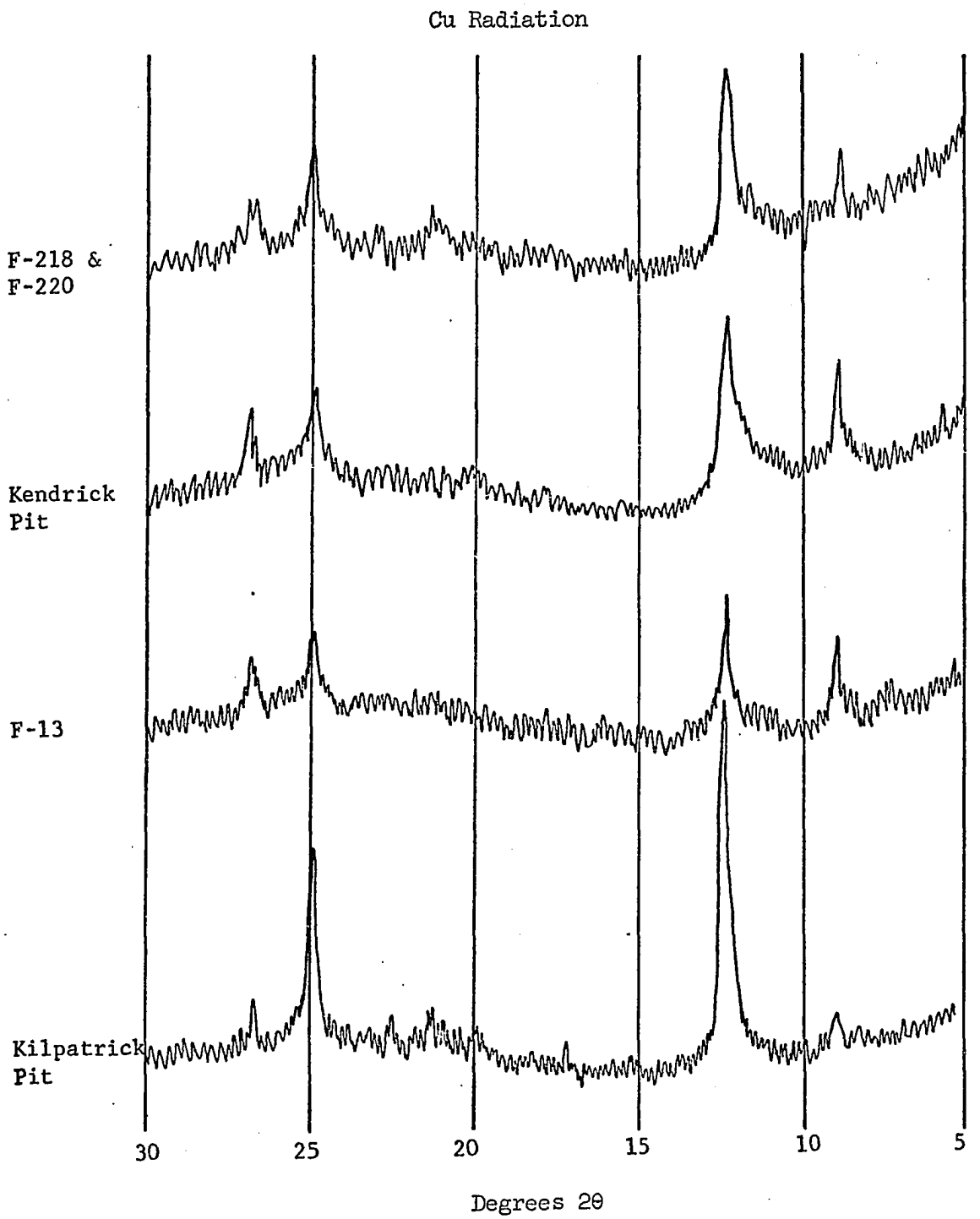

Figure 17. X-ray diffractograms of the oriented less-than-4 micron size fraction of selected samples from the weathered parent bed located in the present zone of oxidation.

CHEMICAL ANALYSIS BY X-RAY FLUORESCENCE

General Statement

Chemical analyses of 17 bulk samples and the less-than-one and less-than-four micron fractions of two size-fractioned samples were conducted quantitatively by means of X-ray fluorescence. For the bulk samples and the less-than-four micron fraction of sample H-1-2, analysis of the FeO, CO_2, organic H, and organic C were performed by John A. Schleicher, Analytical Chemist for the Illinois Geological Survey, utilizing wet chemical techniques. H_2O- and H_2O+ were determined by Schleicher by weight loss determinations, where the former is the percentage of weight loss between room temperature and 110°C and the latter is that between 120° and 1000°C. The Fe_2O_3 values were calculated from Fe_2O_3 undifferentiated values, determined by X-ray fluorescence, by subtracting the Fe_2O_3 equivalent of FeO determined by Schleicher. For the three remaining size-fractioned samples, the H_2O- and H_2O+ contents were determined by the writer utilizing weight determinations as discussed above. The chemical analysis data of the bulk and size-fractioned samples are shown in Tables 2 and 3, respectively.

TABLE 2

CHEMICAL ANALYSES BY X-RAY FLUORESCENCE SUPPLEMENTED WHERE INDICATED

BY WET CHEMICAL AND WEIGHT LOSS ANALYSES (LESS-THAN-250 MESH BULK SAMPLES)

No.	SiO_2	Al_2O_3	*FeO	***Fe_2O_3	K_2O	MgO	Na_2O	CaO	MnO	TiO_2	P_2O_5	S	*Org. C	*Org. H	*CO_2	**H_2O+	**H_2O-	Total
H-1-1	35.56	13.92	11.44	19.22	0.80	1.20	0.14	1.20	0.29	0.45	0.23	1.06	1.31	0.092	4.55	6.84	4.20	102.50
H-1-8	14.20	6.88	28.49	22.35	0.47	0.70	0.12	3.18	0.31	0.18	0.83	0.06	0.23	0.016	15.41	6.83	1.54	101.80
H-1-14	21.30	8.38	17.35	30.43	0.45	1.08	0.11	1.37	0.25	0.27	0.34	0.10	0.85	0.060	6.10	6.97	4.98	100.39
H-1-16	30.40	6.83	20.42	20.38	0.44	1.28	0.13	2.93	0.30	0.26	0.55	0.12	0.22	0.015	10.94	5.12	3.01	103.35
H-6-17	31.30	5.21	33.12	7.91	0.69	0.83	0.17	3.79	0.34	0.36	1.00	1.00	0.74	0.052	23.31	1.96	0.96	112.74
H-6-20	16.30	8.87	31.24	16.86	0.47	0.90	0.14	2.50	0.27	0.22	0.54	0.08	1.42	0.099	16.74	4.70	2.81	104.16
H-6-24	14.00	5.80	33.25	9.63	0.63	1.32	0.08	7.05	0.39	0.23	1.99	0.15	0.38	0.027	22.96	3.70	2.00	103.59
H-6-26	26.30	8.95	21.32	7.84	0.62	1.55	0.11	4.55	0.34	0.30	1.42	0.18	0.43	0.030	10.76	5.05	3.51	93.27
H-11-27	26.64	4.32	28.88	9.70	0.64	1.62	0.15	4.72	0.48	0.22	1.18	0.17	0.37	0.026	20.11	2.78	1.69	103.70
H-11-28	21.52	6.38	23.56	20.35	0.70	1.85	0.11	3.47	0.29	0.26	0.60	0.10	0.26	0.018	13.78	4.71	4.38	102.34
H-11-30	17.51	4.33	12.21	5.93	1.82	1.15	0.09	+25.00	0.15	0.15	2.17	0.13	0.14	0.010	20.98	3.71	2.25	+97.73
H-19-31	18.60	6.03	****	****	0.51	0.96	0.05	2.13	0.16	0.49	0.51	0.05	****	****	****	****	****	****
H-19-33	19.75	6.67	22.58	24.15	0.57	1.08	0.14	2.62	0.31	0.38	0.61	0.07	0.39	0.027	12.24	5.29	4.08	100.96
H-19-34	16.60	6.77	21.30	24.70	0.65	1.03	0.15	3.17	0.20	0.19	0.99	3.86	1.10	0.077	11.45	4.88	3.07	100.19
H-21-35	22.38	9.20	27.57	16.77	0.45	0.90	0.13	1.95	0.34	0.22	0.43	0.08	0.18	0.013	15.37	4.46	3.73	104.17
H-21-37	16.70	7.65	29.40	15.48	0.43	1.18	0.07	2.73	0.28	0.23	0.48	0.09	0.19	0.013	16.80	4.37	3.54	99.99
H-21-40	23.70	10.30	15.33	17.60	0.52	1.57	0.08	2.34	0.22	0.34	0.72	0.09	0.36	0.025	5.76	5.82	4.72	90.00

*Values by wet chemical analysis

**Values by weight loss determinations

***Calculated from Fe_2O_3 undifferentiated (X-ray fluorescence) by subtracting the Fe_2O_3 equivalent of FeO

****Values not determined

TABLE 3

CHEMICAL ANALYSIS OF SIZE-FRACTIONED CLAYS BY X-RAY FLUORESCENCE

SUPPLEMENTED WHERE INDICATED BY WET CHEMICAL OR WEIGHT LOSS ANALYSIS

No.	Particle Size in Microns	SiO_2	Al_2O_3	*FeO	***Fe_2O_3	K_2O	MgO	MnO	TiO_2	P_2O_5	S	*Org. C	*Org. H	*CO_2	**H_2O-	**H_2O+	Total
H-1-2	< 4	39.10	15.90	13.95	14.74	0.80	4.86	0.25	0.85	0.21	0.17	0.36	0.025	6.81	4.43	7.46	109.91

*Values by wet chemical analysis
**Values by weight loss determinations
***Calculated from Fe_2O_3 undifferentiated (wet chemical) by substracting the Fe_2O_3 equivalent of FeO

No.	Particle Size in Microns	SiO_2	Al_2O_3	**Fe_2O_3	K_2O	MgO	MnO	TiO_2	P_2O_5	S	*H_2O-	*H_2O+	Total
H-1-2	< 1	***	***	24.29	***	4.42	***	***	***	***	6.00	10.89	***
H-1-1	< 4	46.30	16.10	22.43	1.08	4.24	0.15	2.36	0.85	0.77	5.65	10.30	103.50
H-1-1	< 1	41.30	16.60	22.14	1.02	3.99	0.08	2.01	0.97	0.58	5.13	11.08	98.26

*Values by weight loss determinations
**Values by X-ray fluorescence (Fe_2O_3 undifferentiated)
***Values not determined

Analyses of the main chemical components of 33 random bulk samples were performed by Bruce Williams Laboratories of Joplin, Missouri (Appendix C). Seven of these samples were chosen as typical for these rocks and utilized as standards for X-ray fluorescence analysis. These standards were supplemented where necessary with U. S. Geological Survey silicate rock standards.

Amorphous iron oxide and finely-divided crystals of goethite were selectively removed from all these samples by the dithionite-citrate technique referred to earlier, and the extracted iron was quantitatively analyzed by atomic absorption spectrophotometry. These results are given in Table 4.

The analytical techniques for the different analyses are given in Appendix A.

Data and Interpretation

Calculated Percent Iron Possible for Each Iron-Bearing Mineral Present in a Typical Sample

One of the major objectives of this study was to determine where the iron in the deposits is located in relation to the constituent minerals. From thin section studies several potential iron-bearing minerals were recognized, including siderite, chamosite, goethite, and minor pyrite and magnetite. The presence of non-structurally coordinated amorphous iron oxide was also detected.

TABLE 4

CHEMICAL ANALYSIS BY ATOMIC ABSORPTION SPECTROPHOTOMETRY OF THE AMORPHOUS IRON SELECTIVELY REMOVED FROM THE BULK SAMPLES (IRON EXTRACTED BY THE DITHIONITE-CITRATE TECHNIQUE)

No.	Fe_2O_3 (Undifferentiated)	No.	Fe_2O_3 (Undifferentiated)
H-1-1	8.25	H-6-23	2.15
H-1-2	9.38	H-6-24	1.07
H-1-5	3.93	H-6-25	3.76
H-1-6	9.86	H-6-26	3.94
H-1-7	7.49	H-11-27	5.91
H-1-8	7.50	H-11-28	5.90
H-1-10	11.34	H-11-29	11.25
H-1-11	12.87	H-11-30	8.43
H-1-12	11.26	H-19-31	8.41
H-1-13	13.95	H-19-32	8.44
H-1-14	11.19	H-19-33	8.42
H-1-15	8.58	H-19-34	13.97
H-1-16	5.93	H-21-35	5.89
H-6-17	2.57	H-21-36	11.29
H-6-18	11.28	H-21-37	8.40
H-6-19	13.96	H-21-38	8.41
H-6-20	8.43	H-21-39	11.27
H-6-21	11.27	H-21-40	5.72
H-6-22	5.92		

Sample H-11-28 was chosen as an average sample to determine the relative percentages of iron incorporated in these various forms. Sample H-11-28 contains a total of 46.53 percent Fe_2O_3, corresponding to 32.57 percent elemental iron, and 13.78 percent CO_2. The relative percent of the elemental iron (32.57 percent) in each iron-bearing mineral type was determined after making the assumption that all the CO_2 in the sample is combined with Fe and Ca. This assumption is possible only if we assume that all the Ca in the sample is in the form of a carbonate and that all of the Mg and Mn in the sample is present in the form of chamosite and siderite, respectively, rather than as carbonates (e.g., dolomite and rhodochrosite). After determining the amount of CO_2 necessary to combine with calcium, that remaining is allocated to Fe.

Based on these assumptions, it was determined that an average of 12.12 percent of the total 32.57 percent elemental iron is structurally-coordinated as siderite, corresponding to approximately 37.21 percent of the total iron content. The remaining 20.45 percent would then be present as chamosite, amorphous iron oxide, pyrite, ilmenite (?), and magnetite. Analyses of the amorphous iron selectively removed from this sample by atomic absorption spectrophotometry yielded a value of 4.13 percent iron which, incidently, differs from the elemental iron equivalent of the Fe_2O_3 content (14.25 percent) listed for this sample in Table 2. This indicates that approximately

30 percent of the ferric iron in these deposits is present as amorphous iron oxide or small finely-divided goethite crystals with the remaining 70 percent most likely present in chamosite. If oxidation does increase the disorder in chamosites as suggested by Brown (1961), then the high ferric iron content in these chamosites could be the reason why they are poorly ordered. Subtraction of the 4.13 percent amorphous iron content leaves 16.32 percent iron which would then be present as chamosite, pyrite, ilmenite (?), and magnetite. If we assume that all the sulfur present in this sample, 0.10 percent, is present as pyrite (FeS_2), then pyrite accounts for approximately 0.10 percent of the remaining 16.32 percent iron.

The titanium content increases in the clay-sized fractions of the size fractions. Therefore, it is suspected that a large part of the titanium present is in the form of ilmenite, even though it was not present in sufficient quantities to give peaks on diffractograms. Assuming that all the titanium in this sample is present in the form of ilmenite, this could account for approximately 0.26 percent of the remaining 16.22 percent iron, leaving 15.96 percent which would be present as magnetite and chamosite. The iron content of the chamosite is approximately 14.38 percent, calculated independently for the less-than-four micron size fraction of sample H-1-2 after the iron present as fine-grained siderite was accounted for. This would leave only 1.58 percent iron present in the form of

magnetite. The iron content would be readily available from all the iron-bearing minerals except chamosite. The total percent available on the basis of these calculations would be 18.19 percent elemental iron which corresponds to approximately 56.79 percent of the total iron present in these samples.

Even though several assumptions had to be made to arrive at the above conclusion, it is felt that the values presented represent a pretty fair first approximation of the relative percentages of iron present in each possible iron-bearing mineral. Any error introduced by one assumption would probably be compensated for by offsetting errors introduced by other assumptions. For example, the loss of iron resulting from the substitution of the Mn^{+2} ion for the Fe^{+2} ion in the siderite structure would be in part compensated for by not assuming that the Mn^{+2} is present as a carbonate (e.g., rhodochrosite) which would tie up part of the CO_2 normally allocated to siderite. Analyses of siderite observed in various publications show Mn percentages up to 24 (e.g., those by Deer, Howie, and Zussman, 1962, p. 273). So the assumption that all the Mn is present in the form of siderite is likely. Likewise, the loss of iron to siderite, which would result by assuming that all the Mg was present as a carbonate would be in part compensated for by substituting Mg^{+2} for Fe^{+2} in the octahedral layer of the chamosite structure, decreasing the amount of non-available iron tied up as chamosite. The assumption that all

the sulfur in the sample is present as pyrite is most probably in error because organic sulfur commonly occurs in association with organic material. In any event, the error introduced by this assumption would not be great because the sulfur content is 0.10 percent for this sample. Likewise, the assumption that all titanium in this sample is present in ilmenite is certainly erronous because normally a certain amount of titanium would be expected to substitute for silica or aluminum in the silicate structures of clay minerals or feldspars. Again, the error introduced by assuming that it is all present as ilmenite would not be too great because the titanium content constitutes only 0.26 percent of the entire sample.

Changes in Mineralogy as Reflected by Changes in Chemical Composition

Bulk Samples. As can be seen from Table 2, the phosphorous content in general increases with a corresponding increase in CaO. The increase in phosphorous is due in part to an increase in collophanite (hydrous calcium phosphate) which within itself helps to increase the relative percentage of calcium. The increase in phosphorous is also normally associated with an increase in calcite. The phosphorous content averages approximately 0.34 percent in the samples analyzed.

The calcium content in these samples is normally variable within a fairly narrow concentration range, but local enrichment in

calcite, such as in nodules or thin layers, results in a major increase in the calcium content (e.g., sample H-11-30).

An increase in the quartz content of samples selected from the transition zones is reflected in the increase in SiO_2 content of the sample (e.g., H-1-1, H-1-16, and H-6-17). Sudden increases in the Al_2O_3 content of bulk samples correspond in almost every case to an increase in the clay content, normally associated with the transition zones. In the case of H-1-1, this is obvious from thin section studies. Subtle increases in the Fe_2O_3 content are always accompanied by a corresponding increase in the amorphous iron oxide content. This reflects an increase in the oxidation potential of the environment subsequent to deposition of the rocks but prior to their deep burial. Likewise, an abnormally high K_2O content corresponds to an increase in the feldspar and/or illite content (e.g., for H-11-30). The sulfur content normally increases in the transition zones, as reflected by samples H-1-1 and H-6-17, and locally it increases due to secondary replacement of other constituents by pyrite (e.g., H-19-34). An abrupt increase in CO_2 reflects an increase in siderite and/or calcite, with a corresponding increase in iron and/or calcium.

Size-Fractioned Samples. Comparison of the SiO_2 and Al_2O_3 in the bulk samples to that in the clay-sized fractions shows an increase of both oxides in the latter, which results from a relative increase in the proportion of clay minerals in the finer size fractions.

Chamosite, kaolinite, and illite, all of which are present in varying proportions in these deposits, are rich in both of these components. A decrease in iron in the finer size fractions reflects a decrease in siderite content. A higher iron content coupled with the presence of CO_2 in the coarser clay-sized fractions show that fine-grained siderite remains with the chamosite during size fractionation. An increase in the K_2O content in the clay size fractions probably represents a relative increase in the proportion of illite. An increase in MgO content suggests a relative increase in a fairly high Mg-chamosite. This is another justification for assuming that most of the Mg is present in chamosite. A substantial increase in TiO_2 in the clay-sized material may be interpreted as a relative increase in fine-grained ilmenite which would remain with the clays. A substantial increase of P_2O_5 in the clays suggests that at least some of the phosphorous in these deposits may be present as finely divided organic phosphorous or as minute collophanite crystals. A progressive decrease in sulfur content with decrease in size suggests that much of the sulfur is present as pyrite. A progressive decrease in CO_2 content with decrease in particle size results from a decrease in siderite in the finer size fractions. An increase in H_2O- and H_2O+ in the clay-sized materials is very easily understood because many clays contain high quantities of interlayer and adsorbed water as well as structurally coordinated water.

The chemical data of the clay-sized material in Table 3 is not typical for normal chamosites. It was impossible to obtain a pure sample of chamosite because even in the finer size fractions it is intimately mixed with kaolinite, as determined by X-ray analysis, and with some illite, siderite, and possibly ilmenite. The specific gravity of chamosites mixed with kaolinite would be lower than that for average chamosites, and this is normally the case for these clays. This phenomenon discouraged any attempts to derive a chemical formula for the chamosite in these deposits.

TRACE ELEMENT GEOCHEMISTRY

General Statement

Quantitative analysis was performed on 40 bulk samples and 5 size-fractioned samples from the Louisiana green ores (Table 5). These samples were analyzed for boron, gallium, vanadium, copper, zirconium, nickel, manganese, and chromium. The less-than-230 mesh size fraction of the pulverized bulk samples was utilized for this study. The preparation and analytical techniques utilized are listed in Appendix A.

The purpose of the quantitative spectrochemical analyses was to predict the paleosalinity and thus the environment of deposition of these sedimentary deposits utilizing a discriminant function based upon the boron and vanadium contents, and hopefully to confirm this environment of deposition by utilizing the remaining trace elements as environmental indicators. The environment indicated from these studies will be compared to the postulated environment as determined from other observations.

Paleosalinity Based on the Boron and Vanadium Discriminant Function

Boron has long been recognized as a potential paleosalinity

TABLE 5

TRACE ELEMENT CONCENTRATIONS IN PARTS PER MILLION

Sample	B	Ga	V	Cu	Zr	Ni	Mn	Cr
H-1-1	185	2	180	< 10	500	75	1080	31
H-1-2	75	< 1	22	< 10	< 10	150	545	12
H-1-3	265	3	265	< 10	960	105	1120	35
H-1-4	270	4	280	< 10	1600	120	1180	37
H-1-5	355	3	390	< 10	1900	140	1200	35
H-1-6	345	4	370	26	910	110	910	34
H-1-7	316	3	280	5	780	120	1010	31
H-1-8	500	4	390	< 10	1550	155	1290	35
H-1-9	370	3	120	< 10	440	90	700	24
H-1-10	315	ND	225	< 10	1100	105	1050	34
H-1-11	290	ND	140	8	950	100	1210	27
H-1-12	285	ND	190	< 10	> 2000	134	1120	31

TABLE 5--Continued

Sample	B	Ga	V	Cu	Zr	Ni	Mn	Cr
H-1-13	320	4	510	11	1800	155	1100	49
H-1-14	150	2	37	< 10	400	66	470	17
H-1-15	280	3	175	< 10	1160	120	1020	35
H-1-16	150	1	30	< 10	> 2000	150	1400	17
H-6-17	170	3	< 10	5	900	22	940	11
H-6-18	280	3	425	5	400	70	1800	38
H-6-19	190	2	80	< 10	120	110	880	19
H-6-20	190	2	55	33	105	60	620	16
H-6-21	200	2	85	< 10	120	80	650	22
H-6-22	165	2	60	< 10	125	85	725	19
H-6-23	210	3	180	< 10	1000	85	125	35
H-6-24	190	3	42	8	200	45	930	15
H-6-25	290	3	310	19	1100	110	1500	35

TABLE 5--Continued

Sample	B	Ga	V	Cu	Zr	Ni	Mn	Cr
H-6-26	270	3	230	7	700	85	1200	31
H-11-27	300	3	45	12	620	65	1450	15
H-11-28	285	2	90	6	560	95	725	16
H-11-29	180	1	40	1	135	80	630	13
H-11-30	270	2	110	< 2	365	105	950	17
H-19-31	320	3	75	< 2	580	60	435	16
H-19-32	150	1	12	< 2	ND	36	260	8
H-19-33	170	2	45	< 2	150	42	425	14
H-19-34	180	2	37	< 2	120	50	500	12
H-21-35	255	3	220	7	710	135	1060	32
H-21-36	295	3	140	5	700	120	980	29
H-21-37	255	3	190	6	1000	110	900	31
H-21-38	265	3	70	9	575	226	1170	27

TABLE 5--Continued

Sample	B	Ga	V	Cu	Zr	Ni	Mn	Cr
H-21-39	310	3	270	7	1100	135	1010	35
H-21-40	160	2	110	4	220	95	580	25

indicator. The utilization of boron content to differentiate marine and fresh-water sediments was first reported by Goldschmidt and Peters (1932a, b in Potter et al, 1963). Subsequent studies by Landergren (1945, 1958), Frederickson and Reynolds (1960), Nichols and Loring (1962), and others established a definite relationship between the concentrations of boron in sediments and the environment of deposition.

Studies by Potter et al (1963) on the distribution of boron in recent and ancient argillaceous sediments indicate that B, Cr, Ga, Ni, and V are significantly more abundant in marine than in fresh-water argillaceous sediments. Upon examining the accuracy and reproducibility of discriminant functions based upon the utilization of B, Cr, Cu, Ga, Pb, Ni and V and various combinations of these to distinguish marine and fresh-water sediments, Potter et al (1963) found that a discriminant function based upon B and V alone can more decisively separate marine and fresh-water sediments. The discriminant function for these two elements is

$$X = 5.3415x + 5.6928y$$

where x and y correspond to boron and vanadium respectively and the number prefixes correspond to weighted factors indicating the amount of each variable contributing to discrimination. Such a discriminant function derived from 33 modern sediments decisively separated the marine and fresh-water environments. Application of this discriminant function to ancient sediments whose environment of deposition had been

independently established by geologic evidence resulted in correct classification of 28 out of 33 sediments (Potter et al, 1963, p. 669).

From a plot of B and V for the modern control group an estimated line of separation between the marine and fresh-water fields was determined by Potter et al (1963, p. 679) as follows:

> The position of the separation line is established by first determining the direction of maximum slope of the discriminant function. This direction is such that projecting the modern control samples onto it provides the maximum possible separation between the two groups of modern sediments. The line normal to the direction of maximum slope of the discriminant function and through the midpoint between the logarithmic averages for the two groups is the estimated line of separation.

Figure 18 demonstrates how the estimated line of separation between marine and fresh-water fields for the Louisiana ore samples corresponds to the original separation line of Potter et al (1963). Out of the 40 bulk samples, 35 fell well within the marine field and only 5 fell within the fresh-water field. This suggests a marine environment of deposition for these deposits with possible local fluctuations between marine and fresh-water conditions. Similar conditions are suggested by the nature of the ore deposits and also by the nature of the overlying and underlying deposits.

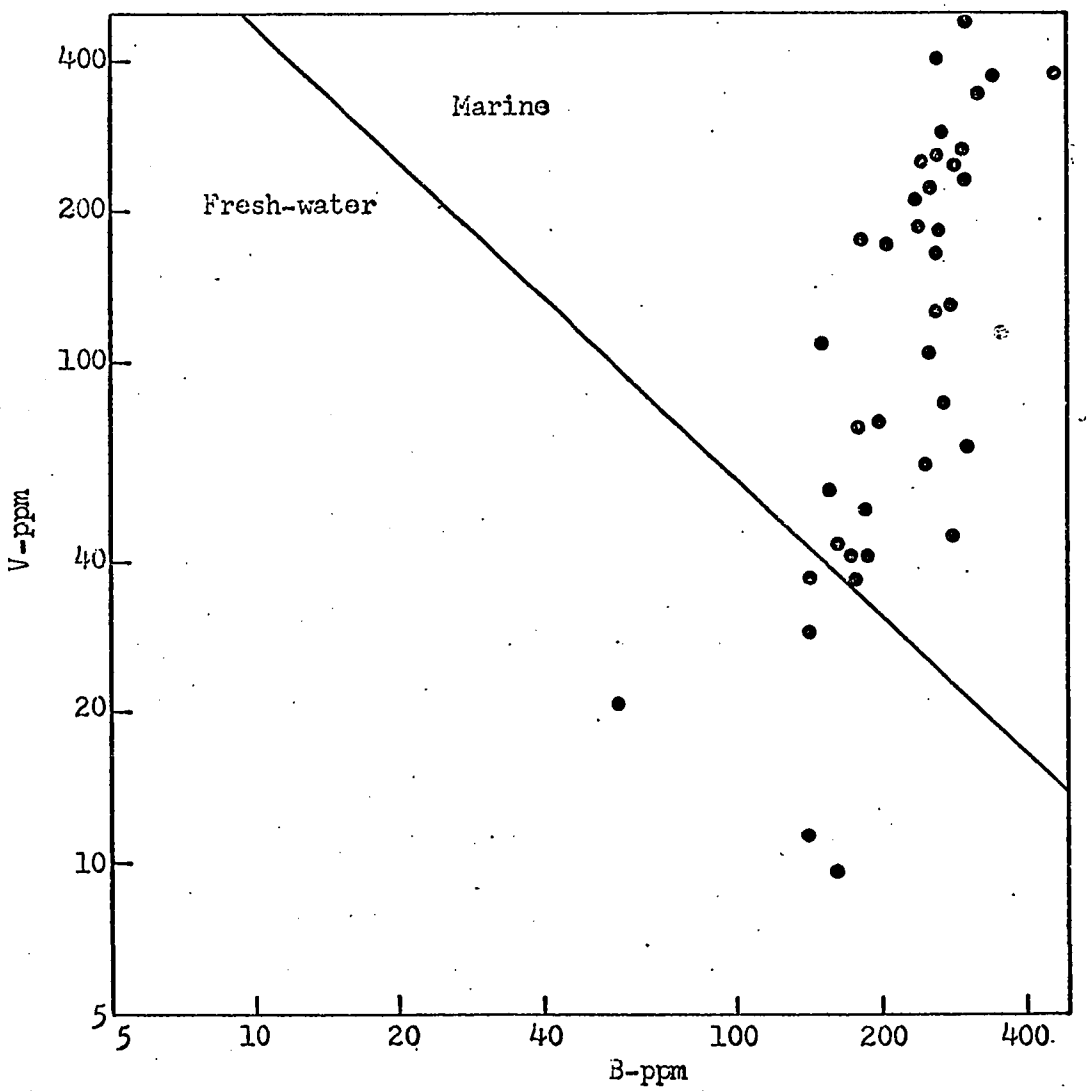

Figure 18. Plot of B and V concentrations of bulk samples of the Louisiana sideritic chamosite ores and estimated line of separation between marine and fresh water fields (after Potter et al, 1963).

Utilization of Individual Trace Elements as Possible Environmental Indicators

Boron

Goldschmidt and Peters reported that boron is enriched in marine but not in the lacustrine iron sediments (in Landergren, 1945, p. 24). After a study of the distribution of boron in the Liassic sediments in Southern Sweden, Palmquish concluded that the high boron content (0.01-0.1 percent B_2O_3) of these ores indicate that they must be considered marine sediments (in Landergren, 1945). Landergren (1945) concluded from studies of Swedish Precambrian iron ores that boron is enriched in those ore types relating to an original marine environment of deposition. He implied that boron enrichment in the marine iron sediments is caused by boron adsorption from sea water.

The boron content in the Louisiana ore deposits ranges from 75 to 500 ppm, averaging 269 ppm. These values are in general higher than those reported by Landergren (1945, p. 25) for typical marine sedimentary iron ores. Perhaps this is suggestive of a higher than normal salinity for these deposits.

Even though the validity of trace elements as environmental discriminators has been demonstrated, relationships between mineral composition, especially for argillaceous sediments, and trace element concentration have not been established. Landergren (1958) found from experimental data on deep sea sediments that approximately 90 percent

by weight of the boron is bound to the clay and medium silt-sized material. Frederickson and Reynolds (1960) conducted studies on the distribution of boron in illite, kaolinite and chlorite, and they concluded that boron seems to be preferentially associated with illite. From geochemical considerations, Degens (1965) was of the opinion that boron should substitute for aluminum in the tetrahedral position of layered silicate minerals.

Vanadium

As stated by Degens (1965, p. 244), "Iron and manganese oxides and hydroxides are known for their ability to scoop up trace elements such as vanadium and nickel in amounts up to 1000 ppm (Krauskopf, 1955; Keith and Degens, 1959)." In his geochemical study of the Blaine Formation of Oklahoma, Everett (1962) proposed that vanadium, chromium, cobalt, and nickel are probably associated with the occurrence of iron. Supposedly, these elements would substitute in iron compounds, be adsorbed on the clay mineral with iron, or substitute for iron in the clay structure (Wu, 1969, p. 64). According to Goldschmidt (1958, p. 495), "The trivalent form of vanadium, which is probably a substantial part of the vanadium in average marine hydrolysate sediments, may be bound in clay minerals in the same way as aluminum." He also states that in oxidate sediments rich in iron the vanadate ion is commonly concentrated to a considerable extent, together with phosphate and commonly

arsenate. In ordinary limonite or hematite sediments of marine origin, the amount of vanadium is normally between 500 and 800 ppm, and rarely less than 100 ppm or more than 1,500 ppm (Goldschmidt, 1958, p. 495). He also points out that concentration of vanadium from sea water into sediments by bottom-mud dwellers like holothurians has allegedly taken place. There is a remarkable uniformity in the concentration of vanadium and boron in these green ore deposits. In some samples the concentrations are exactly the same whereas in others they differ somewhat, but in general, a relative increase or decrease in one corresponds to a similar increase or decrease in the other. Therefore, the factors controlling the distribution functions of vanadium and boron in these deposits must be related. If vanadium is actually concentrated in sediments by bottom-mud dwellers like holothurians, then the presence of extensive worm burrows in these deposits could be construed to imply a similar mode of concentration of this trace element. Because vanadium and boron allegedly concentrate in sedimentary iron ore deposits, the concentration of these trace elements may be directly related to the presence of limonite or chamosite. Regardless of the mode of concentration, both elements are present in concentrations considered to indicate marine conditions.

Copper

The amount of copper in these samples is in general quite low. It ranges from 1 to 33 ppm but averages less than 10 ppm. In general,

these concentrations are lower than the values normally reported for typically marine sediments, but a number of variables could account for this anomaly. Perhaps the concentration of copper in the sea water was lower than that associated with typically marine sediments, or perhaps the distribution functions of copper were not the same for these deposits. As pointed out by Goldschmidt (1958, p. 185), "The actual amount of copper in sea water, previously considered to be quite well known, has become a controversial matter since H. Wattenberg . . . found much less than previously reported." Perhaps there is some correlation between decreased copper concentrations and high vanadium concentrations similar to that which exists in marine animals (Goldschmidt, 1958, p. 186). This fact is thought to corroborate the well established view that vanadium and copper serve closely analogous physiological functions in the conveyance of oxygen by the blood (Goldschmidt, 1958, p. 186). The general absence of marine animals, except for worms, may also help to explain the low concentration of copper in these deposits.

From studies of the relation of copper to various organic groups, Riley (1939, in Goldschmidt, 1958, p. 187) concluded that copper can be removed from sea water by organic matter, and that during periods of organic growth the copper content is slightly increased in the resulting organic matter. Perhaps locally higher concentrations of copper in these deposits may be related to higher concentrations of organic material.

Gallium

The amount of gallium in sea water is low; therefore, the amount of gallium in marine sediments would be expected to be low. This is actually the case for these sediments. The gallium content never exceeds 4 ppm and it commonly is 1 ppm or less. According to Goldschmidt and Peters (1932a, in Rankama and Sahama, 1950, p. 727), the Ga:Fe ratio in sedimentary iron ores is of the order of 1:100,000.

Gallium is probably associated with the clay content of these deposits. Several investigators have suggested that gallium is directly associated with clay minerals (Migdisov and Borisenok, 1963; Goldschmidt, 1958).

Zirconium

According to Rankama and Sahama (1950, p. 566), "Very few determinations are available to show the content of zirconium in sediments. Degenhardt (1957, p. 279) reported that in general the sedimentary rocks contain about the same amount of zirconium as igneous rocks, averaging 156 g Zr/t. He also pointed out that alkalic rocks normally contain about twice as much zirconium as rocks of calcalkalic character with alkalic syenites containing up to 680 g Zr/t. Rankama and Sahama (1950, p. 267) also report that large quantities of zirconium exists in the form of the mineral eudiatite in nepheline syenites. The observations perhaps can help to explain the high

concentration of zirconium in these chamosite ores, attaining over 2000 ppm in some samples. Weathering of alkalic igneous rocks such as the nepheline syenites in Arkansas could supply large quantities of zirconium. In his study, Degenhardt (1957) found $ZrSiO_4$ to be slightly soluble in solutions of bicarbonate of calcium. Zirconium going into solution by such a weathering process would be precipitated in the hydrolyzate sediments by adsorption because zirconium is rather readily removed from solution by hydrolysis and does not form secondary minerals (Rankama and Sahama, 1950). Ronov et al (1961, p. 354) found that the percentages of Al, Ga, Ti, Zr, and Hf are considerably higher in the clays formed under humid conditions as a result of deep chemical weathering than in clays formed under arid conditions in the early stages of weathering of the parent rocks. They also discovered that kaolinitic clays are enriched in zirconium and hafnium and that zirconium is enriched relative to hafnium in the reducing humid environments of the sedimentation basin. According to them, zirconium and hafnium released by the hydrolysis of alumino-silicates and silicates form complexes with the organic acids. Zirconium forms complexes more intensely than hafnium owing to its more pronounced amphoteric properties. This would result in the more efficient removal of zirconium than hafnium and would thus increase its concentration relative to hafnium.

Based on these premises, perhaps a portion of the zirconium

in these ore deposits is adsorbed on the constituent clays, particularly the kaolinitic clays.

Zirconium is commonly contained in resistant minerals which are stable against mechanical and chemical weathering; therefore, zirconium is also concentrated in the resistates. According to Degenhardt (1957, p. 279), zirconium is concentrated in rutile, sphene, magnetite, ilmenite, and apatite. As reported by Ronov et al (1961, p. 354):

> Zirconium and hafnium are concentrated in the clays principally in the silt-sand fraction (0.1-0.01 mm), and their main mass is bound in the accessory zircons and titanium minerals. The quantity of these minerals and the content of Zr and Hf in the clays increases towards the source area indicating the detrital origin of a considerable part of the Zr and Hf and the connection between these elements and deep weathering and accumulation of stable residual material.

The basin of deposition of the Louisiana ores is not far from the original source area for such possible resistates, and as might be expected, the Louisiana ores contain accessory quantities of certain of these zirconium-bearing minerals (e.g., zircon, rutile and apatite). Thus, at least a portion of the high zirconium content in these deposits is present in these stable mineral forms.

Manganese

The fact that manganese in sedimentary rocks is paragenetically related to iron was pointed out by Ronov and Ermishkina (1959, p. 266). Goldschmidt (1958, in Everett, 1962) pointed out that

sedimentary occurrences of manganese are normally associated with iron. According to Ronov and Ermishkina (1959) the ratio of manganese to iron remains approximately unchanged in the sands and clays, but in carbonate rocks this ratio changes toward more manganese indicating that in areas of carbonate sediment accumulation takes place in the presence of geochemical processes which lead to some separation of manganese and iron. In reference to factors controlling the separation and concentration of manganese and iron, Ronov and Ermishkina (1959, p. 266-267) state:

> In accordance with the latest summary of K. B. Krauskopf and a number of earlier papers, the separation of iron and manganese and the concentration of the latter occurs under the influence of various factors, among which essential roles are played by the lower solubility of the trivalent and bivalent iron compounds (for certain values of pH and Eh), the activity of iron and manganese bacteria, and the loss of acid solutions of manganese into an alkaline medium such as usually are ocean waters, subsurface waters of arid regions and contacts with limestones.

Results of studies by Ronov and Ermishkina (1959) show that the maximum manganese content is associated with coastal facies deposits and gradually decreases in amount from the coastal zone in the direction of the open sea towards the pelagic facies deposits. Concentration of manganese primarily in the coastal facies deposits would thus occur when acid streams carrying manganese in the soluble divalent form encountered the alkaline ocean medium, oxidizing the manganese into immobile trivalent manganese, and depositing these along with other

sediments. According to the writers, increased manganese contents in the sediments would shift in the direction of the open sea under weathering conditions in a humid climate whereas under the conditions of an arid climate the zone of maximum manganese concentration migrates in the direction of the continent.

The high concentrations of manganese in these deposits, exceeding 1000 ppm for the most part, possibly suggests that they were deposited as coastal facies deposits near a landmass undergoing weathering in a humid climate. The discontinuous nature of the chamosite lentils which limits their occurrence to a long, narrow band is also suggestive of coastal facies deposits. The laterites and bauxites in the postulated source area for the iron could only have resulted from intense leaching in a humid environment. The presence of enormous quantities of ferrous iron associated with these deposits either indicates that the streams transporting the iron to the basin of deposition had a pH of 7 or less (Krumbein and Garrels, 1952) or that ferric iron transported as colloidal ferric hydroxide in more basic waters was reduced in the environment of deposition by extremely large masses of organic material. Perhaps former large masses of organic material have been subsequently oxidized and consequently disappeared, but the present low organic content of these deposits suggests the first alternative for the presence of the ferrous iron.

The distribution of the manganese in these deposits is

incompletely known, but a major portion of it is present in the form of siderite. Substitution of Mn^{+2} for Fe^{+2} in the siderite structure probably occurred during direct precipitation of siderite from sea water. Rhodochrosite or other primary manganese-bearing minerals were not identified in these deposits. Part of the manganese is associated with the clay content but the nature of this association is incompletely known.

Nickel and Chromium

Control mechanisms for the concentration of nickel and chromium are in general less well known than for the other elements discussed. One of the important studies in the area of the geochemistry of these elements was done by Krauskopf (1956). While conducting experiments on factors controlling the concentration of 13 rare elements in sea water (including Ni and Cr), Krauskopf (1956) found normal sea water to be undersaturated with these elements, even in places where the pH and temperature have extreme values. Therefore, he concluded that a mechanism (or mechanisms) of concentration other than direct precipitation of compounds from normal sea water with these ions present must be responsible. He experimented with several possible control mechanisms, including adsorption, organic reactions and local precipitation of sulfides, to determine how these elements were concentrated. From the results of such experiments, he concluded

that the control of chromium concentration is most reasonable ascribed to local reduction and precipitation of the element as insoluble $Cr(OH)_3$. He further proposed that whereas reduction in sulfide-rich environments may be a possible control mechanism, sulphide is not required because any reducing environment capable of changing chromium to the trivalent form will result in its reduction and removal.

The mechanism of concentration of nickel was more difficult to explain due to negative or inconclusive experimental results, but based on the failure of alternative hypotheses and on indirect evidence of enrichment of these elements in organic sediments and marine organisms, Krauskopf (1956) concluded that the most plausible mechanism of concentration of nickel is by organic reactions. Experimental data ruled out the possibility of adsorption and local sulphide precipitation as possible mechanisms for nickel concentration. The strong adsorption of Co and Ni on the hydrated oxides of iron and manganese is a convenient explanation for the frequent presence of these elements in iron and manganese ores (Krauskopf, 1956).

Rankama and Sahama (1950, p. 623) proposed that because chromium closely resembles ferric iron and aluminum in its chemical properties, ionic size, and ionic charge, it follows these ions during its exogenic cycle. They pointed out that little chromium remains in solutions formed during weathering and as a result chromium becomes enriched in the hydrolyzates.

As pointed out by Potter et al (1963), B, Cr, Cu, Ga, Ni, and V are significantly more abundant in marine than in fresh-water argillaceous sediments. The concentrations of Cr in these rocks, averaging 25.4 ppm, is in excess of that listed by Rankama and Sahama (1950, p. 623) for marine siderite ores (20 ppm). The control mechanism for the concentration of chromium in these deposits is not clearly understood, but the mechanism proposed by Krauskopf (1956) could easily be applicable here because the very nature of the chamositic iron deposits necessitates a reducing environment. Nickel occurs in concentrations in the Louisiana ores, averaging 100 ppm, greater than those listed by Potter et al (1963, p. 685) for ancient marine argillaceous sediments. Perhaps strong adsorption of Ni on the hydrated oxides of iron and manganese as suggested by Krauskopf (1956) is the control mechanism for such high concentrations of Ni in these ores.

PROVENANCE AND ENVIRONMENT

Source

A search of the literature reveals several theories to explain the abnormal concentrations of iron in sea water necessary for deposition of iron, but these theories fall into two general categories. The "from-above" theory assumes that the iron came with streams from eroded, iron-rich areas of adjacent continents whereas the "from-below" theory assumes that the iron comes from below the sea bottom, e.g., from submarine springs or exhalations of volcanic origin. A modification to the "from-below" theory assumes that the iron was derived by mobilization of iron in marine bottom sediments.

In his classical paper on sedimentary iron ores, which ties the environmental characteristics to the observed facies, James (1954, p. 276) concluded that in order to explain deposition of iron-formations it was necessary to have, ". . .the barred or restricted basin of deposition coincident with deep chemical weathering of the land surface." In defense of his proposed source for the iron, James (1954, p. 276) states:

> The factor that led Van Hise and Leith to the volcanic theory was the apparent inadequacy of "ordinary weathering"

> to supply solutions of the proper type for precipitation of iron formations. However, as pointed out by Gruner, Gill, and James, under certain tropical or subtropical conditions the iron and silica content of stream water may be very high and entirely adequate to account for iron-formation deposition.

And in conclusion James (1954, p. 277) postulates, "It seems to the writer that volcanism, though not uncommon during the deposition of the major iron-formations, does not have a close enough correlation in space and time with the iron-rich sediments to be genetically related to those sediments."

Oftedahl (1958, p. 1) postulated that the only probable explanation for the sudden appearance of iron in the sea in quantities sufficient to form large sedimentary iron ore formations is to assume that the iron source is volcanic exhalations from chambers of granitic magma below the sea floor. Kautsky (1958) criticized Oftedahl's theory mainly on the basis that it strongly contradicts previous genetical interpretations of ores in areas where it was applied. In response to Oftedahl's work, Landergren (1958) proposed that geochemical data of the sedimentary iron ores of Central Sweden, to which the theory had been applied, did not support an exhalative-sedimentary theory for their origin. Marmo (1958, p. 277) agrees in general with Oftedahl's exhalative-sedimentary theory, but he ". . .does not fully share Oftedahl's opinions as to the generalization of this factor in ore formation, or concerning the origin of the gaseous exhalations." He

believes that the exhalations may derive either from magmas or from sediments situated close to the hot magma reservoirs but not solely from granitic magma chambers. "Cissarz suggests that submarine springs or exhalations of volcanic origin may have contributed Fe, SiO_2, and CO_2 to the sea water during the deposition of some or all of the Western Macedonian deposits, but recognizes that local evidence is lacking at Tajmiste," (in Page, 1958, p. 14).

Brochert (1960, p. 26) contends that, "Since trivalent iron is practically insoluble in the presence of oxygen. . .the mobilization of iron by weathering solutions in continental regions could not have contributed significantly to the formation of marine iron ore deposits in pre-Devonian times." He further proposes (p. 261) that, "The mobilization and precipitation of iron ore deposits must then have been effected within the oceans themselves." He implies that the iron is mobilized from pre-existing sediments by separating Si-Al components from the iron in a CO_2 zone under reducing conditions. Supposedly, most of the dissolved iron moves towards the oxygen-rich shallow sea where it is deposited as limonite oolites whereas a considerable proportion of the dissolved iron is precipitated in the CO_2 zone itself to form sideritic clay ironstone. Only very little iron reaches the H_2S facies of the deeper zones to be deposited as pyrite.

Carrol suggested that in many deposits transportation of iron took place as a shell of iron oxide at the surface of clay minerals,

and that removal and concentration of the iron might take place after initial sedimentation if the environment became one that permitted reduction and dissolution of ferric oxide. She demonstrated that bacterial activity could result in a change of Eh and pH conditions to those appropriate to the solution of iron oxide, and that solution actually was accomplished (in Garrels and Christ, 1965, p. 384).

Due to the lack of associated volcanic material in the Louisiana deposits, it is assumed that these sedimentary ironstones formed near a fluctuating shoreline in close proximity to a landmass capable of supplying large quantities of iron. The ultimate source of the iron is an interesting problem. Probably it was derived by intense leaching of iron-bearing rocks immediately to the north, e.g., that which produced the extensive laterites and bauxites in Arkansas. This opinion is also shared by Dr. F. C. Loughnan (Personal Communication, 1968). A good example of the results of such an intensive leaching process can be seen in bauxites at Bauxite, Arkansas, where iron-rich nepheline syenites have been reduced to the end product of weathering, bauxite. The chemical alteration products of igneous rocks could also be a source for the necessary alumino-silicates as well as for the detrital quartz, clays, and feldspars intimately associated with the primary iron minerals.

If sufficient concentrations of this iron accumulated in restricted basins, along with an abnormally high silica content, the

combination of these elements along with other ions could, under the proper conditions of salinity, pH, Eh, and temperature, produce the different iron-bearing minerals present in these deposits. Normal sea water is undersaturated in silica (Krauskopf, 1959) and low in iron; therefore, it is imperative that concentrations of these ions increase markedly before crystallization starts.

The mode of transportation and concentration of the iron is more difficult to speculate on than is the source of the iron. The pH and Eh of the transporting medium are the most decisive factors in determining the mode of transportation and concentration of iron. The solubility of iron in the transporting medium is a function of the pH and Eh. Krumbein and Garrels (1952) concluded that for iron transported in true solution the transporting medium would presumably have to have a pH of 7 or less and an Eh in the range approximately -0.1 to +0.3. They stressed that this set of conditions did not include iron carried in colloidal suspension. After conducting experiments on transportation and deposition of iron, Castano and Garrels (1950) concluded that rivers of moderately low pH might well contain considerable quantities of ferrous iron and the resulting iron mineral precipitated when these streams entered ocean basins depended on the Eh, pH, and chemistry of the sea water. River water pH varies considerably, as does the concentrations of iron reported for different rivers, but some rivers have pH values of 7.0 or slightly lower. Average river waters contain

less than one part per million of iron (Taylor, 1949), but some with concentrations up to 61 parts per million have been reported (Moore, 1910, in Taylor, 1949, p. 80). "Experiments by Gruner (1922) and Moore and Maynard (1929) have shown that the solubility of iron is appreciably increased in carbonated waters and solutions of organic acids," (Taylor, 1949, p. 80).

As pointed out by Taylor (1949, p. 80):

> There is considerable divergence of opinion as to the chemical state in which iron is most likely commonly transported. Harder (1919) believes that it is carried mainly as ferrous bicarbonate and to some extent also as ferrous or ferric sulphate or as compounds of organic acids. Van Hise and Leith (1911) suggest it may be as a ferrous salt of silicic, carbonic, sulphuric, hydrochloric or other acids. Aschan (1907) believes it is carried as soluble ferrihumates or ferrohumates, Hayes (1915) as salts of organic acids, as chlorides and sulphates and as ferrous bicarbonate. Gruner (1922) holds the view that iron is largely present in organic colloids or adsorbed by organic colloids. Moore and Maynard (1929) believe that most of the iron is transported as a ferric oxide hydrosol stabilized by the organic colloids in the water with smaller quantities carried as salts of organic and inorganic acids. Gill (1927) suggests that iron may also be transported as a ferrous silicate hydrosol.

The two states more frequently referred to are true solution and colloidal suspension.

Environment

According to James (1954, p. 242), "A number of workers, notably Moore and Maynard and Gruner, have produced evidence to show

that iron is transported most readily as a ferric hydrosol and that it probably is in this form that most iron reaches the sea." Regardless of the mode of transport, once introduced into the environment of deposition, precipitation of the iron as a specific mineral type is dependent specifically upon the Eh and pH of the resulting sea water (Krumbein and Garrels, 1952). As proposed by James (1954, p. 240):

> The depositional environments of the iron-rich rocks clearly belong to their class of "restricted" environments, in which "physiographic, tectonic, or biologic features impose controls on circulation, oxygenation, or concentration of dissolved salts." In this type of environment, the oxidation-reduction potential, Eh, may range from positive (or oxidizing) at the surface to strongly negative (or reducing) at depth; the hydrogen-ion concentration, pH, may show a range that indicates mild alkalinity at the surface, changing to neutral or even slightly acid at depth. Concentration of dissolved salts may show wide variation, particularly when free circulation of water to the open ocean is inhibited.

Iron entering such a basin as ferric hydroxide would be precipitated by salt water, and iron entering the oxidizing surface waters of this basin in true solution would be converted to and precipitated as insoluble ferric hydroxide. As this colloidal ferric hydroxide settles into lower and more reducing waters of this basin, it is likely that the iron would be reduced and either go into solution or be replaced or reprecipitated as a ferrous mineral in equilibrium with the new environment. This line of reasoning is in agreement with James' (1954, p. 244) conclusion that:

> The solubility of iron in surface waters of the basin

is almost negligible. Using values obtained from Krumbein and Garrels (57), we may assume a pH of about 8.0 and an Eh of about +0.2, at which the activity of Fe^{++} plus Fe^{+++} ions is about $10^{-10.5}$, and ferric hydroxide is a stable precipitate. But as the flocculent material slowly settles, it may, in a "restricted" basin, sink into an environment more acid and less oxygenated. In such an environment a typical value for pH would be 7.5 with an Eh of -0.1, at which the activity of Fe^{++} plus Fe^{+++} is about $10^{-4.7}$, and the stable iron mineral is $FeCO_3$. This tremendous increase in solubility would cause the flocculent hydroxide to either go into solution and thus greatly increase the Fe^{++} content of the water, or, if the solubility product of $FeCO_3$ were exceeded, to be reacted with or to form a ferrous precipitate.

Krumbein and Garrels (1952) prepared diagrams showing the fields of chemical stability of certain groups of minerals as functions of pH and oxidation-reduction potentials. Since the precipitation of minerals under any given set of temperature and salinity conditions depends upon the activity and activity products of the ions involved, construction of the Eh-pH fields of stability for all species were based upon calculations involving these physico-chemical constants (Krumbein and Garrels, 1952, p. 10). If the activities are known, the pH and Eh can be calculated from known equations. By substituting these calculated values in the Nernst equation ($E = Eo + \frac{RT}{nF} \cdot \ln C$), the writers arrived at values of Eh and pH at which the various chemically precipitated minerals can exist in a stable state. They applied this method to the problem of the origin and classification of chemical sediments as a function of the Eh and pH. Figures 19, 20, and 21 show the stability zones of

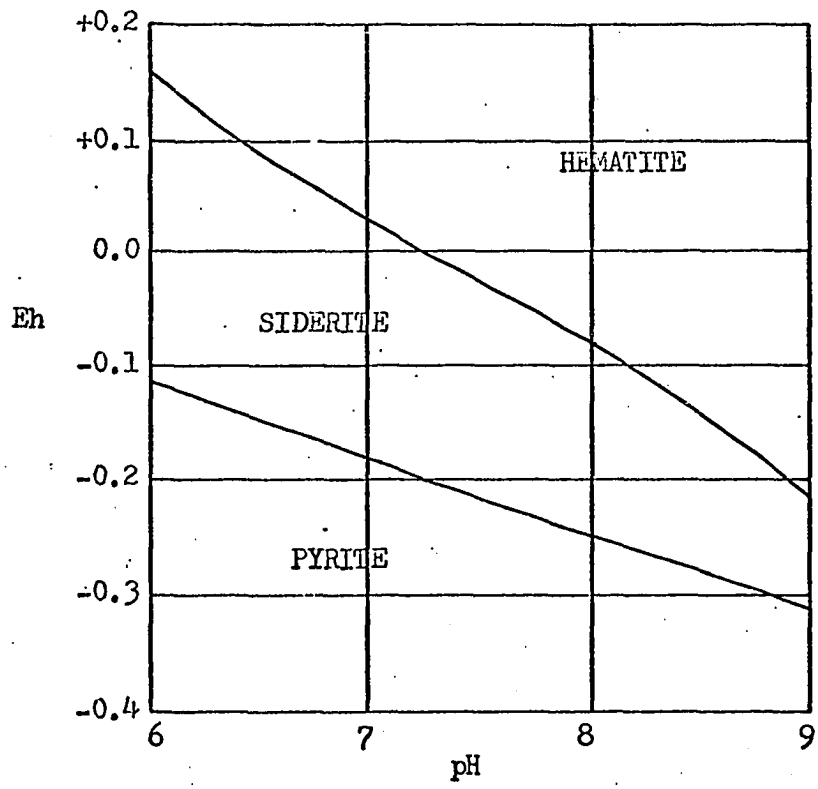

Figure 19. Fields of stability of hematite, siderite, and pyrite (From Krumbein and Garrels, 1952, p. 12).

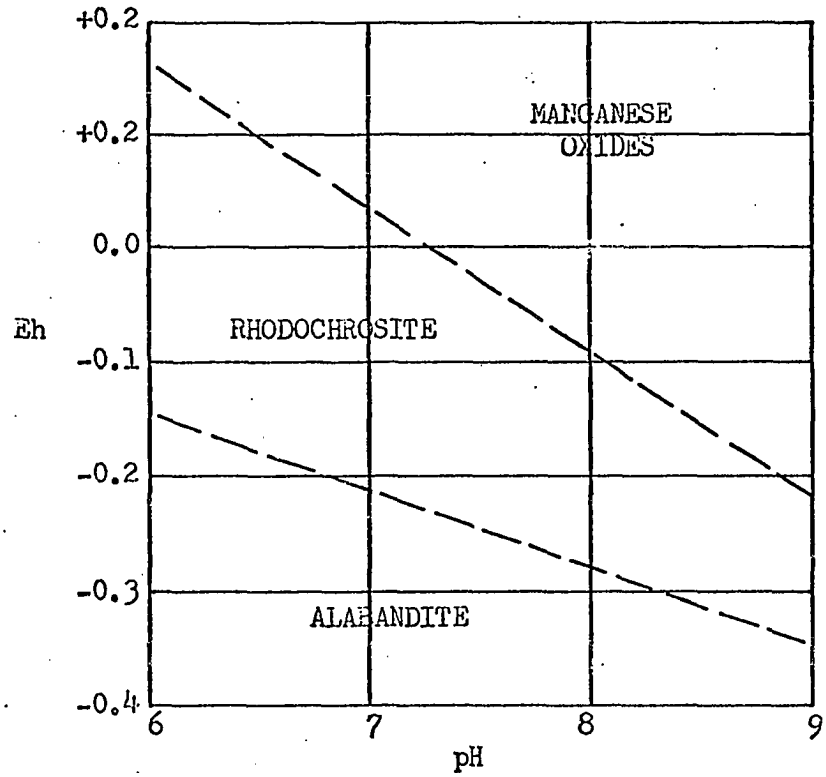

Figure 20. Approximate fields of stability of manganese oxides, rhodochrosite, and alabandite (From Krumbein and Garrels, 1952, p. 14).

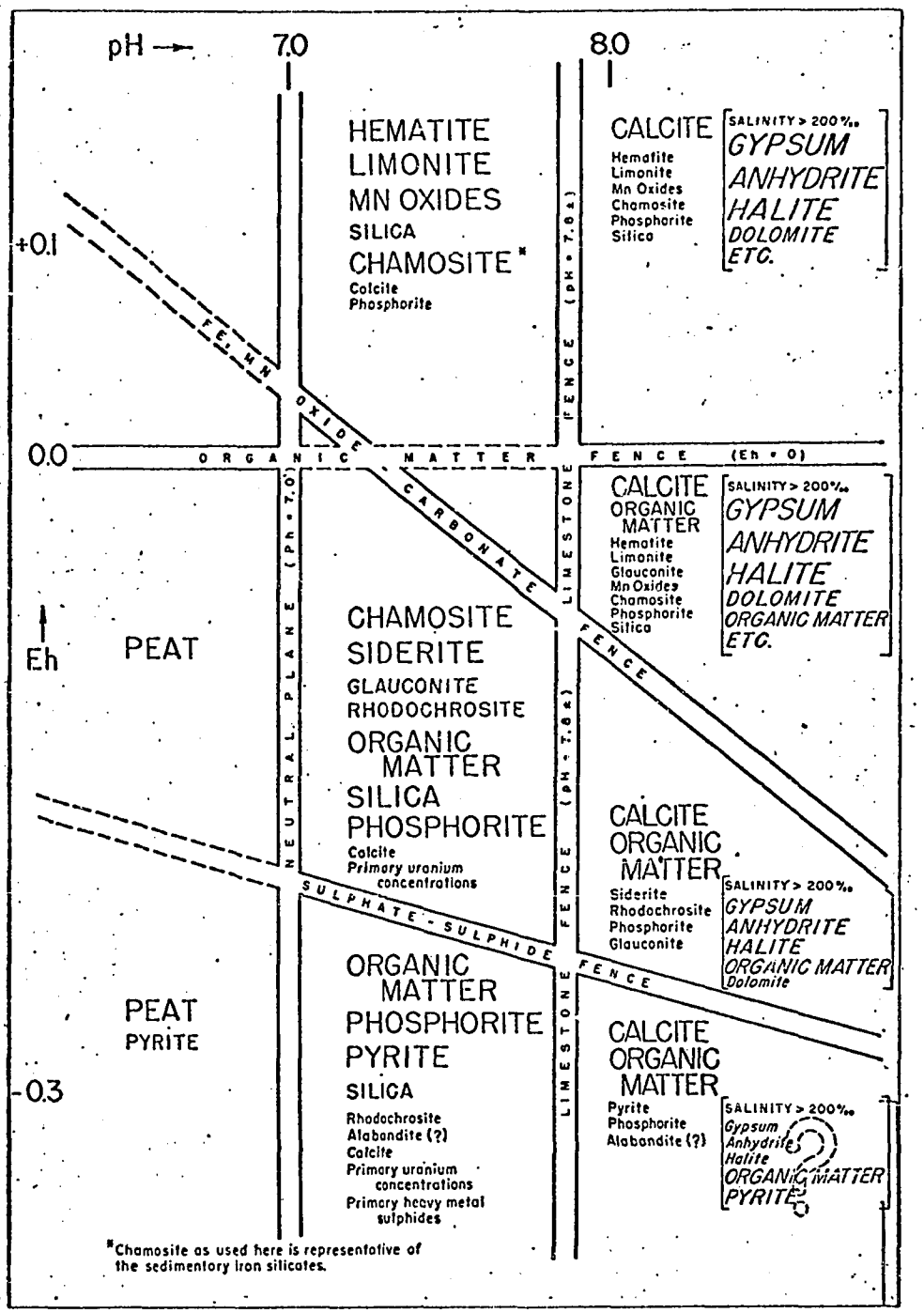

Figure 21. Sedimentary chemical end-member associations in their relations to environmental limitations imposed by selected Eh and pH values. Associations in brackets refer to hypersaline solutions (From Krumbein and Garrels, 1952, p. 26).

iron and manganese minerals, calcite, and phosphorite which were constructed by Krumbein and Garrels from values determined by computing the activity of ferrous and ferric ions, carbonate ions, sulfide ion, and the hydroxyl ion on the one hand, and by computing the concentrations of the trivalent and bivalent iron and the sulfide ion on the other hand (in Sokolova, 1962, p. 10).

Thus, in marine mediums of constant salinity and temperature the precipitation of minerals such as hematite, siderite, and pyrite depends on the activity of the ferrous and ferric ions and the concentration of carbonate, sulfide, and hydroxyl ions. From the diagrams referenced above, it is seen that siderite or pyrite and the manganese minerals alabandite or rhodochrosite are stable for negative Eh values and a pH of 7 and more while hematite or manganese oxides are stable for positive Eh values. Very broadly, then, the activity product of hematite is most likely to be exceeded in solutions of high Eh and high pH, for they would have a high Fe^{+++}/Fe^{++} ratio (determined solely by Eh) and a high hydroxide concentration. Siderite would be favored by solutions of low Eh and high pH, providing a high Fe^{++}/Fe^{+++} ratio and high carbonate ion concentration. Pyrite would be favored by solutions of low Eh and high pH also, for they promote the formation of both Fe^{++} ion and $S^{=}$ ion. Krumbein and Garrels (1952) found the stability fields to be essentially independent of temperature, pressure and composition of the sea water system from which the

minerals precipitated. They further concluded that the solubility of carbonates and phosphates depends only on the pH (not affected by Eh), and they are only precipitated under alkaline conditions.

Krumbein and Garrels' (1952, p. 26) fence-diagram showing the fields of occurrence of typical chemical end-member associations in terms of Eh and pH shows a mineral assemblage which corresponds very closely to the assemblage constituting the North Louisiana chamosite deposits (Figure 20). This assemblage, consisting of the primary constituents chamosite, siderite, organic matter, silica, and phosphorite and the accessory minerals rhodochrosite, glauconite and calcite would indicate an environment in which the pH was 7.0 to 7.8±, and the Eh was 0.0 to -0.2±. The Louisiana ores are composed chiefly of chamosite and siderite with minor organic matter, calcite, pyrite, magnetite, ilmenite (?), collophanite and variable quantities of limonite. Most of the limonite (or goethite) is probably a secondary alteration product resulting from late or post-depositional oxidation of primary siderite and chamosite due to an increase in the oxidational potential of the then existing environment. Slight upward or downward shifts of Eh reflecting temporary or local changes in Eh could account for the presence of minerals such as ilmenite and pyrite. "Magnetite, although stable under approximately the same Eh conditions as siderite, will form in preference to siderite under alkaline pH conditions," (Huber, 1958, p. 137). Slight changes towards more alkaline conditions

locally could therefore account for the irregular distribution of magnetite in these deposits.

Studies of equilibrium stability relations among iron minerals under variable conditions of Eh, pH, P_{CO_2} and P_{O_2} led Garrels and Christ (1965, p. 228) to conclude that:

> In terms of the primary sedimentary iron ores, it is obvious that a siderite facies can be obtained by having a high dissolved CO_2 and by removing sulfide sulfur from the system; a silicate facies, by removing sulfur and high CO_2 content, while preserving enough silica to yield chert; a magnetite facies, by reducing sulfur, CO_2, and maintaining silica at a value undersaturated with respect to amorphous silica.

Castano and Garrels (1950) after conducting experiments on the deposition of iron, with special reference to the Clinton Iron Ore Deposits, concluded that iron-bearing solutions moving into aerated ocean waters containing calcium carbonate will precipitate ferric oxide and that with the addition of silt and perhaps a slight lowering of pH they may be expected to precipitate chamosite. The silt would presumably serve as nuclei for crystal growth during precipitation of chamosite. They further concluded that if streams discharge into an area of stagnant water where organic debris tends to accumulate, the minerals might well be chamosite (if silt is present) or siderite and pyrite.

A study of the literature reveals that the general consensus of opinion regarding the origin of bedded sedimentary iron deposits

is that they are chemically precipitated sediments predominantly of marine origin, that they are in the main shallow water deposits, and that the iron was derived from continental sources by the normal processes of erosion.

Castano and Garrels (1950) concluded that the Clinton Iron Ore Deposits were shallow water deposits on the basis of the existence of extensive surface markings, cracks, and tracks of crustaceans and worms in the shales and sandstones of these deposits. The Wabana ores in Newfoundland show ripple marking and current bedding while erosion surfaces are indicated by the presence of abundant worm burrows (Hayes, 1915).

The occurrence of extensive worm borings in the Louisiana sedimentary ores coupled with the occurrence in some places of current bedding in sections of some exposed lentils strongly suggest that they are also shallow water deposits. A shallow environment of deposition for these deposits is also suggested by their characteristic vertical gradation in both directions into sandstone beds consisting of poorly sorted detrital quartz, muscovite mica, clays, and abundant carbonaceous plant debris and fossil wood suggestive of backswamp or deltaic deposition. The restriction of these deposits to a narrow NW-SE trending belt by lateral facies changes is also suggestive of nearshore, shallow water deposits. Landward facies changes are marked by a progressive landward increase in clastic sandstones, shales and organic

material while basinward changes reflect increases in marine clays, sand and fossils. All evidence indicates that these deposits were laid down near a fluctuating shoreline as part of the major upper Cook Mountain-lower Cockfield regressive phase between the underlying marine lower Cook Mountain and the overlying non-marine Cockfield. The fluctuating shoreline may have been that of the open gulf as it exists today or that of a lagoon freely connected with the open gulf.

Most of the chamosite and siderite of these deposits is considered to be primary. In typical chamosite oolites the concentric growth rings of cryptocrystalline chamosite around quartz nuclei could only have formed by direct crystallization. Chamosite oolites intimately mixed with clays and other detrital material may represent reconstituted faecal pellets as suggested by Porrenga (1965). Taylor (1949, p. 81) proposed that, "There is no evidence whatever in the Northampton Sand to suggest that chamosite is other than a primary precipitate . . ."

Most of the siderite groundmass is thought to have been precipitated directly from waters where the partial pressure of CO_2 was low enough to exceed the solubility product of $FeCO_3$ and the Eh of the environment was non-oxidizing. Precipitation would be encouraged in warm waters in which the degree of dissociation of the bicarbonate would be relatively high and/or in waters where the removal of carbon dioxide in the process of photosynthesis actively takes place (Taylor, 1959, p. 81). The carbon dioxide must no longer be present in

sufficient quantities to maintain all the iron as soluble bicarbonate. Some primary siderite was also laid down as fine siderite muds and was later recrystallized to form siderite spherulites and granular aggregates of siderite. Because the solubility of CO_2 in water decreases with increasing temperature, it is likely that the conditions in the basin of deposition were quite warm. Neutral to slightly reducing conditions would have been essential. Reduced circulation due to local restrictions to water circulation and/or to depletion of the oxygen content by oxidizing large masses of organic material would produce this effect. Because increasing CO_2 decreases the pH of the depositional media and lower pH values increase the solubility of siderite, it stands to reason that the partial pressure of CO_2 was an extremely important factor in determining the deposition or non-deposition of siderite.

There is some diagenetic chamosite but quantitatively it is not significant. There is considerable secondary siderite. This results from recrystallization of finely-divided siderite originally widely disseminated in clay muds as granular siderite or siderite spherulites. This is a relatively simple chemical equilibrium process by which concentrated aggregates of material have lower free energy than the same material widely disseminated. Siderite is also a very prolific diagenetic replacement mineral, and it accounts for the major part of the secondary siderite. In discussing the diagenetic

changes expected in mineral associations within certain stability fields, Krumbein and Garrels (1952, p. 16) state:

> The usual effect of diagenesis is to cause a decrease in Eh and relatively little change in pH. If an original deposit of hematite were subjected to such a change, so that the Eh dropped into the siderite field of stability, one might expect to find at least a little siderite replacing hematite. On the other hand, if the Eh change were drastic and caused a rapid drop all the way down into the pyrite field, one might find some pyrite replacing hematite.

This line of reasoning is relatively straight forward when considering replacements among chemically related iron minerals, but the replacement of quartz, chamosite, feldspars, etc., by siderite is somewhat more difficult to explain. In such situations, complete disruption of silicate structures are involved. The solubility of silica is little affected by pH values between 1 and 9 but rises rapidly at values greater than 9 (Krauskopf, 1959). The writer interprets this to mean that either the pH of the environment of deposition changed to much more alkaline conditions during late stages of deposition or that the pH of residual pore fluids after accumulation of the deposits was considerably higher. Either case would necessitate a restricted environment with abnormal concentrations of alkali metal ions because normal sea water seldom exceeds pH 8.5.

Sideritization in the North Louisiana ores is similar to that reported for the Northampton ores, and the statement by Taylor (1949, p. 82) that "While this extensive sideritization is evidently largely

of post-accumulation date it seems probable that it was a penecontemporaneous reaction" seems to apply to the North Louisiana ores. Perhaps some of the sideritization of these ores occurred in a manner similar to that given by Hayes (in Taylor, 1949, p. 82):

> In the case of the Wabana ore Hayes (1915) believes that replacement of chamosite and other minerals by siderite took place in the lower layers of the sea floor where ammonium carbonate resulting from the decomposition of organic matter reacted with iron salts in the sea water with formation of the corresponding ammonium salts and the precipitation of siderite. Thus, "while hematite and chamosite were forming at the surface of deposition, the siderite was contemporaneously formed in the immediately underlying sediments."

In summary, these ores are shallow marine, or possibly even brackish. Trace element studies indicate alternation between normal marine and brackish (but predominantly marine) environments of deposition for these deposits. Basically, the ore deposits were formed in a reducing environment, but local sporadic changes to mildly oxidizing conditions is reflected in alternating brown and green growth rings of chamosite oolites. Mixed assemblages of oolites consisting of some more highly oxidized than others suggests that local oxidizing and reducing conditions alternated on the sea floor with currents mixing the different types.

CONCLUSIONS

Sideritic chamosite lentils occur in at least four distinct stratigraphic levels within a 150 foot stratigraphic section of the upper Cook Mountain and lower Cockfield. On exposure to surface weathering conditions, they alter to brown ore which consists of goethite or limonite veins and ledges in the clayey matrix of the altered parent lentils. The flat-lying nature of the beds of the D'Arbonne platform results in exposure of the parent lentils over wide areas of north-central Louisiana. The major ore deposits are located in an area approximately forty miles in length and twenty miles in width which trends northwest-southeast between the northeast portion of Webster Parish and the south-central part of Lincoln Parish. The development of present topography and/or facies changes within the parent ore lentils has resulted in isolated ore districts within the overall region, but these are normally quite extensive.

The fresh parent lentils consist predominantly of green or gray green chamosite oolites and pellets in a matrix of clear or pale yellow microcrystalline siderite or less commonly in a matrix of green chamosite. Averaged point counts of the constituent minerals in

selected size fractions yield 53 percent siderite (with minor magnetite, ilmenite (?) and pyrite), 42 percent chamosite (with minor quantities of kaolinite, illite and nontronite (?)), with the remaining 5 percent being composed of detrital quartz, feldspar, mica, and other minor minerals. In general, the siderite persists throughout and tightly cements the parent lentils. The siderite is normally associated with only minor quantities of calcite but locally calcite enrichment results in calcite becoming the dominant matrix material. This phenomenon occurs rarely, however, and then is restricted to small rounded or nodular bodies of finely crystalline calcite. Siderite is also present as granular masses and secondary spherulites in chamositic muds and is thought to be secondary, produced by recrystallization of siderite originally disseminated through the chamosite muds. Siderite is also an active replacement mineral and commonly replaces chamosite, detrital quartz, and organic matter.

In addition to these minerals, most samples examined contained amorphous limonite coatings and/or finely divided goethite grains. Quantitative analysis of this iron, extracted by means of the dithionite-citrate technique, shows that such occurrences constitute an average of 6.5 percent by weight of the total rock specimen.

Minor collophanite occurs in these deposits. Quantitatively, the percent of this phosphorous-bearing mineral is insignificant compared to the other constituent minerals, but from an economic point

of view, its relative percentage is very significant in terms of potential value of the iron. On selecting a processing technique for these ores, the high phosphorous content, averaging approximately 0.34 percent in the green ores and 0.39 percent (Durham, 1964) in the brown ores, must be considered.

Once exposed to surface or near-surface conditions, the sideritic chamosite beds are altered by weathering processes. Chemically reactive surface waters charged with carbon dioxide attack the siderite, and to a lesser extent the chamosite, of the parent lentils, oxidizing and leaching their iron content. The liberated iron is concentrated as goethite and/or limonite veins or ledges within an associated clayey residue from which the iron has been leached.

Chemical analyses of the unaltered parent lentils by X-ray fluorescence yield an average iron content of approximately 47 percent Fe_2O_3. Utilizing a sample typical for these deposits, the relative percentages of iron tied up in the various potential iron-bearing minerals recognized in thin section, were determined after making certain assumptions based on the proportion of certain elements to the CO_2 content of this sample. Based on these assumptions, it was calculated that an average of 12.12 percent of the total 32.57 percent elemental iron in this sample is structurally coordinated in siderite. This value corresponds to approximately 37 percent of the total iron

content. Of the remaining 20.45 percent it was calculated that 4.13 is present as limonite coatings and/or finely divided crystals of goethite, 0.10 percent as pyrite, 0.26 percent as ilmenite (?), 1.58 percent as magnetite, and 14.38 percent as chamosite. Based on the assumption that the iron is available from all the minerals except chamosite, the total iron available on the basis of these calculations would be 18.19 percent elemental iron, corresponding to approximately 56 percent of the total iron present in this sample. The presence of such a high available iron content in the enormous green ore reserves available (over 121 million long tons mapped) could add significantly to the economic potential of the brown iron ore deposits.

These sedimentary ironstones formed near a fluctuating shoreline in close proximity to a landmass capable of supplying large quantities of iron. The iron necessary for these deposits was most probably derived from extensively leached igneous rocks in areas immediately to the north, e.g., Arkansas.

The iron was most probably transported either as colloidal ferric hydroxide in oxidizing river water or in true solution as ferrous ion and/or as ferrous bicarbonate in rivers presumably having a pH of 7 or less and an Eh in the range -0.1 to +0.3. Most of the siderite and chamosite were precipitated directly from solution in warm, shallow marine to brackish waters with a pH ranging from approximately 7.0 to 7.8 and an Eh ranging from approximately 0.0

to -2.0. A reducing environment such as this might be expected to result in areas of reduced circulation due to restrictions of water circulation and/or in areas where depletion of the oxygen content resulted from oxidation of large masses of organic material.

The presence of minor limonite and/or goethite crystals suggests sporadic changes to mildly oxidizing conditions. The occurrence of alternating brown and green growth rings of chamosite in typical growth oolites also reflects such sporadic changes. Mixed assemblages of oolites, consisting of some more highly oxidized than others, possibly suggest that local oxidizing and reducing conditions alternated on the sea floor with currents mixing the different types.

The chamosite and most of the siderite in these deposits is considered primary. In typical chamosite oolites the concentric growth rings of cryptocrystalline chamosite around quartz nuclei could have formed only by direct crystallization from solutions with a relatively low Eh and neutral or higher pH. Chamosite pellets consisting of chamosite intimately mixed with clay, quartz and other detrital material may represent reconstituted faecal pellets as suggested by Porrenga (1965). Chamosite present as "false" oolites and as chamositic muds is also thought to represent primary depositional material.

The presence of directly precipitated siderite in these deposits places certain restrictions on the environment of deposition.

The Eh and pH range and the CO_2 content of the environment are certainly restricted to definable limits. Siderite becomes insoluble and precipitates directly from waters where the partial pressure of CO_2 is relatively low, the Eh is 0.0 or less, and the pH is 7 or above. Precipitation would be encouraged in warm waters in which the degree of dissociation of the bicarbonate would be relatively high and/or in areas where the removal of carbon dioxide by the process of photosynthesis was active.

The presence of diagenetic replacement siderite in these deposits reflects changes in the environment either during late stages of deposition or in the microenvironment of the pore fluids after accumulation. The replacement of quartz, chamosite, and feldspars by siderite would presumably require a pH of at least 9 to disrupt the silicate structures before replacement could proceed, assuming that the solubility product of $FeCO_3$ had already been exceeded. Such an abnormal environment would necessarily be a restricted type with abnormal concentrations of alkali metal ions because normal sea water seldom exceeds a pH of 8.5.

That the environment of deposition for these deposits was shallow is reflected in the occurrence of extensive worm borings and current bedding in some sections of some exposed lentils. A shallow environment is also suggested by the characteristic vertical gradation of these deposits in both directions into beds typical of backswamp

deposition. The restriction of these deposits to a narrow NW-SE trending belt by lateral facies changes is also suggestive of near-shore, shallow water deposits. Trace element studies indicate alternation between normal marine and brackish, but predominantly marine, environments of deposition for these deposits.

CITED REFERENCES

Aschan, C., 1907, Die bedeutun wasserloslichen humus-stoffe sumpferge: Zeit. Prak. Geol., v. 15, p. 56-62.

Bannister, F. A., and Hollingworth, S. E., 1948, Two new British minerals: Nature, London, v. 162, p. 565.

Brindley, G. W., 1951, The crystal structure of some chamosite minerals: Mineralog. Mag., v. 29, n. 212, p. 502-525.

Brindley, G. W., and Youell, R. F., 1953, Ferrous chamosite and ferric chamosite: Mineralog. Mag., v. 30, p. 57.

Brochert, H., 1960, Genesis of marine sedimentary iron ore: Inst. Mining and Metallurgy Trans., v. 69, London, p. 261-279.

Brown, G., ed., 1961, The X-ray identification and crystal structures of clay minerals: London, Mineralog. Soc., 544 p.

Brown, G., and Norrish, K., 1952, Hydrous micas: Mineralog. Mag., v. 29, n. 218, p. 929-932.

Carrol, D., 1958, Role of clay minerals in the transportation of iron: Geochim. et Cosmochim. Acta, v. 14, p. 1-27.

Castano, J. R., and Garrels, R. M., 1950, Experiments on the deposition of iron with special reference to the Clinton iron ore deposits: Econ. Geology, v. 45, n. 8, p. 755-770.

Cayeux, L., 1922, Les minerais de fer oolithique de la France, Fasc. II, minerais de fer secondaires: Minist. Trav. Publics, Etudes gites mineraux de la France, Paris, 1051 p.

Cissarz, A., 1954, Zur petrographie und genesis sudwestmazedonischer eisensilikaltagerstatten: Bull. Serv. geol. geophys., Serbie, v. 11, p. 261-340.

Cullity, B. D., 1959, Elements of X-ray diffraction: Reading, Mass., Addison-Wesley, 514 p.

Deer, W. A., Howie, R. A., and Zussman, J., 1962, Rock-forming minerals, v. 5, non-silicates: London, William Clowes and Sons, 371 p.

Degens, E. T., 1965, Geochemistry of sediments: Englewood Cliffs, N. J., Prentice-Hall, Inc., 342 p.

Degenhardt, H., 1957, Untersuchungen zur geochemischen verteilung des zirkoniums in der lithosphare: Geochim. et Cosmochim. Acta, v. 11, p. 279-309.

Durham, C. O., Jr., 1964, Iron ore of Central North Louisiana: La. Dept. Conserv., Geol. Survey Bull. 41, 127 p.

Durham, C. O., Jr., and White, W. S., 1960, A guided geological tour through North and Central Louisiana, in Interior salt domes and Tertiary stratigraphy of North Louisiana: Shreveport Geol. Soc., 1960 Guidebook, p. 83-147.

Eckles, Edwin B., 1938, The brown iron ores of Eastern Texas: U.S. Geol. Survey Bull. 902, 157 p.

Everett, A. G., 1962, Clay petrology and geochemistry of Blain Formation (Permian), northern Blain County, Oklahoma: unpublished M.S. Thesis, University of Oklahoma, 108 p.

Folk, R. L., 1959, Petrology of sedimentary rocks: Austin, Texas, Hemphill's Publishing Co., 154 p.

Frederickson, A. F., and Reynolds, R. C., Jr., 1960, Geochemical method for determining paleosalinity: Clays and Clay Minerals, v. 8, p. 203-213, New York, Pergamon Press.

Garrels, R. M., and Christ, C. L., 1965, Solutions, minerals and equilibria: New York, Harper and Row, 450 p.

Gill, J. E., 1927, Origin of the Gunflint iron-bearing formation: Econ. Geol., v. 22, p. 687-728.

Goldschmidt, V. M., 1958, Geochemistry: London, Oxford Univ. Press, 730 p.

Goldschmidt, V. M., and Peters, C., 1932a, Zur Geochemie des Bors: Nachr. Ges. Wiss., Gottingen, Math-physik. Kl., III, 402.

_____ 1932b, Zur Geochemie des Bors, II: Nachr. Ges. Wiss., Gottingen, Math-physik. Kl., III, 528.

Gruner, J. W., 1922, The origin of sedimentary iron ore formations, the Biwabik Formation of the Mesabi Range: Econ. Geology, v. 17, p. 407-460.

Hallimond, A. F., 1925, Iron ores: Bedded ores of England and Wales: Great Britain Spec. Rept. Miner. Resour., Petrography and Chemistry, v. 29, 139 p.

Harder, E. C., 1919, Iron-depositing bacteria and their geologic relations: U.S. Geol. Survey Prof. Paper 113, 89 p.

Hayes, A. O., 1915, Wabana iron ore of Newfoundland: Canada Geol. Survey Mem. 78, 163 p.

Huber, N. K., 1958, The environmental control of sedimentary iron minerals: Econ. Geology, v. 53, n. 2, p. 123-140.

Huner, J., 1939, Geology of Caldwell and Winn Parishes: La. Dept. Conserv., Geol. Survey Bull. 15, 356 p.

Jackson, M. L., 1964, Soil clay mineralogical analysis, in Soil Clay Mineralogy, a symposium (eds Rich, C. I., and Kung, G. W.): Chapel Hill, Univ. N. Car. Press, p. 245-294, p. 281-282.

James, H. L., 1951, Iron formation and associated rocks in the Iron River District, Michigan: Geol. Soc. American Bull. 62, p. 251-266.

_____ 1954, Sedimentary facies of iron-formation: Econ. Geology, v. 49, p. 235-293.

Jones, H. L., 1962, The geology of the iron ore deposits of the Sugar Creek Area, Bienville, Claiborne, and Lincoln Parishes, La.: unpublished M.S. Thesis, Louisiana State University, 108 p.

Kautsky, G., 1958, The theory of exhalative-sedimentary ores proposed by Chr. Oftedahl, a criticism: Geol. Foren. Stockholm Forh, v. 80, n. 492, p. 283-287.

Keith, M. L., and Degens, E. T., 1959, Geochemical indicators of marine and fresh-water sediments, p. 38-61, in Researches in geochemistry (ed. Ableson, P. H.): New York, John Wiley and Sons, Inc., p. 38-59.

Kerns, R. L., 1967a, Particle-size separation of clays: Okla. Geology Notes, v. 27, p. 167-174.

Krauskopf, K. B., 1955, Sedimentary deposits of rare metals: Econ. Geology, v. 50, p. 411-463.

_____ 1956, Factors controlling the concentration of thirteen rare metals in sea-water: Geochim. et Cosmochim. Acta, v. 9, p. 1-32B.

_____ 1959, The geochemistry of silica in sediments: Soc. Econ. Paleontologist and Mineralogists Spec. Pub. 7, p. 4-20.

Krumbein, W. C., and Garrels, R. M., 1952, Origin and classification of chemical sediments in terms of pH and oxidation-reduction potentials: Jour. Geol., v. 60, n. 1, p. 1-33.

Landergren, S., 1945, Contribution to the geochemistry of boron: Arkiv Mineralogi och Geologi, v. 19A, n. 26, p. 1-31.

_____ 1958, On the distribution of boron on different size classes in marine clay sediments: Geol. Foren. Stockholm Forh., v. 80, n. 492, p. 104-107.

_____ 1958, Comments to "A theory of exhalative-sedimentary ores": Geol. Foren. Stockholm Forh, v. 80, n. 492, p. 288-290.

Marmo, V., 1958, On the theory of exhalative-sedimentary ores: Geol. Foren. Stockholm Forh, v. 80, p. 277-282.

Martin, J. L., 1943, Geology of Webster Parish, La.: unpublished Ph.D. Thesis, Louisiana State University, 248 p.

_____ 1954, Surface stratigraphy, in Geology of Webster Parish: La. Dept. Conserv., Geol. Survey Bull. 15, p. 71-106.

Mehra, O. P., and Jackson, M. L., 1960, Iron oxide removal from soils and clays by a dithionite-citrate system buffered with sodium bicarbonate: Clays and Clay Minerals, v. 7, p. 317-327, New York, Pergamon Press.

Migdisov, A. A., and Borisenok, L. A., 1963, Geochemistry of gallium in sedimentation under humid conditions: Geokhimiya, n. 12, p. 1113-1128.

Moore, E. S., 1910, The occurrence and origin of some bog iron deposits in the district of Thunder Bay, Ontario: Econ. Geology, v. 5, p. 528-538.

Moore, E. S., and Maynard, J. E., 1929, The solution, transportation, and precipitation of iron and silica: Econ. Geology, v. 24, p. 272-303, p. 365-402, p. 506-527.

Murray, G. E., 1961, Geology of the Atlantic and Gulf Coastal Province of North America: Harper and Bros., 692 p.

Nelson, B. W., and Roy, R., 1958, Synthesis of the chlorites and their structural and chemical constitution: Am. Mineralogist, v. 43, p. 707.

Nicholls, G. D., and Loring, D. H., 1962, The geochemistry of some British carboniferous sediments: Geochim. et Cosmochim. Acta, v. 26, p. 181-224.

Oftedahl, C., 1958, A theory of exhalative-sedimentary ores: Geol. Foren. Stockholm Forh, v. 80, n. 492, p. 1-19.

Orcel, J., Henin, S., and Caillere, S., 1949, Sur les silicates phylliteux des minerais de fer oolithiques: Acad. Sci. Comptes Rendus, Paris, v. 229, p. 134.

Page, B. M., 1958, Chamositic iron ore deposits near Tajmiste, Western Macedonia, Yugoslavia: Econ. Geology, v. 53, n. 1, p. 1-21.

Palmquist, S., 1935, Geochemical studies on the iron-bearing Liassic Series in Southern Sweden: Medd. Lunds geol.-miner. Instn., v. 2, n. 60, 204 p.

Porrenga, D. H., 1965, Chamosite in recent sediments of the Niger and Orinoco Deltas: Geologie en Mijnbouw, v. 44e, p. 400-403.

Potter, P. E., Shimp, N. E., and Witters, J., 1963, Trace elements in marine and fresh-water argillaceous sediments: Geochim. et Cosmochim. Acta, v. 27, p. 669-694.

Rankama, K., and Sahama, Th. G., 1950, Geochemistry: Chicago, Univ. Chicago Press, 912 p.

Riley, G. A., 1939, Limnological studies in Connecticut: Ecol. Monogr., v. 9, p. 53-94.

Ronov, A. B., and Ermishkina, A. I., 1959, Distribution of Manganese in sedimentary rocks: Geokhimiya, n. 3, p. 254-278.

Ronov, A. B., Vainshtein, E. E., and Tuzova, A. M., 1961, Geochemistry of hafnium, zirconium, and some other hydrolyzate elements in clays: Geokhimiya, n. 4, p. 343-355.

Smith, C. R., 1957, Queen City-Sparta relationships in Caddo Parish, Louisiana: Am. Assoc. Petroleum Geologists Bull., v. 46, p. 2517-2522.

Sokolova, E. I., 1962, Physicochemical investigations of sedimentary iron and manganese ores and associated rocks: Israel Program for Scientific Translations (Cat. no. 206), 220 p., Translated from Izdatel'stvo Akademii Nauk. SSR by Shochet, D., 1964: New York, Daniel Davey and Co., Inc., 1964

Stenzel, H. B., 1939, The Yegua Problem, in Contributions to Geology: Bur. Econ. Geology, n. 3945, p. 847-904.

Taylor, J. H., 1949, Petrology of the Northampton Sand Ironstone Formation: Great Britain Geol. Surv. Mem., London, 111 p.

Van Hise, C. R., and Leith, C. K., 1911, The geology of the Lake Superior Region: U.S. Geol. Surv. Mon., v. 12, n. 52, 641 p.

Wattenberg, H., 1943, Erganzung zu der milleilung: Zur Chemie des Meerwassers: ober die in spuren vorkommenden elemente: Zeitschr. Anorg. u. Allg. Chemie, v. 251, p. 86-91.

Williams, H., Turner, F. J., and Gilbert, C. M., 1954, Petrography: an introduction to the study of rocks in thin sections: San Francisco, W. H. Freeman and Co., p. 368-372.

Worley, G. T., 1962, Geology of the Arcadia Salt Dome Area, Bienville Parish, La.: unpublished M.S. Thesis, Louisiana State University, 77 p.

Wu, D. C., 1969, Clay Mineralogy of the Upper Flowerpot Shale in Major and Blaine Counties, Okla.: unpublished Ph.D. Thesis, University of Oklahoma, 104 p.

APPENDIX A

ANALYTICAL PROCEDURES AND TECHNIQUES

Sample Preparation

Large samples of the bulk material were prepared for selective iron extraction. They were crushed until they passed through a 120 mesh screen, and after homogenization, exact quantities of each rock powder (less than five grams in every case) were weighed and placed in a 250 milliliter centrifuge tube. After the iron was removed from these samples by means of the dithionite-citrate technique discussed in the next section, the treated samples were dispersed in distilled water in one-liter beakers and further disaggregated and dispersed by means of the ultrasonic transducer. The less-than-four and less-than-one micron equivalent spherical diameter particles of each sample were segregated from the suspended sample by fluid withdrawal according to Stokes' Law settling graphs. Further size fractionation of selected samples was performed by the high speed centrifugation method in hopes of obtaining more nearly monomineralic samples of clay-sized particles. The less-than-one micron fraction was further subdivided into 1-1/2,

1/2-1/4, 1/4-1/8, and 1/8-1/16 micron fractions by continuous flow centrifugation utilizing the flow rate and centrifuge revolutions per minute settings recommended by Kerns (1967a) for collection of certain size fractions.

Preferred orientation slides of the selected size fractions were prepared by sedimenting the clay suspension on glass slides and then drying the slides in an oven at approximately 55°C. This procedure preferentially aligns the clay fraction and enhances the basal diffraction maxima by orienting the c-crystallographic axis of the clay minerals normal to the slide.

Randomly oriented powder slides of the dried size-fractioned material were made by sieving the material directly onto vaseline-coated slides or by packing the powder in an aluminum sample holder.

Selective Removal of Amorphous Iron Oxide

The presence of amorphous iron oxide in untreated samples created extreme difficulty in obtaining diffractograms of either the random powder slides or preferentially-oriented slides of clay fractions. In choosing a technique to remove amorphous iron oxides from samples several factors had to be considered. The process should selectively remove oxide coatings without attacking the iron structurally coordinated in the iron-bearing clay minerals present. Further, it should not attack the layer silicate minerals with resulting increase or

decrease in cation exchange capacity, and ideally the technique should be fast and free from analytical difficulties. Such a technique was proposed by O. P. Mehra and M. L. Jackson (1960). Their dithionite-citrate-bicarbonate method employs sodium dithionite ($Na_2S_2O_4$) as a reducing agent, sodium bicarbonate as a buffer, and sodium citrate as a chelating or complexing agent for iron. Operation at a neutral pH makes it possible to achieve the prerequisites mentioned above. The procedure for removal as listed by Mehra and Jackson (1960, p. 350) is as follows:

> A suitable amount of the sample (4 g of many soils or 1 gm of clay per 100 ml tube) containing 0.5 g of extractable Fe_2O_3 or less, is placed in a 100 ml. centrifuge tube and 40 ml. of 0.3 M Na-citrate solution and 5 ml. of 1 M $NaHCO_3$ solution are added. The temperature is brought to 80°C in a water bath, then 1 g. of solid $Na_2S_2O_4$ ($\frac{1}{2}$ g. suffices for clays low in free iron oxides) is added by means of a spoon, and the mixture is stirred constantly for 1 min. and then occassionally for a total of 15 min. At the end of the 15 min. digestion period, 10 ml. of saturated NaCl solution (and 10 ml. of acetone, particularly needed for allophanic soils) is added to the tube to promote flocculation. The suspension is then mixed, warmed in a water bath, and centrifuged for 5 min. at 1600-2200 rev./min. The clear supernatant is decanted into a 500 ml. volumetric flask (or a 1000 ml. flask if the volume exceeds 500 ml.) and the solution is kept for Fe, Al and Si determinations.
>
> For samples which originally contained more than 5 percent of extractable Fe_2O_3, the treatment in the previous paragraph is repeated once or twice (sample combined into fewer tubes for the second treatment) with decantation into the same 500 ml. volumetric flask as before. A final washing (two or more for samples of more than 1 g. of residue) is made with the Na-citrate solution (with NaCl and acetone if necessary for flocculation), which is combined with the previous decantates for Fe determination. If the colloid does not flocculate, 10 ml. of acetone is added (HCl and $CaCl_2$ solutions are avoided).

> The solution is mixed and warmed in a water bath. Care is taken that solutions containing acetone do not boil. Centrifugation for 5 min. is repeated. A pure white color of the residue should not be expected, as some soils and colloids contain cream or green colored colloids and coarse, black mineral particles. The sample is kept in methanol, acetone or water, without drying. The sample, freed of extractable Fe_2O_3 but not dried at any time during the procedure, is ready for cation exchange capacity determination or (Jackson, 1956, p. 72) boiling in 2 percent Na_2CO_3 for dispersion and segregation for X-ray diffraction analysis, differential and integral thermal analysis, infrared analysis, elemental analysis, electron microscope examination, or other procedures.

This procedure was followed but with the following modifications. A 250 ml. centrifuge tube was utilized instead of the recommended 100 ml. tube. An additional gram of $Na_2S_2O_4$ was added at the end of 5 and 10 minutes during the 15 minute digestion period (Jackson, 1964, p. 282).

Analysis of the Selectively-Removed Iron Oxide by Atomic Absorption Spectrophotometry

The iron selectively removed from the samples by the dithionite-citrate technique was analyzed by atomic absorption spectrophotometry. The Perkin Elmer 303 Spectrophotometer located in the Botany and Microbiology building and the Beckman Model Number DB spectrophotometer located in the Chemistry building were utilized for this purpose. Standards with iron concentrations of 2, 5, 10, 20, 30, 40, and 50 parts per million were prepared by diluting aliquots of a standard iron solution containing 1000 parts per million iron to the correct proportions. These samples were aspirated in the spectrophotometers, and the

percent transmission, which is dependent on the concentration of the element analyzed for, was read directly from the percent transmission indicator. The percent absorption, the desired factor, may be read directly from available tables which have been calculated to give percent transmission values for corresponding percent absorption values. Or these values may be obtained from the following equation:

$$\text{Percent Transmission} = 2 - \log \text{percent Transmission}$$

A standard curve was prepared by plotting the percent absorbance against the parts per million for the particular standards representing these values.

The unknown samples were diluted until the concentration of the iron was low enough, less than 50 ppm, to give values detectable by the unit. The concentration of iron in the unknown samples was then read directly from the standard plot, in parts per million, utilizing the converted percent absorbance values.

The parts per million of iron in each sample may be converted to weight percent of the total sample by taking into account the original weight of the sample and the dilution factor of each sample as follows:

$$\frac{\text{Conc. of Fe (ppm) X Dilution factor (ml)}}{\text{Original wt. sample (gm)}} = \text{Weight Percent Iron in Sample}$$

Analytical X-ray Techniques

X-ray diffraction patterns were obtained with the Siemens

X-ray diffractometer and automatic recorder with nickel-filtered copper (K-alpha) and zirconium-filtered molybdenum (K-alpha) radiations. The reason prompting utilization of molybdenum radiation in X-ray analysis of these unusual rocks is discussed in detail in the Clay Mineralogy section and will not be dealt with here. The goniometer was operated at one degree 2θ per minute, and the diffracted radiation was detected by a scintillation counter.

Diffraction patterns of preferentially oriented slides of treated clay fractions, those with the amorphous iron selectively removed, were obtained before and after solvation of the samples in a saturated ethylene glycol atmosphere at 60 degrees centigrade overnight. Slides of oriented clays were examined before and after heat treatments in a high temperature oven to determine heating modifications. Sedimented slides of acid-treated clay fractions, samples from which the chamosite had been removed by treatments with warm 10 percent hydrochloric acid, were utilized to confirm the presence of kaolinite.

Randomly oriented powder slides of bulk samples were utilized to distinguish the different minerals present. Diffractograms of randomly-oriented powder slides were utilized to detect the presence of minor quantities of kaolinite and to distinguish between trioctahedral and dioctahedral clay minerals, based upon d-spacing of the (060) reflection. A marked increase in the intensity and definition of the reflections present was detected for powder samples held in

aluminum sample holders. Diffractograms of randomly oriented powder slides of acid-treated clay size fractions were essential in distinguishing the variety of kaolinite present.

X-ray Fluorescence Analysis

General Theory

Chemical analysis by fluorescence is possible because each element emits characteristic radiation when bombarded with X-ray quanta of sufficient energy. The target is bombarded with primary radiation, causing emission of characteristic fluorescent radiation. Secondary characteristic radiation is then diffracted from the analyzing crystal into the counter. In accordance with the Bragg Law, radiation of only a single wavelength is reflected for each angular setting of the crystal and the intensity of this radiation can be measured with a suitable counter. Qualitative analysis is possible by identification of the diagnostic radiation emitted by the element utilizing tables of the K and L lines of all elements and a table of corresponding wavelengths and 2θ values of the analyzing crystal. For quantitative analysis, it is necessary to measure the intensity of the characteristic fluorescent radiation which is proportional to the concentration of the element detected. This relation is not linear, however, due to:

1. Matrix absorption - The absorption coefficient of the matrix varies as the concentration varies.

2. Multiple excitation - If the wavelength of the fluorescent is smaller than the K absorption edge of another element in the sample, the latter will also emit fluorescent radiation due to this radiation in addition to excitation radiation due to the primary source.

Two other major problems exist in fluorescent analysis:

1. Intensity of the fluorescent radiation is much less than that of the incident beam on the sample, and it is further reduced by diffraction on the analyzing crystal. If the diffracted beam entering the counter is very weak, a large counting time will be necessary to measure the intensity with acceptable accuracy. High intensity is desirable to reduce the counting time, therefore in such situations a tungsten target tube with as high a power rating as possible is normally utilized. The exciting radiation is then that part of the continuous spectrum and such L lines of tungsten as have shorter wavelengths than the K absorption edge. Because the intensity of a particular line from the sample is usually compared with the intensity of the same line from a standard, the output of the X-ray tube must be stabilized or the tube must be monitored.
2. Resolution is difficult when the wavelength of fluorescent radiation for two elements present is very close. Reflecting

flat and curved crystals of LiF and NaCl give greater reflected intensity but less resolution than the curved transmitting crystals of mica.

In quantitative analysis the non-linear relationship between intensity and concentration require that the intensity of the sample be compared with a curve for a suitable sample. The sample is analyzed for one element at a time and preparation of standards for each given element analyzed is necessary. Uniform samples of known concentration of the elements in question are combined with a matrix similar to the matrix of the unknown. That the matrix should be similar to that of the unknown is necessary because different matrices have different absorption affects.

X-ray periodic charts are available that give the analyzing crystal best suited for a particular element. The 2θ value corresponding to the desired wavelength for the element concerned is set on the goniometer. The intensity of the known is measured at the prescribed angle by means of the counter. After measuring the peak intensity, the standard is then turned slightly off this peak angle and the background radiation is then measured. This difference in intensity is then plotted against the weight percent of the oxides in the standard. A curve is then derived from a set of standards of different weight percentages, and this information may be utilized to determine the weight percent of the oxides in the unknown. A

plot of the intensity difference of the unknown oxide determines the position on the standard curve at which weight percent may be read directly.

Advantages of chemical analysis by X-ray fluorescence are:

1. Analyzing time is very short once standards and working curves are prepared.
2. Accuracy is superior to optical spectroscopy for elements ranging from 1 to 100 percent; optical spectroscopy is superior below 1 percent.
3. Non-destructive method.

Disadvantages of chemical analysis by X-ray fluorescence are:

1. Ordinarily, the method is limited to elements with atomic numbers greater than around 22. Elements of atomic numbers between 5 and 22 have to be analyzed in a vacuum or in an atmosphere of light gasses using a gas flow proportional counter because of the low energy of the characteristic fluorescent radiation of these elements.
2. Higher light elements cannot be detected in a heavy matrix due to absorption.
3. White radiation of the tube causes a background effect.
4. This method is not very sensitive to trace elements.
5. Characteristic radiation of the target material will normally

appear in the emergent radiation.

Procedure

For quantitative X-ray fluorescence analyses, a Siemens X-ray spectrometer was used with a chromium tube and evacuated chamber for the lighter elements and a tungsten tube for the heavier elements. Topaz, lithium fluoride, KAP and PET analyzing crystals were utilized. Seven bulk samples of the parent bed which had been chemically analyzed by wet methods were utilized as standards and supplemented where necessary with U.S.G.S. standards. These known standards were utilized to construct a set of standard curves. Counts per minute were plotted against weight percent of the oxides, as reported for wet chemical analyses. The standard curve was then constructed by drawing a straight line through these points. The weight percent of the unknown oxide was read directly off the curve from the number of counts per minute determined for each unknown.

The samples were prepared for analyses by hand-grinding each sample until it passed through a 250 mesh screen. After the samples were thoroughly mixed, 3.2 grams of the powdered sample were added to 0.8 grams of Polyvinal Alcohol (20 percent PVA), remixed, and pressed under 30 tons pressure in a press to make brickettes. The brickettes are one inch in diameter and are surrounded by PVA rims.

Emission Spectrographic Analysis

Quantitative trace element analysis for boron, gallium, vanadium, copper, zirconium, nickel and chromium in 40 samples was performed utilizing a Jarrel-Ash, 1.5 meter, Elbert mount spectrograph. These spectrochemical analyses were performed with the assistance of Mr. Kenneth Sargent, former graduate student at the University of Oklahoma.

Standards with concentrations of 10, 25, 100, 250, 500, and 1,000 parts per million of these elements were prepared with spectrographically pure compounds diluted with a carbonate to approximate the matrix of the unknown samples as closely as possible. One part of the standard was thoroughly mixed with one part of analytical grade graphite and two parts of cobalt (added as an internal standard) and thoroughly mixed on an automatic shaker. Then the samples, ground to less than 250 mesh, were diluted 1:9 with spectrographic grade graphite and homogeneously mixed. Ten milligrams of each standard and each sample were then loaded into a spectrographic graphite electrode. These were then placed in the electrode holder opposite the counter electrode and burned to completion in a DC arc of 5 amperes with a constant 6 mm analytical gap maintained between the opposing electrodes. The burning time was preprogrammed for 45 seconds. Emission spectra were recorded on 35 mm Eastman Kodak SA-1 film and the percent transmission of light through the spectral lines was read on a Jarrel-Ash

Console microphotometer.

The intensity ratio of the spectral lines of the unknown elements to the cobalt reference line was read directly from an emulsion curve prepared empirically by Kenneth Sargent for this particular type film. Empirical curves (straight lines) were then drawn on a Slidel calculating board by plotting the intensity ratio of the standards as the ordinate and the concentrations of the trace elements of the standards, in ppm, as the abscissa. The trace element content of the unknown samples was then read directly from the abscissa, corresponding to the intersection of the intensity ratio and the empirical line.

Because determination of the trace element content is based upon the ratio of the intensity of an element spectral line with that of a nearby cobalt line, errors are not introduced by variations in ignition time, ignition amperages, incomplete burning, or exposure time because these variations would not affect this ratio.

Differential Thermal Analyses

DTA gives information concerning the nature of the reaction (endothermic or exothermic), the temperature range at which the reaction takes place, and the sequence and intensity of reactions taking place under specified conditions (particle size, pressure, heating rate, etc.). Characteristic endothermic reactions due to dehydration and to loss of crystal structure and exothermic reactions due to the formation

of new phases at elevated temperatures are shown. This type of analysis measures energy changes brought about by reactions involving weight losses and structural rearrangement. The area under the curves reflects the amount of energy involved in the thermal transformations but comparison from one pattern to another quantitatively is unfeasible. For comparison of like samples standard techniques must be followed, i.e., heating rates must be uniform from sample to sample. Consequently, the peaks and troughs are not reflections of equilibrium reactions due to many such variable parameters. The temperature of the peaks is dependent upon particle size, perfection of stacking, interlayer cation, internal substitution, heating rate, pressure, etc.

Differential thermal analyses of both the bulk samples and the size-fractioned samples were conducted by means of a Robert L. Stone Model DTA-13M furnace and recording assembly. The system was constantly purged by nitrogen gas with a flow rate of approximately 25 millimeters per hour. The samples were loaded in the sample holder and heated to 1020°C at a rate of 10°C per minute.

Effluent Gas and Gas Chromatography Analyses

Gas liberated by samples during the reactions produced by heating was detected by the Effluent Gas Analyses Unit, and the gas was collected and analyzed by gas chromatography. Samples for analysis were prepared by grinding to less than 250 mesh and then small pellets

were made by pressing small aliquots of the homogenized sample with a miniature die. These were loaded into platinum discs and placed in the sample holder attachment of the DTA unit. The heating program and rate was essentially the same as that for DTA runs. Gas liberated during heating reactions was detected by the DTA Effluent Gas Analysis attachment. DTA and EGA curves are printed simultaneously during this procedure.

The gas detected by EGA was identified by passing it directly from the EGA unit through solutions containing different indicators for different gases. The presence of CO_2 released during decomposition of organic matter or carbonates was qualitatively analyzed for by passing liberated gas through a 10 percent solution of calcium hydroxide, with the resulting precipitation of calcium carbonate if the gas was CO_2. Sulfur dioxide released during decomposition of pyrite or oxidation of organic sulfur was analyzed for by passing the gas through a dilute solution of KI using starch as an indicator. A change in color from light purple, produced by addition of the starch, to clear or colorless is the test for the presence of SO_2.

A second technique developed for qualitative analysis of released gases consisted of bubbling gas produced by a home-made gas generator through solutions containing different indicators. The gas generator was constructed from fused silica tubing by the Physics Glass Blowing Shop. It is approximately 18 inches long and consists of an

inner $\frac{1}{4}$-inch silica tube with a shorter, outer 3/4-inch silica tube closed at one end and fused to the inner tube at the other end. A portion of the smaller inner tube extends outward from the point of fusion with the larger outer tube and acts as an outlet for gas produced. A third, $\frac{1}{4}$-inch fused glass tube was fused around a hole in the outer large tube just below the point of fusion with the inner small tube and acts as an inlet tube for the purging gas. The gas generator was fitted to the front of a high temperature furnace by drilling a formfit hole through a fiber glass plate cut to fit snugly in the furnace opening. The sample was poured through the intake tube into the gas generator, and the generator was then inserted into the oven by passing it through the hole in the fiber glass plate. Plastic tubing was then utilized to connect the intake tube to a gas flow gage connected in turn to a nitrogen tank. The outlet tube to the gas generator was then connected to a glass container similar in design to the gas generator. This device, equipped with an inlet and outlet tube, contained the indicator solutions. As the samples were heated, the whole system was purged with nitrogen gas with a slow flow rate. The lighter nitrogen carrier gas passed on through the outlet of the indicator tube but other gases became mixed with the indicator solutions and produced reactions peculiar to that particular gas and the indicator affected.

APPENDIX B

CORE DESCRIPTIONS

Rock cores of the parent siderite-chamosite lentils consist of essentially the same mineral assemblage and variations in the cores are restricted to changes in the relative proportions of the constituent minerals. Changes in the mineralogy and rock texture within any one core is repeated time and again in cores from other areas; therefore, core descriptions here will be restricted to one typical core, H-6. Even the rock types in the overlying and underlying beds, into which these lentils characteristically grade, are invariably similar.

The cores were designated with the prefix "H" and are followed by numbers which run consecutively throughout the ore region. Thin sections taken from these cores, starting with core H-1 and proceeding from the top to the bottom of it and each succeeding core considered, are designated by attaching an additional number on the end of the core designation, e.g., H-1-1, representing thin section number one from the top of core H-1.

Core H-6

SE¼, NE¼, NE¼, SE¼ Sec. 11, T22N, R7W, in the extreme north-central portion of the Mahon District, Claiborne Parish, Louisiana.

Unit No.		Thickness (feet)
9	Quartz sand, very fine-grained, clear, angular to subangular, with large quantities of muscovite and organic matter, all in light to dark gray sideritic clay matrix with discontinuous, light gray, clayey siderite stringers.	0.50
8	Sideritic bed, reddish brown, extremely indurated, consisting of predominantly fine-grained quartz sand with muscovite, organic matter and a very high percentage of siderite.	0.50
7	Sideritic chamosite, dark green chamosite, tightly cemented by siderite, contains varying proportions of burrows and bore holes subsequently filled with light-colored, sideritic mud giving rock a mottled appearance, being more oxidized and leached of its iron content and containing a much higher clay content and more siderite-filled burrows near the upper and lower portions of the unit, less tightly-cemented, rotten-looking, 4-inch interval near center of core characterized by light specks of granular allophane (?) giving the interval a speckled appearance.	7.00
6	Siderite stringer, reddish purple, strongly indurated, with a sugary texture.	0.20
5	Sideritic chamosite, dark grains in dirty sideritic clay matrix with progressively more quartz, clay and siderite-filled burrows near bottom of unit.	1.00
4	Sideritic stringer, consisting of dark chamosite grains in dirty, clayey, oxidized sideritic cement, near top of unit, grading downward into more compact, reddish brown, granular siderite with a sugary texture.	0.85

Unit No.		Thickness (feet)
3	Sideritic chamosite, tightly cemented with slightly oxidized siderite, containing numerous, rounded siderite-filled burrows and borings and discontinuous sideritic stringers, being more oxidized and leached, less consolidated and containing more quartz and sideritic clay near lower portion of interval.	2.15
2	Quartz, fine-grained, with organic material, in clayey to granular sideritic cement.	0.50
1	Clay, dark gray, compact, waxey.	1.00
	Measured Total	13.70

Core Locations, Overburden Thickness, Green Ore Thickness, and Total Drilling Depths

Hole No.	Location	Thickness of Overburden (in feet)	Thickness of Green Ore (in feet)	Total Drilling Depth (in feet)
H-1	SW¼, SW¼, SW¼, SE¼ Sec. 27, T22N, R7W, Mahon District, Claiborne Parish.	37.5	13.0	60.0
H-2	SW¼, SE¼, SE¼, SW¼, Sec. 23, T22N, R7W, Mahon District, Claiborne Parish.	20.0	9.0	70.0
H-3	SW¼, SE¼, SE¼, NW¼, Sec. 23, T22N, R7W, Mahon District, Claiborne Parish.	45.0	15.0	65.0
H-4	SW¼, SE¼, SE¼, SW¼, Sec. 13, T22N, R7W, Mahon District, Claiborne Parish.	22.0	11.5	40.0
H-5	SE¼, SE¼, NW¼, NW¼, Sec. 18, T22N, R6W, Mahon District, Claiborne Parish.	18.0	9.0	30.0
H-6	SE¼, NE¼, NE¼, SE¼, Sec. 11, T22N, R7W, Mahon District, Claiborne Parish.	43.0	9.5	60.0
H-7	SE¼, SE¼, SW¼, SE¼, Sec. 15, T22N, R7W, Mahon District, Claiborne Parish.	50.5	13.5	100.0
H-8	SW¼, SE¼, SE¼, SW¼, Sec. 22, T22N, R7W, Mahon District, Claiborne Parish.	48.5	4.5	75.0
H-9	SW¼, SE¼, SW¼, SW¼, Sec. 35, T22N, R7W, Mahon District, Claiborne Parish.	13.5	9.5	30.0

Hole No.	Location	Thickness of Overburden (in feet)	Thickness of Green Ore (in feet)	Total Drilling Depth (in feet)
H-10	NW¼, SW¼, NE¼, SW¼, Sec. 25, T22N, R7W, Mahon District, Claiborne Parish.	37.0	9.0	60.0
H-11	SW¼, NE¼, NE¼, NE¼, Sec. 6, T19N, R4W, Crossroads District, Lincoln Parish.	42.0	8.0	60.0
H-12	SW¼, NW¼, NW¼, NW¼, Sec. 5, T19N, R4W, Crossroads District, Lincoln Parish.	75.0	10.0	90.0
H-13	SE¼, SE¼, SW¼, SW¼, Sec. 32, T20N, R4W, Crossroads District, Lincoln Parish.	41.5	11.0	60.0
H-14	NE¼, NE¼, NW¼, SE¼, Sec. 6, T19N, R4W, Crossroads District, Lincoln Parish.	40.0	8.5	60.0
H-15	SW¼, SE¼, NW¼, NE¼, Sec. 7, T19N, R4W, Crossroads District, Lincoln Parish.	55.0	14.0	80.0
H-16	NW¼, NW¼, NE¼, NW¼, Sec. 7, T19N, R4W, Crossroads District, Lincoln Parish.	32.5	7.0	50.0
H-17	SW¼, NW¼, SW¼, SW¼, Sec. 6, T19N, R4W, Crossroads District, Lincoln Parish.	15.5	7.5	35.0
H-18	SW¼, NE¼, NE¼, SE¼, Sec. 12, T19N, R5W, Crossroads District, Lincoln Parish.	37.0	13.8	54.0
H-19	SE¼, SE¼, NE¼, SW¼, Sec. 34, T19N, R6W, Mt. Mariah District, Claiborne Parish.	22.0*	19.0	53.0

*Overburden consists of brown ore derived by weathering of the parent green ore.

Hole No.	Location	Thickness of Overburden (in feet)	Thickness of Green Ore (in feet)	Total Drilling Depth (in feet)
H-20	SW¼, NE¼, SW¼, SW¼, Sec. 34, T19N, R6W, Mt. Mariah District, Claiborne Parish.	**	**	50.0
H-21	SE¼, SW¼, SE¼, SW¼, Sec. 27, T22N, R8W, Ruple Church District, Claiborne Parish.	25.0	10.0	44.0
H-22	SW¼, NW¼, NE¼, SW¼, Sec. 35, T22N, R8W, Ruple Church District, Claiborne Parish.	21.0	9.0	40.0
H-23	SW¼, NE¼, SE¼, SE¼, Sec. 36, T22N, R8W, Ruple Church District, Claiborne Parish.	11.0	8.0	31.0

** Not present.

Thin Section Numbers, Depths Below Surface, and Distances from Top of Beds

Thin Section Number	Depth Below Surface (in feet)	Distance From Top of Bed (in feet)
H-1-1	37.17	2.17
H-1-2	38.25	3.25
H-1-3	38.83	3.83
H-1-4	39.33	4.33
H-1-5	40.08	5.08
H-1-6	40.67	5.67
H-1-7	40.83	5.83
H-1-8	41.17	6.17
H-1-9	41.67	6.67
H-1-10	41.91	6.91
H-1-11	42.33	7.33
H-1-12	42.50	7.5
H-1-13	42.75	7.75
H-1-14	43.08	8.08
H-1-15	44.08	9.08
H-1-16	45.17	10.17
H-6-17	41.58	1.58
H-6-18	42.17	2.17
H-6-19	42.83	2.83
H-6-20	44.00	4.00
H-6-21	45.25	5.25
H-6-22	46.91	6.91
H-6-23	50.42	10.42
H-6-24	51.25	11.25
H-6-25	51.91	11.91
H-6-26	53.00	13.00
H-11-27	45.50	0.50
H-11-28	45.75	0.75
H-11-29	47.33	2.33
H-11-30	49.75	4.75
H-19-31	26.67	[illegible]
H-19-32	28.75	[illegible]
H-19-33	29.83	3.83
H-19-34	44.08	17.08
H-21-35	26.67	2.67
H-21-36	27.67	3.67
H-21-37	28.42	4.42
H-21-38	28.67	4.67
H-21-39	29.08	[illegible]08
H-21-40	30.08	[illegible]

APPENDIX C

WET CHEMICAL ANALYSES BY BRUCE WILLIAMS LABORATORIES, JOPLIN, MISSOURI

*Analysis No.	Core No.	Depth (feet)	SiO_2	Al_2O_3	Fe	MgO	CaO	P	S	CO_2	Loss on Drying (105°C)	Water of Hydration	Loss on Ignition (1000°C)
334	H-0	00.00-00.25	18.40	6.14	22.50	0.53	16.25	0.08	0.06	20.20	1.68	2.92	22.92
335	H-0	00.25-00.50	23.70	10.21	30.50	1.50	3.13	0.07	0.02	9.90	2.56	5.64	14.54
336	H-0	02.33-02.50	28.10	6.77	27.50	1.68	2.88	0.17	0.15	17.80	1.68	0.63	18.43
337	H-0	03.00-03.25	60.85	6.59	14.50	0.73	1.25	0.07	0.07	1.10	2.26	1.62	4.72
338	H-0	04.50-04.83	45.80	5.11	20.00	1.45	2.50	0.13	0.05	13.30	1.10	0.98	14.28
339	H-11	45.00-45.50	28.60	10.31	27.50	1.63	2.50	0.16	0.04	8.60	3.31	4.17	12.77
**340	H-11	47.50-48.00	19.70	2.18	34.25	1.90	3.13	0.15	0.02	14.40	2.41	2.89	17.29
341	H-11	49.00-49.50	21.35	9.14	31.25	1.96	3.13	0.29	0.06	12.20	2.46	3.65	15.85
342	H-11	49.50-50.00	17.50	7.06	20.00	0.29	19.75	0.15	0.02	21.40	1.42	2.73	24.13
343	H-11	50.25-50.33	28.40	4.64	28.75	0.96	3.25	0.14	0.03	17.60	1.41	1.23	18.83
344	H-11	50.00-50.75	19.85	4.33	30.50	3.44	3.38	0.24	0.03	22.20	0.95	0.40	22.60
345	H-13	36.50-36.83	26.50	4.62	27.50	2.00	4.38	0.24	0.18	21.24	0.68	0.19	21.43
346	H-13	36.83-37.33	52.37	6.11	16.25	1.45	2.50	0.07	0.12	12.10	1.27	0.20	12.38
347	H-13	37.50-37.66	36.40	3.74	22.50	2.72	3.38	0.03	0.08	19.50	0.65	0.20	19.70
**348	H-13	38.00-38.33	28.58	8.31	27.50	1.61	1.50	0.16	0.04	12.20	2.29	3.53	15.73
349	H-13	39.50-40.00	23.40	6.01	28.75	2.86	3.75	0.17	0.04	20.85	1.52	0.05	20.90
**350	H-13	45.00-45.50	55.22	6.88	16.00	0.19	2.50	0.13	0.03	8.70	1.37	0.52	9.22
351	H-13	47.66-48.18	29.58	5.03	25.00	2.51	4.00	0.42	0.06	20.40	0.67	0.53	20.93
352	H-13	48.18-48.83	36.00	8.48	24.00	1.05	3.13	0.31	0.29	9.60	1.67	2.21	11.81
353	H-14	35.33-35.50	42.36	2.73	20.00	3.68	3.75	0.07	0.08	18.20	0.20	0.30	18.50
354	H-14	37.00-37.42	26.30	8.48	28.75	0.80	2.50	0.18	0.02	13.80	2.60	1.70	15.50
355	H-14	39.66-40.00	22.60	8.76	29.25	2.52	3.13	0.18	0.06	13.20	2.60	3.30	16.50

APPENDIX C--Continued

*Analysis No.	Core No.	Depth (feet)	SiO_2	Al_2O_3	Fe	MgO	CaO	P	S	CO_2	Loss on Drying (105°C)	Water of Hydration	Loss on Ignition (1000°C)
356	H-14	46.42-46.83	37.70	7.91	22.50	2.17	2.88	0.18	0.23	10.60	1.90	1.70	12.30
357	H-14	46.83-48.00	29.80	3.98	25.00	1.72	4.38	0.38	0.20	18.70	1.00	2.21	20.91
358	H-14	48.00-48.75	42.70	8.89	20.56	1.54	2.50	0.12	0.47	8.50	1.80	2.30	10.80
**359	H-18	35.18-35.66	32.20	6.60	21.50	2.90	3.75	0.07	0.29	20.70	1.90	NP	20.70
360	H-18	35.66-36.00	14.82	4.27	32.50	1.54	3.75	0.11	0.12	26.90	1.20	0.20	27.10
361	H-18	37.50-38.00	20.06	8.23	31.75	1.94	2.75	0.16	0.02	15.30	2.60	2.30	17.60
362	H-18	39.18-40.00	17.84	6.90	33.00	2.68	2.50	0.18	0.06	16.70	2.10	2.80	19.50
**363	H-18	46.00-46.66	24.00	28.24	29.00	1.76	3.13	0.12	0.03	13.60	2.20	2.60	16.20
**364	H-18	47.25-47.83	19.84	7.02	32.00	2.39	3.13	0.14	1.66	15.10	1.85	1.70	16.80
**365	H-18	49.00-49.18	32.47	10.34	25.00	1.01	2.50	0.18	0.07	10.10	2.30	2.70	12.80
366	H-18	49.18-50.00	31.08	4.27	25.00	0.91	4.38	0.32	0.05	21.10	0.90	0.10	21.20

*Louisiana Geological Survey analyses number designations
**Samples utilized as standards for X-ray fluorescence analyses
NP Not present